ELECTRODEPOSITION OF CERMETS, (Part 2).

David William Snaith

In Candidacy for the Degree of

Doctor of Philosophy

University of Aston in Birmingham

November 1974

SUMMARY

Modern engineering requirements are frequently near the limits of application of conventional materials. For many purposes, particularly tribological, the most satisfactory solution is frequently the application of a resistant coating to the surface of a common metal. Electrodeposited cermet coatings have proved very satisfactory: some of the factors underlying the cermet electrodeposition process have been investigated.

A ceramic particle in contact with an electrolyte solution will carry a charge which may affect the kinetics of the suspended particle under electroplating conditions. Measurement has been made of this charge on particles of silicon carbide, chromium diboride and quartz, in contact with solutions of copper sulphate/ sulphuric acid in terms of the electrokinetic (zeta) potential and also as surface charge density. The method used was that of streaming potential and streaming current measurement. The electrolyte composition used was 1:1 Cu^{2+}:H^{+}, i.e. that of the common electroforming bath. Very high concentrations and a wide range of temperature were used in order that the values of charge in a practical plating electrolyte should be found. Measurements were also made using solutions of copper sulphate, sulphuric acid and potassium hydroxide separately.

The heats of adsorption of cations on silicon carbide and quartz from the acid copper sulphate electrolyte were determined and the adsorption shown to be physical in nature.

Copper-based cermet materials have been produced by electrodeposition at a number of current densities and temperatures using suspensions of the above-named ceramics in the acid copper sulphate bath. The particle inclusion density was correlated with the charge carried by the particle and to the electrical field strength in the electrolyte. It was shown that with this electrolyte, which

has high micro-throwing power, it was not possible to deposit non-conducting quartz particles even although they carried a high positive charge.

It is suggested that the mechanism of particle deposition involves hydrodynamic transfer of the particle to the outer Helmholtz plane on the cathode, a field assisted transport through the double layer and finally mechanical keying of the particle by electrodeposited metal.

Acknowledgements

The author wishes to thank Mr. P. D. Groves and Dr. I. Jenkins for encouragement and helpful discussion during the course of this work.

CONTENTS.

Introduction.

The results of the first phase of a study of cermet electrodeposition [1] were very encouraging and gave a useful insight into the possible mechanisms of the process. The object of the present work, which follows directly from this initial study, was to determine the effects of high electrolyte concentrations and of variations of temperature on the electrokinetic (zeta) potential of a number of ceramic materials and to study in more detail the relationship of the zeta potential to the codeposition of ceramics with metal and hence to further elucidate the mechanisms of the codeposition process. The long term aim is to achieve sufficient understanding of the mechanism of the process that any combination of particulate material and electrolyte can be readily evaluated by electrochemical measurements instead of by prolonged plant tests, to determine whether or not it might give satisfactory codeposits. Suitable variables for measurement may be the electrokinetic properties of the particulate material and the deposition characteristics of the plating electrolyte. The positions in the metal structure at which particles are deposited may be very significant: distribution may be completely random or concentrated at dislocations, grain boundaries or any other physical features such as edges and hollows.

At the present time there is good reason for studying this process in detail: more specialised materials are constantly being demanded to meet the needs of advanced technology and raw materials of many sorts are becoming increasingly scarce. Surface coating processes like this one enable desirable properties to be obtained without the need to produce an entire article in a scarce material or one which is difficult to fabricate. In addition, properties otherwise unobtainable can be achieved in many cases.

CHAPTER I. COMPOSITE MATERIALS.

For many purposes the ideal material for fabrication does not exist and for centuries attempts have been made to improve upon existing materials. Examples of such attempts include iron-bound wood, steel reinforced concrete and more recently fibre reinforced synthetic plastics. Each of these attempts involved the combination of two materials which had complementary properties, the resulting composite material having properties better than those of either component. Many naturally occurring materials are composite in structure.

In order to obtain improvements in properties such as high strength and stiffness with light weight, high strength at high temperature, good oxidation resistance at high temperature or resistance to abrasive wear a considerable amount of development work has been done in recent years on the production of composite materials. The background to the development and use of such materials was summarised in the first stage of this work.[1] The general principles involved in preparation and application of such materials were considered. Much of the published work involved plastics as matrix materials, reinforcing fibres being of a variety of materials. Of particular interest was carbon fibre. A considerable amount of work in which fibres or granules were incorporated into a metallic matrix by non-electrolytic means was reported.

The use of composite materials has enabled certain problems to be overcome in recent years, for example the production of high strength and light weight rocket motor cases from boron fibre/epoxy resin. Unfortunately there have been some serious failures due to an incomplete understanding of the characteristics of these materials. In this context the failure of the Rolls-Royce RB 211 "carbon fibre" engine was notable as, following the very successful

RB 111 engine, it illustrated the potential dangers of scaling-up operations with these new materials.

1.1 Plastic matrix materials.

Because the uncured (liquid) matrix material can readily be cast around the reinforcement and subsequently cured these materials are relatively easily produced. If the matrix and reinforcement are carefully chosen excellent lightweight materials are obtained for room and moderate temperature applications. Of the available reinforcing materials carbon fibre is very popular because of its high specific strength. Carbon fibre/epoxy material has recently found application in airframes.[2]

Plastic matrix materials cannot be used at elevated temperatures because of their inherent susceptibility to thermal and oxidative degradation. The methods of preparation and the properties of these materials are not of great significance to the work described in this thesis.

1.2 Metal matrix materials.

The use of metal as matrix material makes possible the use of composite materials at elevated temperatures. It is more difficult to fabricate composites having metal matrices than those with plastic matrices. This is particularly true for aluminium, magnesium and the refractory metals.[3] As metal matrix composites, even those with alumium or magnesium, generally have lower specific properties, e.g. tensile strength, stiffness, than those with plastic the use of metal matrix materials is limited to those cases where a metal matrix gives special advantages. Examples of such applications are those at high temperatures, where electrical or thermal conductance are required, where increased strength is needed or reduced flammability required.

A great variety of metal matrix composites have been produced and a number of different methods used. The type of application of the finished material necessarily determines the exact nature of the material produced: if it is to be wear and abrasion resistant a particulate reinforcement is suitable whereas if high strength is required a fibrous reinforcement is necessary. For highest strength materials a high and even aligned-fibre density is required. This is difficult to achieve by mechanical mixing processes as these generally involve either powder metallurgical methods or the use of liquid metals which may attack a fibre and weaken it. [4,5] The main non-electrolytic methods by which metal matrix composites can be produced were reviewed in the earlier work [1] and have been well discussed by other workers. [3,6,7,8]

If metal matrix composites are produced by electroforming the preparation method will depend upon the type of material required. For the production of high strength materials with a high density of aligned fibres a considerable amount of work has been done on methods involving filament winding with concurrent electroforming. [7,8,9-14] Where high specific strength and stiffness were required carbon fibre was again a very popular reinforcement although far from ideal as a reinforcement for metals. [7,15,16] For production of composites having granular reinforcing, suitable for abrasion and wear resistance, the method used is a variation on the following: the finely powdered reinforcing material is dispersed in the electroplating bath, being maintained thus by some form of solution agitation. Under plating conditions the powder is codeposited together with the metal. Much work has been done on improving this process in recent years and the earlier work was discussed thoroughly. [1] Recent developments include application in reclamation procedures for jet aeroengines [17] as well as in general anti-wear use.

Electrodeposition processes have the great advantage over any of the mechanical mixing processes for production of composite materials that the process is carried out cold, thus avoiding thermal damage to the reinforcement, and under conditions which cause no mechanical damage to the reinforcement. In addition, in the case of the electrodeposited anti-wear coating, it is possible to apply it in places where any other technique is impossible.[17]

1.3 Mechanism of formation of particle reinforced composites by electrodeposition.

Previous work[1] had indicated that the electrocodeposition process for ceramic/metal composites, "cermets", was influenced by the charge carried by the ceramic particle in suspension. It was also shown that, as expected, the charge which a particle carried was changed when the concentration of electrolyte with which it was in contact was changed. In the case of silicon carbide, on which the main investigation was carried out, the charge which was initially negative decreased as the ionic strength of the solution was increased. This decrease was apparently independent of the nature of the ions present i.e. it was simply an ionic strength effect. These results also suggested that if the concentration of electrolyte in contact with the particles of ceramic was increased further the charge on the particle might undergo sign reversal, becoming positive. A positively charged particle would be more consistent with the cathodic deposition of particles. Some indication was gained, during a brief investigation using chromium diboride, that the greater the positive charge on a ceramic particle the greater was the probability that it would be deposited on a cathode under electroplating conditions. Some confirmation of this opinion was gained, at this time, from Foster.[18]

The present work has studied the effect on the charge on the ceramic particle of increasing the concentration of electrolyte to very high values and to changes in temperature. The electrolyte chosen was a mixture of copper sulphate and sulphuric acid. Investigations have been made using a number of ceramic materials over a range of temperature.

To find whether or not a relation could be found between the charge on a particle and its tendency to deposit under plating conditions an extensive programme of electrodeposition has been carried out.

CHAPTER 2. THE ELECTROCHEMICAL DOUBLE-LAYER

When a ceramic particle, or other solid material, is brought into contact with an electrolyte solution a potential difference is set up between the solid and liquid phases. This is caused by the presence of adsorbed ions and orientated solvent dipoles at the solid surface.

Any change in this interphase potential difference which is brought about through a change in electrolyte or in temperature must necessarily be caused by alteration in the structure of the double layer which exists between the low or nonconducting ceramic particle and the bulk of the solution. The structure of the double-layer, from the simple capacitor model up to the currently accepted model was discussed in detail in the earlier part of this work.[1] This current model shows the orientation of solvent dipoles, the presence of adsorbed anions the locus of centres of which constitute the inner Helmholtz plane and, on the outer Helmholtz plane, a layer of excess charge merging into a diffuse "Gouy-Chapman" layer which extends into the bulk of the solution. When a liquid stream is forced, by hydrostatic pressure, through a porous diaphragm of ceramic particles contained in a tube, or through a capillary tube, a potential difference is set up between the ends of the tube. This is the streaming potential which arises because the liquid stream displaces and carries with it the diffuse part of the double layer near to the interface. Under steady state conditions this movement of charge constitutes an electric current which is proportional to the pressure difference. This current is entirely dissipated by back-conduction through the liquid when no current is flowing in an external circuit. The current must thus be proportional to the streaming potential set up between the ends of the tube. Streaming potential and current are related to sedimentation, electroosmosis and electrophoresis;

all are known as electrokinetic phenomena. Equations relating the measureable quantities for an electrolyte/solid interface for the above phenomena in terms of the electrokinetic (zeta) potential have been derived, initially by Helmholtz [19] and later by Smoluchowski. [20] A concise rederivation of their equations is given by Kortüm. [21] The zeta potential is the value of potential in the glide plane of the double layer and corresponds to the outer Helmholtz plane (OHP). [1,22] This is shown diagrammatically in fig. 2.1.

2.1 The Helmholtz-Smoluchowski equations.

The equations relevant to the present work are those for streaming and electrophoresis. If surface conductance is neglected the equation for streaming potential is

$$E = \frac{\zeta P D_o}{4\pi\eta_o K}$$

and that for electrophoresis is

$$V = \frac{\zeta X D_o}{4\pi\eta_o}$$

where E is the streaming potential, ζ is the electrokinetic potential, P the applied hydrostatic pressure, D_o the dielectric coefficient, η_o the viscosity, K the conductivity, V the velocity of a particle in an electric field of strength X. The subscript zero refers to the values of viscosity and dielectric coefficient of the continuous phase in zero electric field. Usually in the calcultion of zeta potential the bulk values of D and η are used, however, the mean value of D in the double layer may be less than in bulk and the value of η varies, particularly as it is a function of ψ, the field in the double layer. For most purposes the simplified model of viscosity remaining at its bulk value up to the plane of shear is sufficiently accurate. [23]

In the establishment of the "classical" Helmholtz-Smoluchowski equation certain assumptions are made: that capillary or pore radius r is large compared with $\frac{1}{K}$, the thickness of the double layer and that surface conductance can be neglected. When the ionic

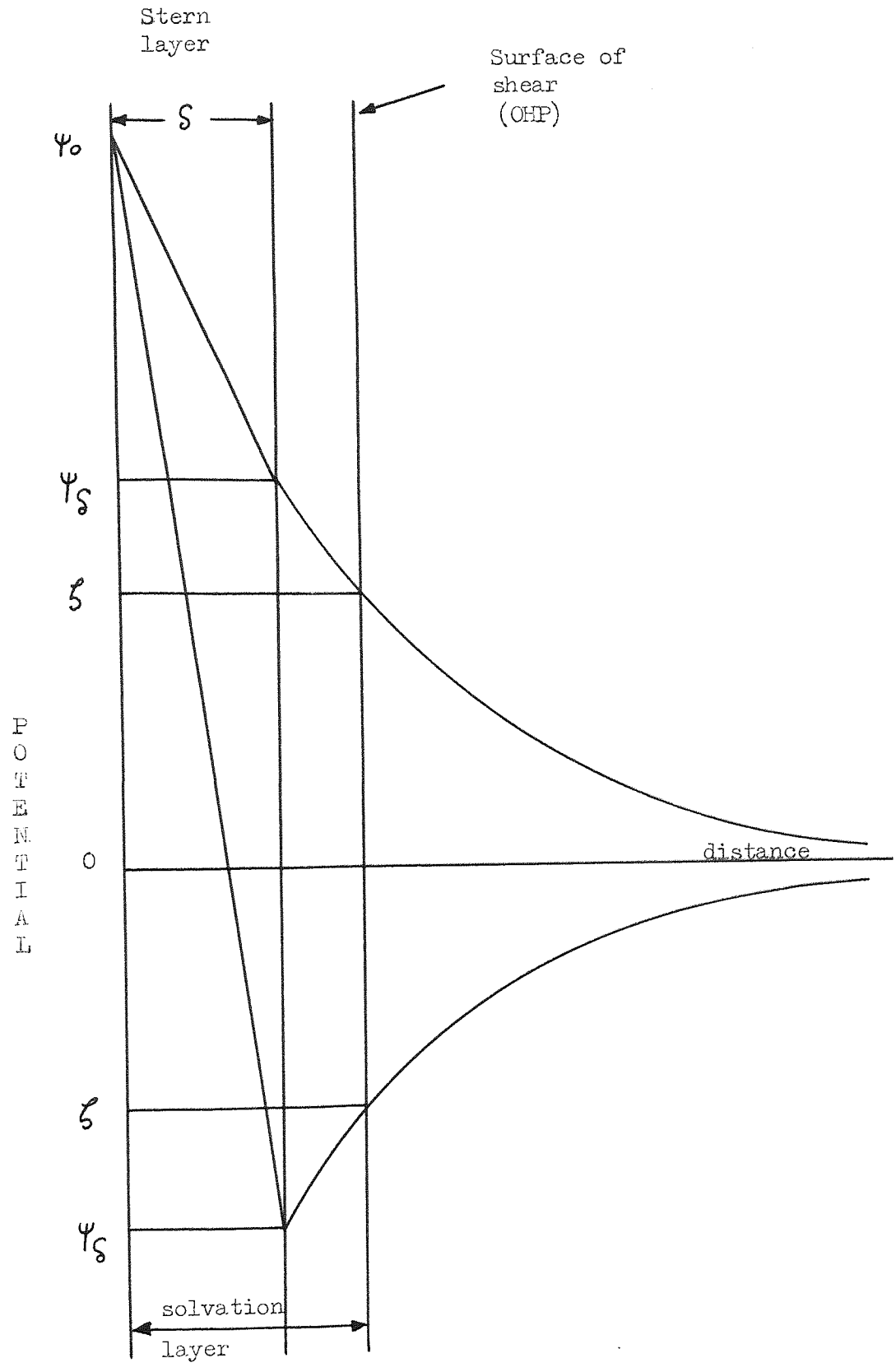

Fig. 2.1. Potential decay curves for an electrical double layer on a surface of potential ψ_0. The lower curve is for strong adsorption in the Stern layer.

concentration of the electrolyte is very low this condition $r \gg \frac{1}{K}$ is no longer satisfied. Conductivity also is very low and the effects of surface conductance can become noticeable. Under these conditions deviations from the classical equation can be observed.[24,25] At high electrolyte concentrations, particularly in the presence of multivalent ions, the double layer will contract and the effect of surface conductance, which remains almost constant with concentration,[26,27,28] becomes negligible. This is also true for concentrations greater than about 10^{-3}M for small univalent ions.[29]

2.2 Effects on D and η of the field within the double layer.

Within the double layer the local electric field may be very high since the potential may fall as much as 100 mV in a distance of 2 nm from the surface giving a local field of 5×10^5 Vcm^{-1}. Calculated results show that the viscosity of water rises sharply and the dielectric coefficient falls with increase in the field[30,31,32,33] hence $\frac{D}{\eta}$ falls sharply with $\frac{d\psi}{dx}$, with local field strength at any point in the double layer. This is illustrated in fig. 2.2.

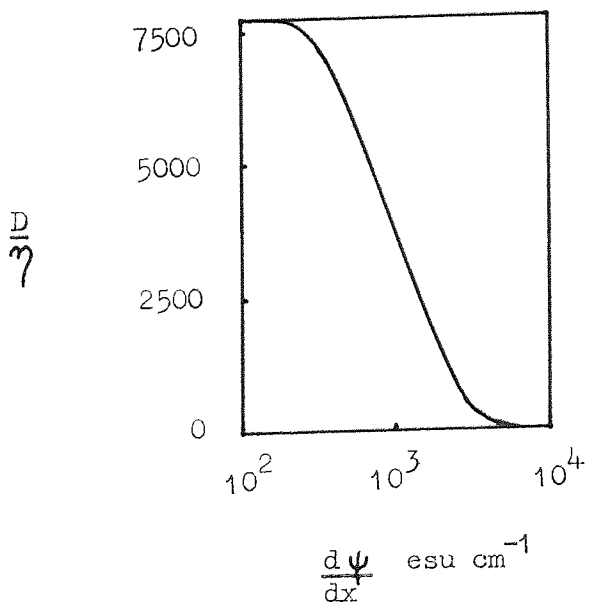

Fig. 2.2. Variation of $\frac{D}{\eta}$ with field strength, from data of refs. 31 and 32.

In the calculation of zeta potential it is assumed that D and η are constant, with values of D_o and η_o right up to a plane of shear at which η suddenly becomes infinitely great i.e.

$$\int_0^{\zeta} \frac{Do}{\eta o} d\psi = \frac{Do\zeta}{\eta o} = \int_0^{\psi_o} \frac{D}{\eta} d\psi .$$ The term $\frac{D_o\zeta}{\eta o}$

in the Helmholtz-Smoluchowski equations should therefore be replaced by $\int_0^{\psi_o} \frac{D}{\eta} d\psi$, where ψ_o is the electrostatic potential in the interface, at zero distance from it, relative to the subjacent aqueous phase. The equation of electroosmotic flow is thus given [34] as

$$v = \frac{X}{4\pi} \int_0^{\psi_o} \frac{D}{\eta} d\psi$$

From this equation and the Helmholtz-Smoluchowski equation

$$v = \frac{X}{4\pi} \cdot \frac{Do}{\eta_o} \cdot \zeta$$

$$\zeta \frac{D_o}{\eta_o} = \int_0^{\psi_o} \frac{D}{\eta} d\psi$$

and $$\zeta = \frac{\eta_o}{D_o} \int_0^{\psi_o} \frac{D}{\eta} d\psi$$ where as usual the subscript zero refers to values in zero electric field. If the presence of the field had no effect on D_o and η_o then the ratio $\frac{\zeta}{\psi_o}$ calculated by evaluating the integral $\int_0^{\psi_o} \frac{D}{\eta} d\psi$ should be equal to 1. In fact calculations show that $\frac{\zeta}{\psi_o}$ increases towards 1 with decreasing field strength or ionic strength,[35] assuming no specific interaction between ions. This suggests that in very dilute solutions and in low fields use of D_o and η_o is justified in the calculation of ζ. For concentrations of up to about 0.1M of small univalent counter-ions the

ratio $\frac{\zeta}{\psi_o}$ in many systems is about 0.5. Above this concentration specific effects become more important and ultimately reversal of charge can occur.[35] If D_o and η_o are used in calculations and if under the conditions used $\frac{\zeta}{\psi_o}$ is about 0.5 then the calculated zeta potential will be about 0.5 of the value from the interface to the bulk of the solution, i.e. half of its "true" value.

Polyvalent heavy metal ions such as Th^{4+} are strongly absorbed onto a surface of negative ψ_o such as glass. Their presence may even cause ζ to be of opposite sign from ψ_o, which is little changed even when ζ becomes markedly positive. This suggests that the heavy metal ions are strongly bound to the surface forming a solid Stern layer. It has been shown that absorption of singly charged ions can similarly take place.[36,37] (Surfaces other than glass may have a negative value of ψ_o. At the interface between water and an inert solid water molecules will orientate such that there are always more with their oxygen end towards the interface owing to dispersion interactions. The solid will thus become slightly negative.[38]) Because of the strongly bound Stern layer the electrokinetic movement of liquid and ions must be possible only outside this layer and it is reasonable to suppose that ζ can be calculated from this plane of strongly bound ions rather than from the plane of negative ions or orientated dipoles which determine ψ_o.[35] In the current work high concentrations of electrolyte have been used. As indicated above, under such conditions $\frac{\zeta}{\psi_o}$ would become much less than 1 and would be likely to reverse in sign as the electrolyte concentration was increased.

2.3 The effects of surface conductance.

Surface conductance, which is associated with an increased concentration of ions at a charged surface, may appreciably reduce the value of electrokinetic effects. Consider an ionogenic material, such as glass, placed in an aqueous solution of an

electrolyte. The surface of the glass will contain silicic acid groups from which some cations, e.g. H^+ or Na^+, can split off into the water while the silicate group remains part of the solid sheet. The glass will now have a negative charge which, although it will cause redistribution of the ions of the electrolyte near the surface, will not alter its actual conductivity. Only the mobile cations (forming a diffuse double layer) added to the system by the ionisation of the silicate groups will alter the conductivity. This increment is known as the surface conductivity. It is generally in the order of $1 \times 10^{-9} \Omega^{-1} cm^{-1}$ and increases only slightly with increase in electrolyte concentration;[35] it is therefore significant only when very dilute solutions are used. In the present work solutions, mostly of copper sulphate plus sulphuric acid, have been used at concentrations between approximately 1×10^{-5} and 5×10^{-1} molar; the most dilute solution has a conductivity in the order of $1 \times 10^{-6} \Omega^{-1} cm^{-1}$. For such solutions the effect of surface conductivity was neglected.

For the conditions used in this work it was considered that use of the Helmholtz-Smoluchowski equations was justified. The ceramic material was studied by streaming and these equations can satisfactorily be applied to results from streaming measurements made on diaphragms prepared from the 37 µm powders used.[1,39]

2.4 Calculation of zeta potential and surface charge density.

Zeta potentials were calculated from both streaming potential and streaming current measurements by use of the Helmholtz-Smoluchowski equation for streaming. Surface charge densities were calculated using these values of zeta potential and the calculated double-layer thicknesses in the equation for surface charge density due to Smoluchowski. Calculation of zeta potential, whether from streaming current or streaming potential measurements involved determination of the mean value of the ratio streaming

potential (or current) to hydrostatic pressure over the pressure range used i.e. the mean value of $\frac{E}{P}$ or $\frac{I}{P}$ where E was the streaming potential, I the streaming current and P the hydrostatic pressure. To speed the calculation of these ratios and also the calculation of the zeta potentials from the very large amount of experimental data a computer was used: (ICL 1903, with 16K store). The program, which is given in appendix 1, was written to include a "least squares" procedure to determine $\frac{E}{P}$ or $\frac{I}{P}$ from the experimental data and also to include all necessary conversion factors to give the zeta potential in milivolts.

2.4.1. Calculation of zeta potentials using streaming potential measurements.

The Helmholtz-Smoluchowski equation was used in the form

$$\zeta = \frac{E}{P} \times \frac{4\pi\eta K}{D}$$

where ζ is the electrokinetic (zeta) potential, E the streaming potential, P the hydrostatic pressure applied between the ends of the diaphragm, η the viscosity of the solution, K the conductivity of the solution and D its dielectric coefficient. This equation is the one used in the earlier work.[1]

2.4.2. Calculation of zeta potentials using streaming current measurements.

The streaming equation was modified to allow calculations to be made using current measurements. If the resistance of the cell circuit is R, the resistance of the measuring circuit r and the "cell constant" of the streaming cell is $\square$

then $$K = \frac{1}{R} \times \square \text{ and } E = I\,(R + r).$$

Hence $$\zeta = \frac{I\,(R + r)}{P} \times \frac{4\pi\eta}{D} \times \frac{\square}{R}$$ which rearranges to

$$\zeta = \frac{I}{P} \times \frac{4\pi\eta}{D} \times \left(\frac{r}{R} + 1\right) \square$$

where I is the observed streaming current.

It was required that zeta potentials calculated from streaming current data should be expressed in milivolts as usual: the appropriate conversions used in the change from potential to current measurements are given in appendix 1.

2.4.3. Calculation of surface charge density.

The surface charge density on the ceramic was calculated using the expression

$$q = \frac{\zeta D}{4\pi d} \quad \text{due to Smoluchowski,}$$

where q is the surface charge density in esu cm^{-2}, D is the dielectric coefficient, d is the double layer thickness in cm and ζ is the zeta potential calculated as in 2.4.1. and 2.4.2., above.

N.B. One appreciable advantage obtained by expressing the results in terms of surface charge density instead of as zeta potential is that the dielectric coefficient D is eliminated between the two equations:

from 2.4.1. and 2.4.3.

$$\zeta = \frac{E}{P} \cdot 4\pi\eta K \cdot \frac{1}{D} = q \cdot 4\pi d \cdot \frac{1}{D}$$

$$\therefore \quad \frac{E}{P} \cdot 4\pi\eta K \cdot \frac{1}{D} = q \cdot 4\pi d \cdot \frac{1}{D}$$

and

$$\frac{E}{P} \cdot \eta K = q \cdot d$$

hence the dielectric constant, appearing in the denominator in both expressions, can be eliminated. The advantage of this is twofold, firstly that as dielectric constant changes with concentration of solution and with temperature it is necessary to make the (very difficult) measurements of it for each solution and each concencentration and secondly the dielectric coefficient within the double layer is not a constant, (see sections 2.1. and 2.2.).

The thickness, d, of the double layer is given by the relationship

$$d = (3 \times 10^{7} \times |Z| \times C^{\frac{1}{2}})^{-1}$$

where C is the molar concentration of a Z : Z electrolyte and d is in cm.[40]

CHAPTER 3. MEASUREMENT OF ZETA POTENTIAL AND SURFACE CHARGE DENSITY.

Determination of zeta potential and surface charge density on the ceramic particles under investigation was via streaming current and streaming potential measurements. The measurements were made using vertical columns of the particulate materials. It was decided in this phase of the work that much higher electrolyte concentrations should be used than hitherto and that studies should be made over a range of temperatures. In order that sufficiently large streaming currents and potentials should be generated, at the higher electrolyte concentrations, for accurate measurement it was necessary to use higher hydrostatic pressures than in previous work. The cell used in the earlier work inherently allowed very accurate measurements at low values of hydrostatic pressure. However it was cumbersome to use and had a tendency to draw in air if pressures appreciably in excess of 100 mm Hg were used. For these and other reasons the cell design was considerably changed.

3.1. Design of the improved streaming apparatus.

3.1.1. The general design of the cell is shown in Fig. 3.1.

This cell was very much larger than the original cell. It had a considerably longer powder column in order that much higher hydrostatic pressures could be used without an increase in liquid flow rate and turbulence. It consisted of two vertically mounted flanged glass tubes, (Quickfit FG15), 15 mm in internal diameter and 170 mm in length. The ceramic powder diaphragm occupied the upper of these tubes and was, as in previous work, retained by a sheet of filter-paper (Whatman 541) supported on a sheet of perforated platinum. The filter-paper and platinum sheets were clamped between the flanges of the tubes, and the joint was made solution-tight by means of a sealing compound, ("Bostik 1"). Electrical measurements were made using platinum electrodes coated with platinum black: these were mounted above and below the

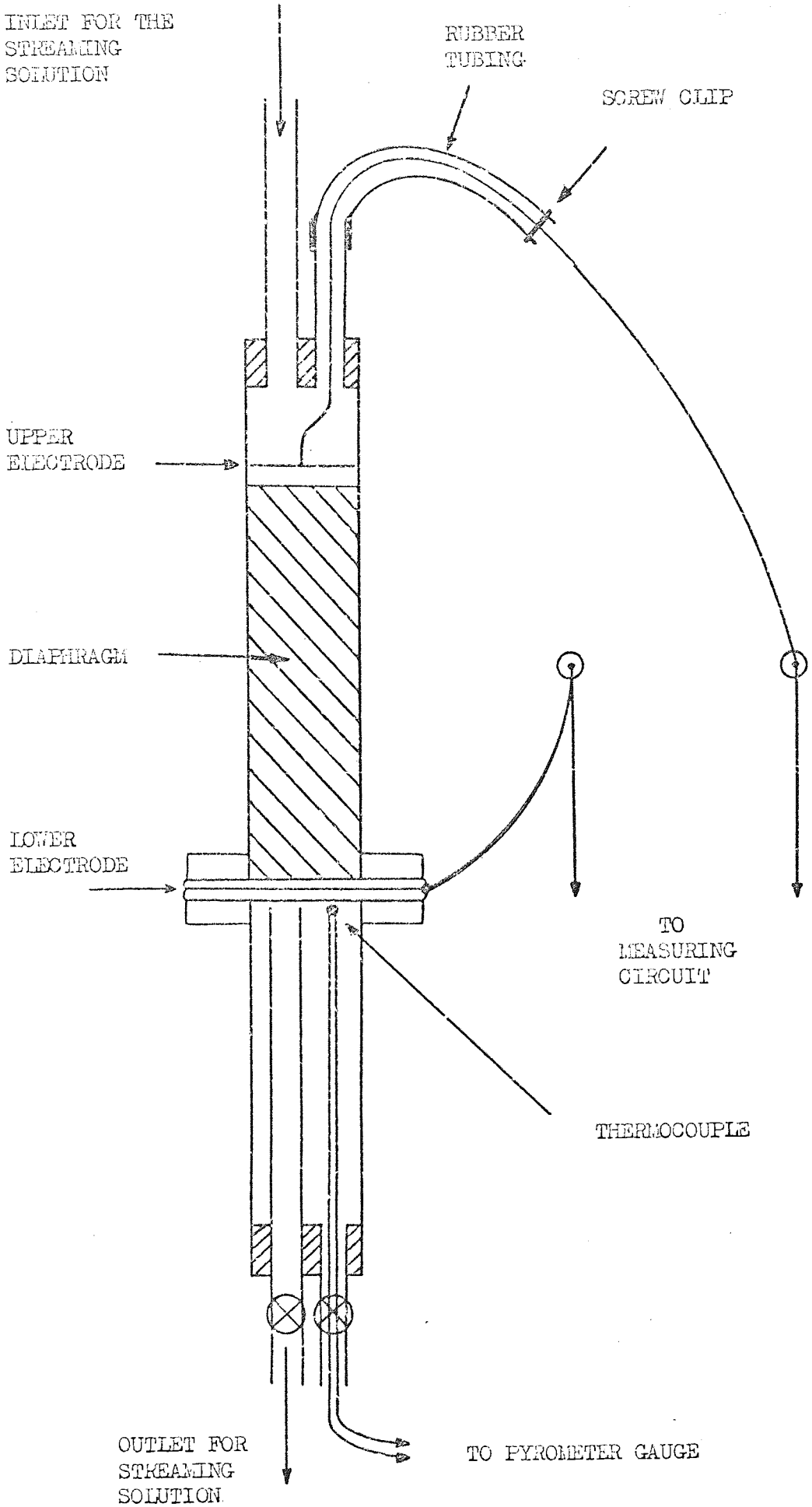

Fig. 3.1. General design of the streaming cell.

diaphragm of ceramic and as close to it as possible without touching. The perforated platinum sheet supporting the diaphragm also acted as the lower electrode. This electrode system proved to be very satisfactory in service and did not appear to suffer from polarisation or from other problems.

3.1.2. Measurement of streaming potential and streaming current.

Streaming potential was measured using a pH meter (Pye, model 291) as a high-impedance milivoltmeter, for the higher potentials, and a precision dial potentiometer (Pye 7565 Universal Precision Potentiometer) for the lower ones. Measured values of potential were identical whether measured by pH meter or potentiometer: the potentiometer, together with a sensitive electronic galvanometer, was essential for making measurements in the region of the polarity change.

Streaming currents were measured using an electronic microammeter. (WPA K201).

Electrical connections were made throughout using earthed coaxial leads, the guard being earthed to reduce the likelihood of electrical interference.

3.1.3. Application of hydrostatic pressure between the ends of the diaphragm.

Hydrostatic pressure of up to 220 mm Hg was applied by the simple but effective method of raising the solution reservoir, a 5 litre aspirator, using a rope and pulley and measuring the pressure directly by means of a surveyor's tape. This system was checked against a manometer for various flow rates and was found to be satisfactory. Many advantages were gained over the use of a pump and manometer, principally that any desired pressure was readily obtained and maintained steady and that the solution at no time came into contact with mercury in a manometer. This latter was particularly important as solutions of high concentrations were to

This system for applying pressure was well suited to the total-solution-loss system which was preferred to a recirculatory one as the possibility of contamination was reduced.

3.1.4. Temperature control.

In order to control the temperature accurately at a number of values it was necessary to satisfy two requirements. These were firstly that the streaming solution should be raised to the required temperature before entering the cell and secondly that the cell should be maintained at this temperature so that the solution was not cooled during the streaming process. The former was achieved by passing the solution, immediately prior to its entering the cell, through a heat exchanger immersed in a thermostat bath. A suitable heat exchanger was produced from 2 metres of 3 mm bore thin-wall glass tubing coiled into a spiral. The streaming solution was passed from this heat exchanger directly into the top of the cell. To maintain the cell at the chosen temperature it was completely enclosed in an insulated box: this was made of 20 mm thick expanded polystyrene sheet and one wall was an unlagged wall of the thermostat bath. Water from the thermostat bath was pumped through a copper-tubing spiral, which acted as a heating "radiator", coiled around the cell walls. The temperature of the solution leaving the diaphragm was measured using a chromel/constantan thermocouple mounted immediately below the lower electrode.

The general arrangement of the apparatus is shown in fig 3.2.

3.1.5. Measurement of the conductivity of the solution present in the diaphragm.

The value for solution conductivity used in calculations was determined on the solution/diaphragm system directly. The bulk conductivity of the solution was also measured in each case. By taking these two values it was possible to confirm that the neglect of surface conductance was justified as both bulk and solution/

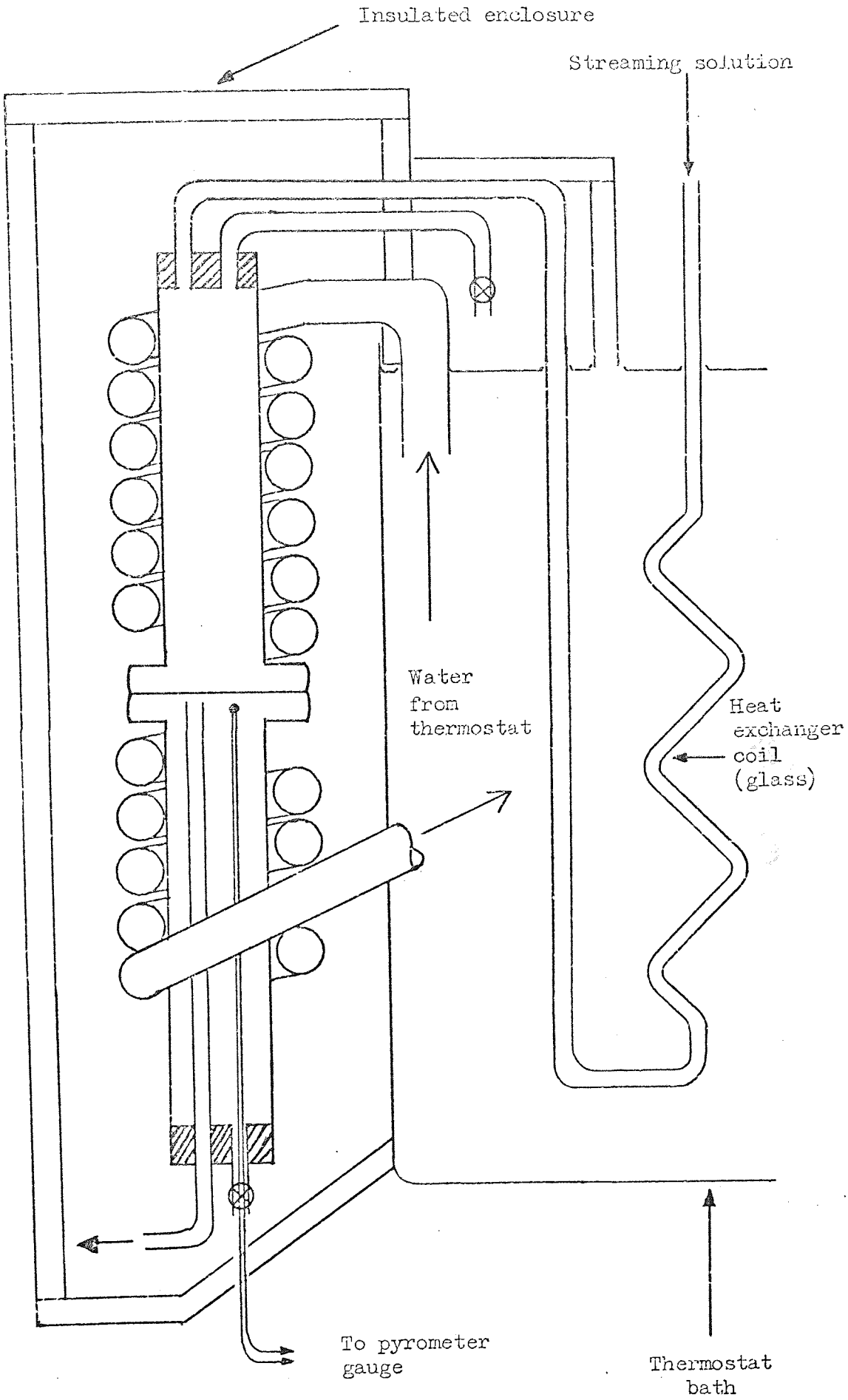

(a)

Fig. 3.2. General design of the streaming apparatus.

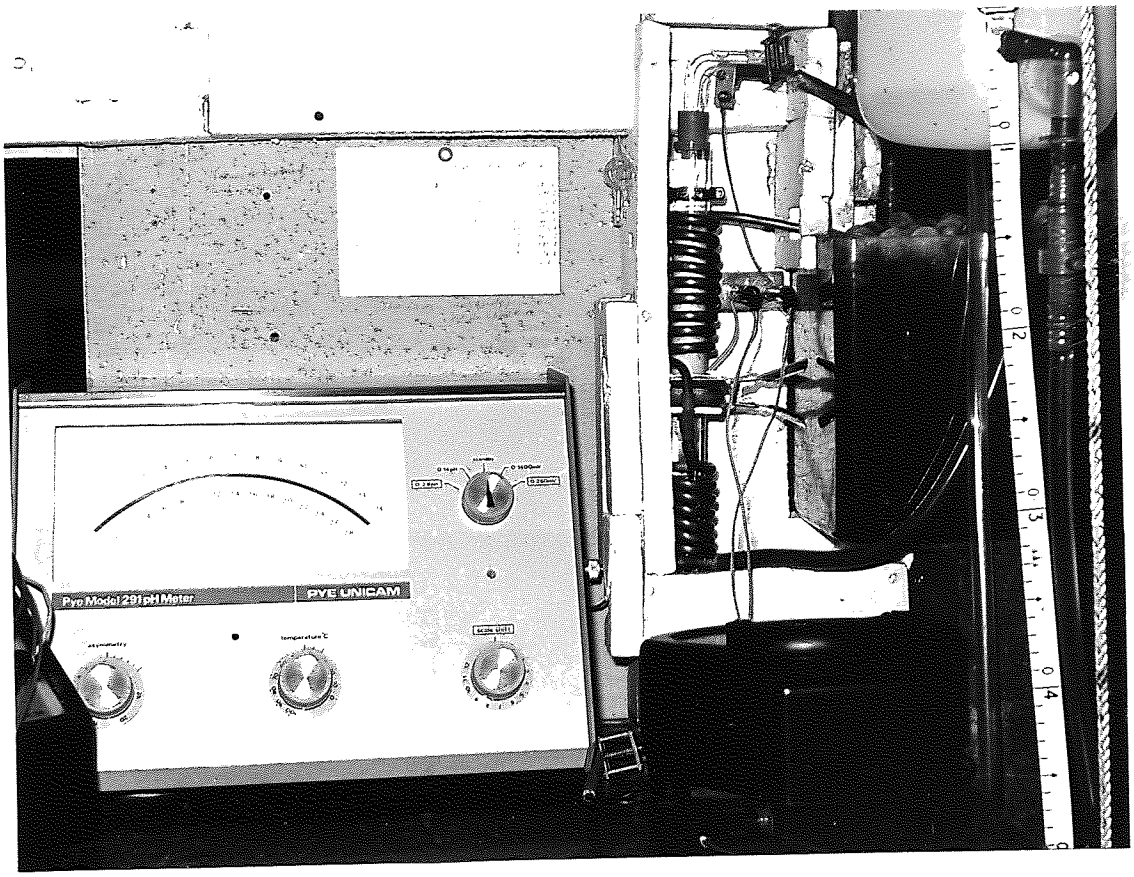

(b)

Fig. 3.2. Apparatus used for streaming studies.

diaphragm conductivities changed by the same proportion for a given concentration change of the solution. Measurement of solution/diaphragm conductivity allowed the calculation of the conductivity of solution present in the diaphragm. Measurements of conductance of the system were made using as "conductance cell" electrodes the platinum electrodes of the streaming cell. Measurements were made while solution was streaming slowly. To determine the "cell constant" of the diaphragm system potassium chloride solutions, firstly 0.1 molar and then 1.0 molar, were placed in the diaphragm. The conductance of the diaphragm system was measured as before for each of these solutions and the "cell constant" was calculated using the relationship

$$\text{conductance} \times \text{cell constant} = \text{conductivity} \qquad 41$$

Calculations from data obtained using 0.1 and 1.0 molar potassium chloride gave the same value for the cell constant, as expected. Using this same expression the conductivities of all the solutions used were calculated and these values used in calculation of the zeta potential and surface charge density. All conductance measurements were made using a Philips PR 9501/00 conductance bridge.

3.2 Materials used.

The choice of electrolyte and ceramic was a copper sulphate/sulphuric acid electrolyte and of silicon carbide, chromium diboride and quartz powders. A limited investigation was made using potassium hydroxide solutions with silicon carbide and quartz powders and a further short investigation was made using copper sulphate and sulphuric acid, separately, with silicon carbide.

The electrolyte used in the main investigation was of composition Cu^{2+} : H^{+} of 1:1 molar. This was chosen because it is a simple solution which finds wide application in commercial electroplating and electroforming practice and because it was the electrolyte used in the earlier part of this work.[1]

Solutions of total molar concentrations as follows were used: 6×10^{-6}, 3.2×10^{-5}, 1.28×10^{-4}, 5.12×10^{-4}, 2.05×10^{-3}, 8.19×10^{-3}, 3.28×10^{-2}, 1.32×10^{-1} and 5.28×10^{-1} molar. This highest concentration was one quarter of the concentration commonly used as a plating solution.

The potassium hydroxide solutions, in the same concentration range as the copper sulphate/sulphuric acid solutions, were used with silicon carbide and quartz to establish the effect of alkaline solutions on the ceramics used and to establish whether the use of alkaline instead of acidic solutions altered significantly the way in which the zeta potential and the surface charge density on the ceramic material changed with electrolyte concentration. The short investigation of the effects of copper sulphate and sulphuric acid alone on the charge on the ceramic was carried out using silicon carbide to confirm the findings of the earlier work using the original cell, that is that the change in zeta potential (and surface charge density) is for the systems studies an ionic strength effect rather than a specific ion effect.

3.2.1. Preparation of solutions.

All solutions were prepared from analytical grade reagents using "conductance" grade water prepared by deionisation of distilled water using a three-tank system: anionic, strong cationic and finally mixed-bed exchange resin. The water so prepared was stored in an aspirator fitted with a soda-lime guard tube to exclude carbon dioxide.

All glassware used in handling solutions was prepared for use by initially soaking in concentrated sulphuric acid to remove any soluble alkaline material in the surface of the glass, which could otherwise subsequently have leached out, followed by steaming out to remove all traces of electrolytes.

3.2.2. Preparation of ceramic powders for streaming.

In the earlier work silicon carbide of particle size 37/um had been used for streaming and this size shown to be very satisfactory. It was chosen again for use in the present streaming work. The three materials chosen for study were silicon carbide, chromium diboride and quartz: the former two because they had previously been used and the latter because it was a commonly used oxide. The silicon carbide could be purchased as 37/um powder (The Carborundum Company Ltd., 280 grit) and required only removal of "fines" but the chromium diboride and quartz were obtainable only in size range - 300 mesh to dust (Borax Consolidated Ltd., Jas. Podmore and Son). The required size of powder was separated from the mixture for these latter materials by water elutriation using a considerably modified laboratory elutriator (Griffin and George Ltd., "Laboratory Elutriator"). This is shown diagramatically in appendix VI together with the details of the calculations of the water flow rates required.

3.3. Preparation of ceramic powder diaphragms.

Powder diaphragms were prepared, from the 37/um powder, by simple sedimentation through conductance water in the upper or "diaphragm" tube of the streaming cell, the powder being added as a slurry in conductance water. The materials were all used "as supplied" after elutriation as previous work had indicated that the past history of the material did not affect its subsequent electrokinetic properties.[1]

N.B. This conclusion was confirmed by subsequent work using quartz and potassium hydroxide solutions, as shown in fig 4.13, for potassium hydroxide on quartz.

3.4. Measurement of streaming potential and current.

3.4.1. Silicon carbide diaphragms.

3.4.1.1. Streaming potential measurement.

Copper sulphate/sulphuric acid electrolyte was used at concentrations from 8×10^{-6} to 5.28×10^{-1} molar (total) at temperatures of 10°, 25°, 40°, 55° and 70°C. Copper sulphate solution and sulphuric acid solutions were used individually at concentrations from 8×10^{-6} to 8.19×10^{-3} molar at 25°C. Potassium hydroxide was used at concentrations from 2.28×10^{-5} to 3.74×10^{-1} molar at 25°C.

3.4.1.2. Streaming current measurements.

Copper sulphate/sulphuric acid electrolyte was used at concentrations from 8×10^{-6} to 5.28×10^{-1} molar (total), as for streaming potential measurement, at the temperatures of 10° and 70°C.

3.4.2. Quartz diaphragms.

3.4.2.1. Streaming potential measurements.

Copper sulphate/sulphuric acid electrolyte was used at concentrations from 8×10^{-6} to 5.28×10^{-1} molar (total) at temperatures of 10°, 25°, 40°, 55° and 70°C as for the silicon carbide diaphragms. Potassium hydroxide was used at concentrations from 2.28×10^{-5} to 3.74×10^{-1} molar at 25°C, also as for silicon carbide diaphragms.

3.4.2.2. Streaming current measurements.

Copper sulphate/sulphuric acid electrolyte was used in the same range of concentrations and temperatures as for streaming potential measurements.

3.4.3. Chromium diboride diaphragms.

Streaming potential measurements were made using the copper sulphate/sulphuric acid electrolyte over the concentration range from 8×10^{-6} to 5.28×10^{-1} molar (total) at temperatures of 25°,

CHAPTER 4. RESULTS OF STREAMING MEASUREMENTS.

The results of streaming measurements are shown, plotted as zeta potential and surface charge density against electrolyte concentration, in figs 4.1 to 4.17. Because of the very wide range of concentration used and the correspondingly great range in the zeta potentials and surface charge densities obtained the results are plotted log/log. In all cases the dependent variable is plotted on the abscissa: all the results in the earlier published work [1,42] were plotted in this way and for consistency this has been continued.

4.1 The effect of temperature.

For all of the solution/ceramic systems studies an increase in temperature gave a decrease in the positive value of the zeta potential and the surface charge density at all concentrations of solution. This can be seen in figs 4.1 to 4.11.

4.2 The effect of concentration.

For all combinations of ceramic and electrolyte and for both streaming potential and streaming current measurements an increase in electrolyte concentration gave an increase in the positive value of zeta potential and of surface charge density. At very low concentrations zeta potential and surface charge density were negative, silicon carbide most and chromium diboride least so. As concentration was increased from the lowest value this negative value decreased, leading to charge reversal and then increasing positive values in each case. For any given concentration above that for charge reversal chromium diboride had the highest value and silicon carbide the lowest. This can be clearly seen in fig 4.12. The zeta potential changes on all materials with both copper sulphate/sulphuric acid and with potassium hydroxide solutions showed increase with solution concentration tending approximately to linearity at the higher concentrations when plotted log/log.

The changes in surface charge density with concentration were similarly linear for copper sulphate/sulphuric acid solutions but for potassium hydroxide solutions showed some tendency to become more nearly constant with concentration when this was increased to very high levels, as shown in figs 4.15 and 4.16.

4.3. Electrolyte concentration required for charge reversal.

The concentration required for charge reversal varied for each solution/ceramic combination and also, as discussed in 4.1., with temperature. The way in which the zeta potential (and the corresponding surface charge density) varies in the region of the charge reversal can be seen in figs 4.1 to 4.17. In order to show the change for chromium diboride it was necessary to use the values of bulk electrolyte conductivity instead of those calculated from conductance measurements on the solution/diaphragm system (see 3.1.5.). This was because the bridge available did not allow accurate conductance measurements to be made of this system at the lowest concentration used, i.e. 8×10^{-6} molar.

N.B. The "cell constant" of the solution/diaphragm system was greater by about 10:1 than that of a typical dip cell. The graph of zeta potential change calculated from bulk conductivity values against concentration is shown in fig 4.10. The solution concentrations for charge reversal at 25° are as follows.

4.3.1. Silicon carbide.

Copper sulphate/sulphuric acid	2.2×10^{-3} molar (total)
Copper sulphate	2.4×10^{-3} molar
Sulphuric acid	2.6×10^{-3} molar
Potassium hydroxide	3.3×10^{-2} molar

4.3.2. Quartz.

Copper sulphate/sulphuric acid	2.5×10^{-3} molar (total)
Potassium hydroxide	3.1×10^{-2} molar

4.3.3. Chromium diboride.

Copper sulphate/sulphuric acid	1.2×10^{-5} molar (total).

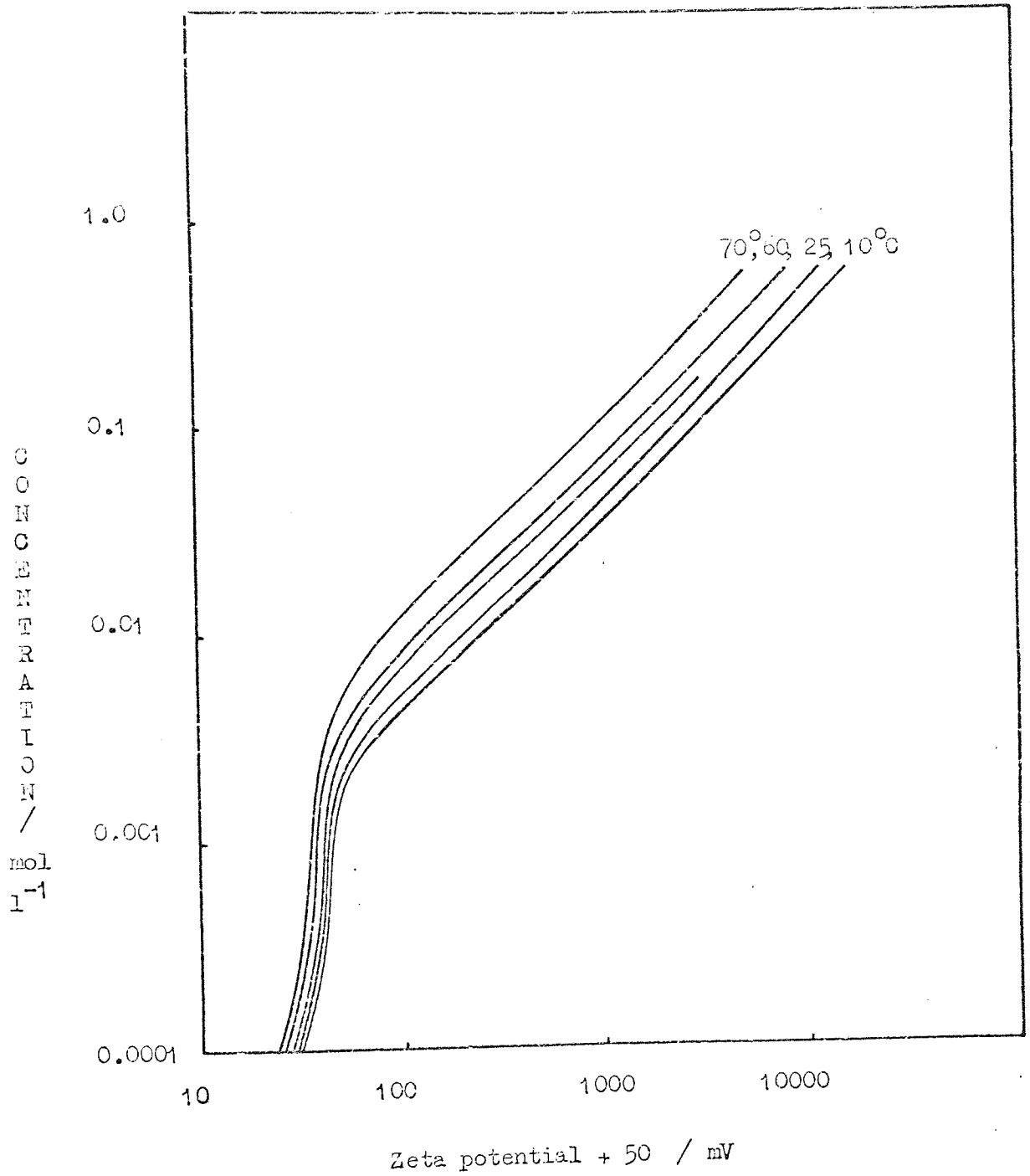

Fig.4.1. Change of zeta potential with concentration and with temperature: silicon carbide in copper sulphate/sulphuric acid solutions, from streaming potential measurements.

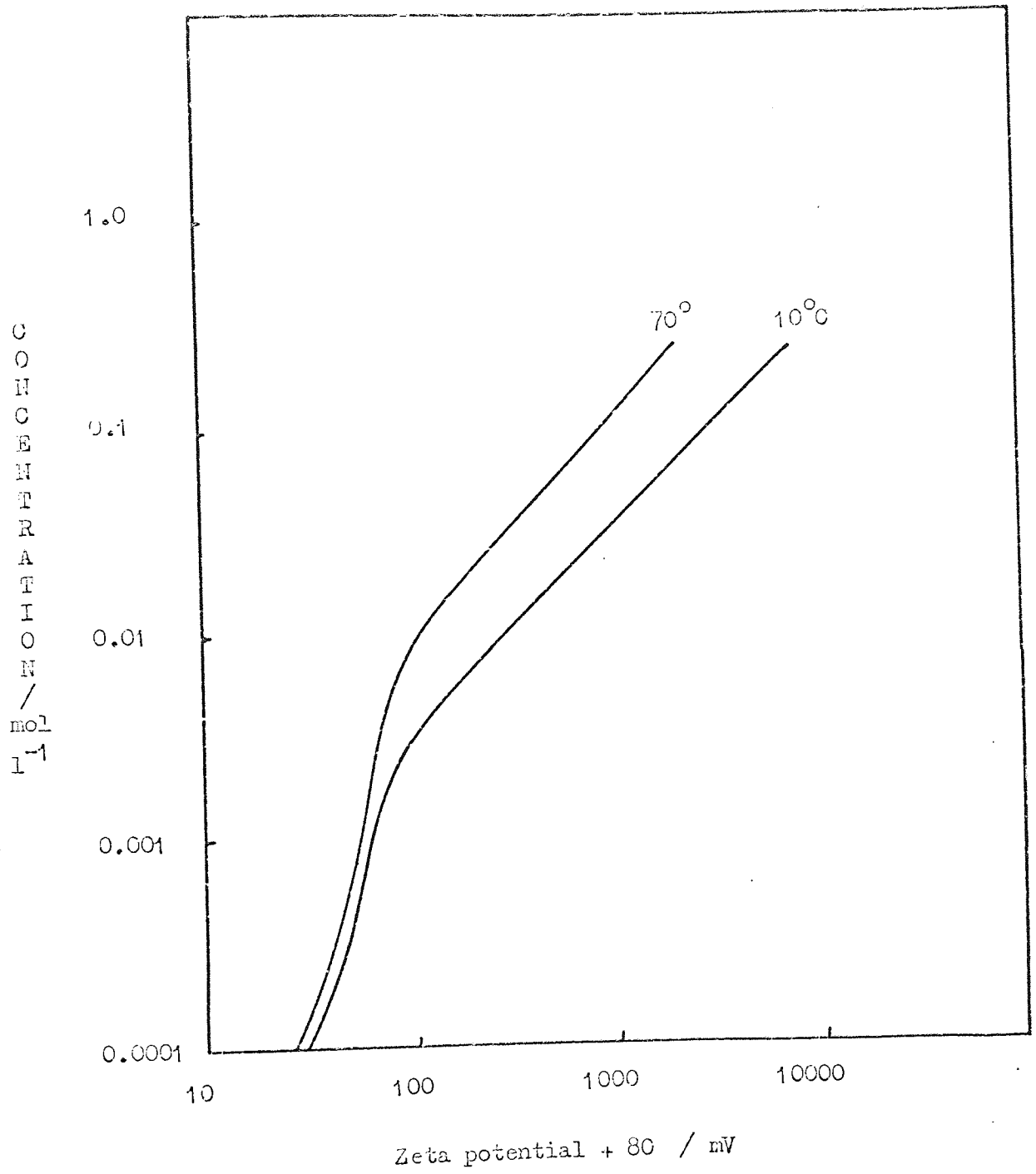

Fig. 4.2. Change of zeta potential with concentration and with temperature: silicon carbide in copper sulphate/sulphuric acid solutions, from streaming current measurements.

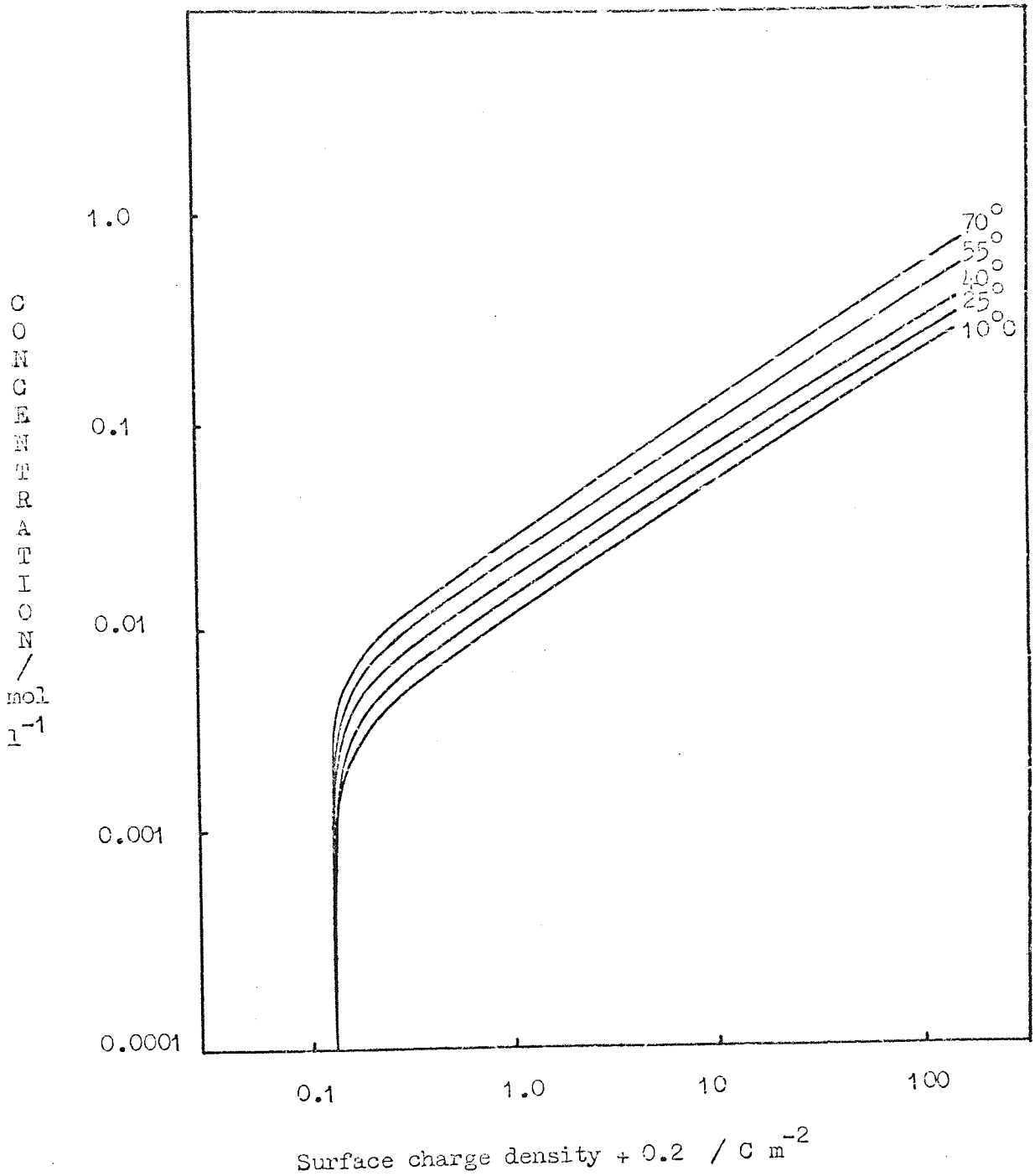

Fig. 4.3. Change of surface charge density with concentration and with temperature: silicon carbide in copper sulphate/sulphuric acid solutions, from streaming potential measurements.

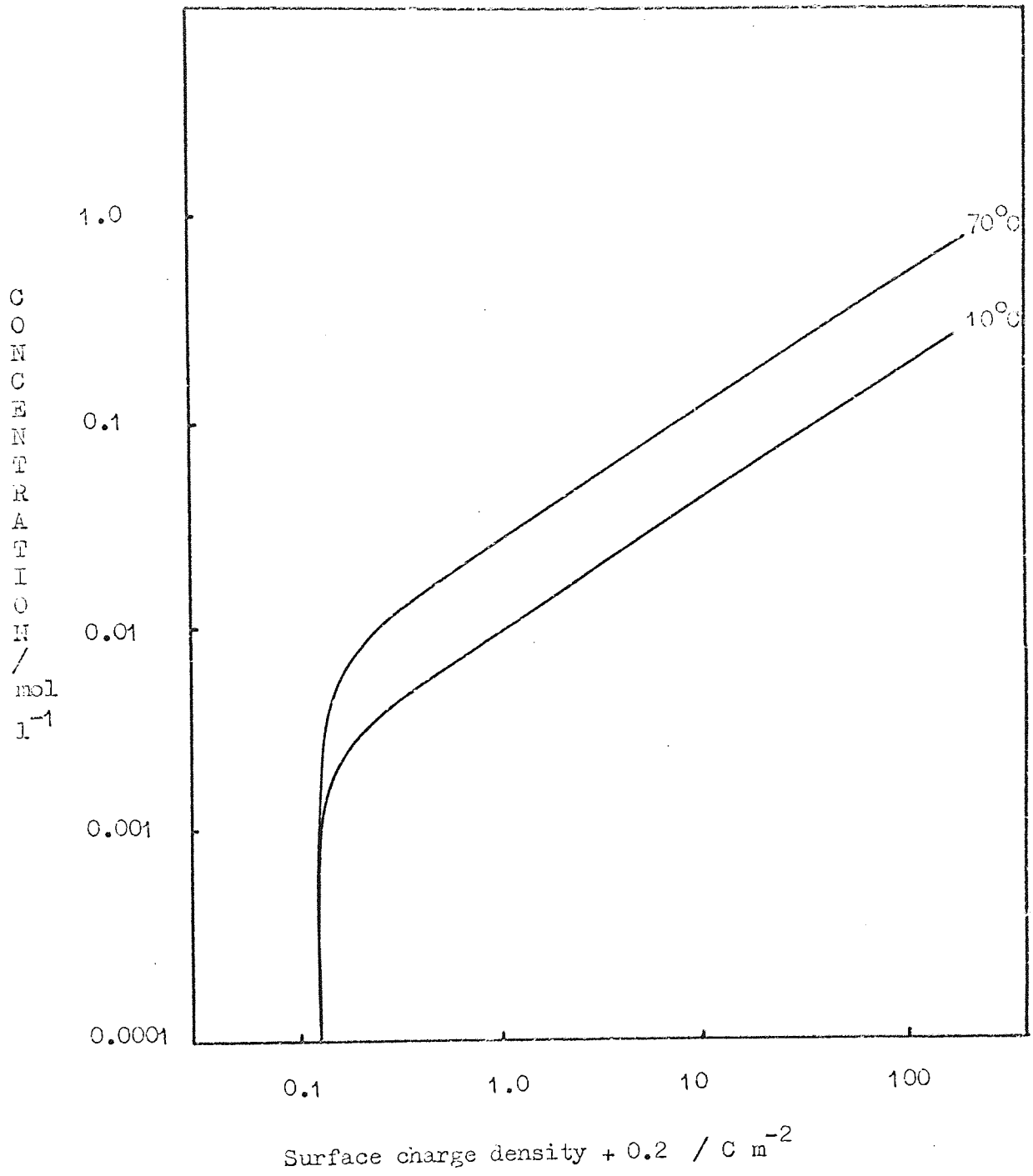

Fig. 4.4. Change of surface charge density with concentration and with temperature: silicon carbide in copper sulphate/sulphuric acid solutions, from streaming current measurements.

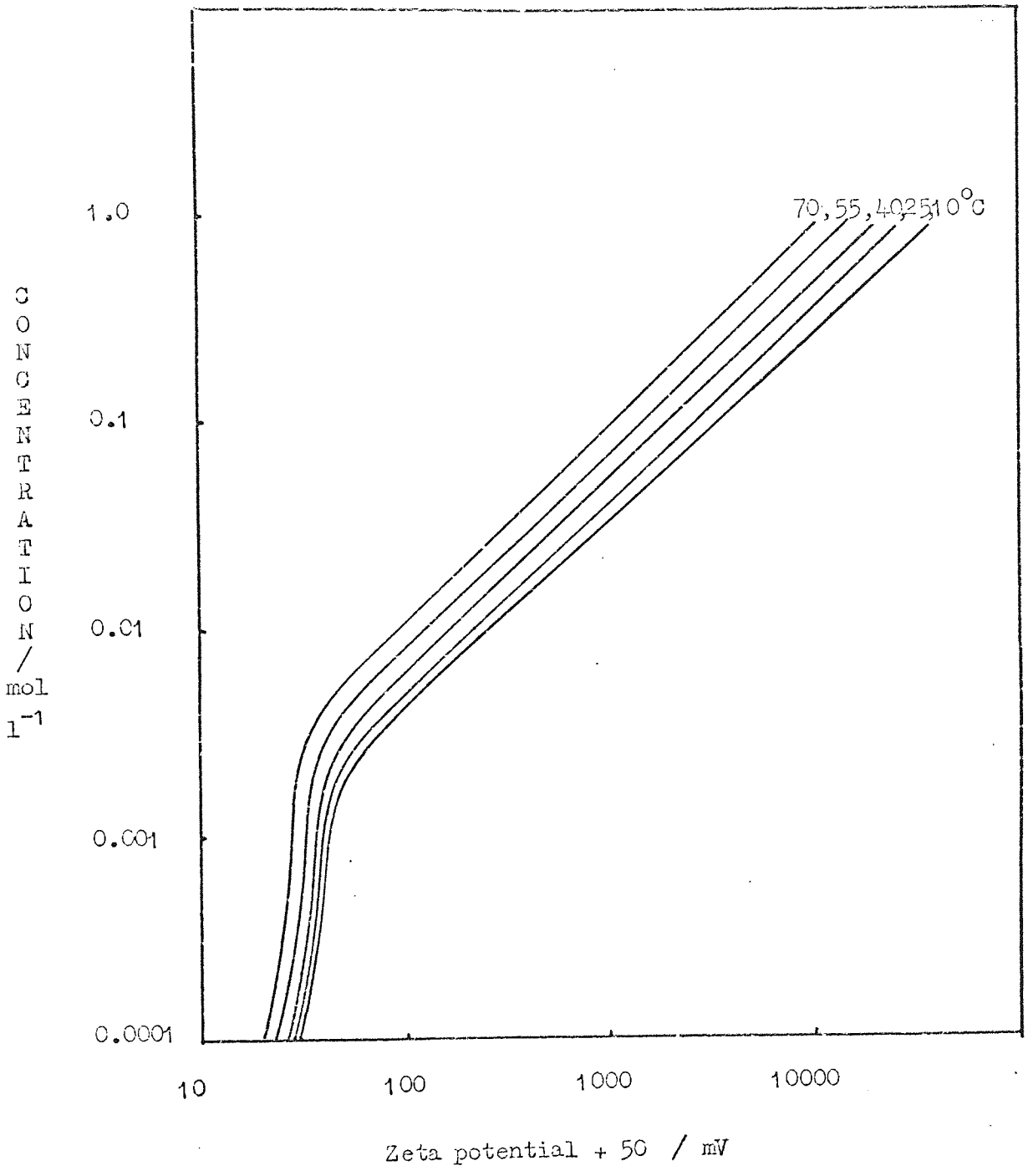

Fig. 4.5. Change of zeta potential with concentration and with temperature: quartz in copper sulphate/sulphuric acid solutions, from streaming potential measurements.

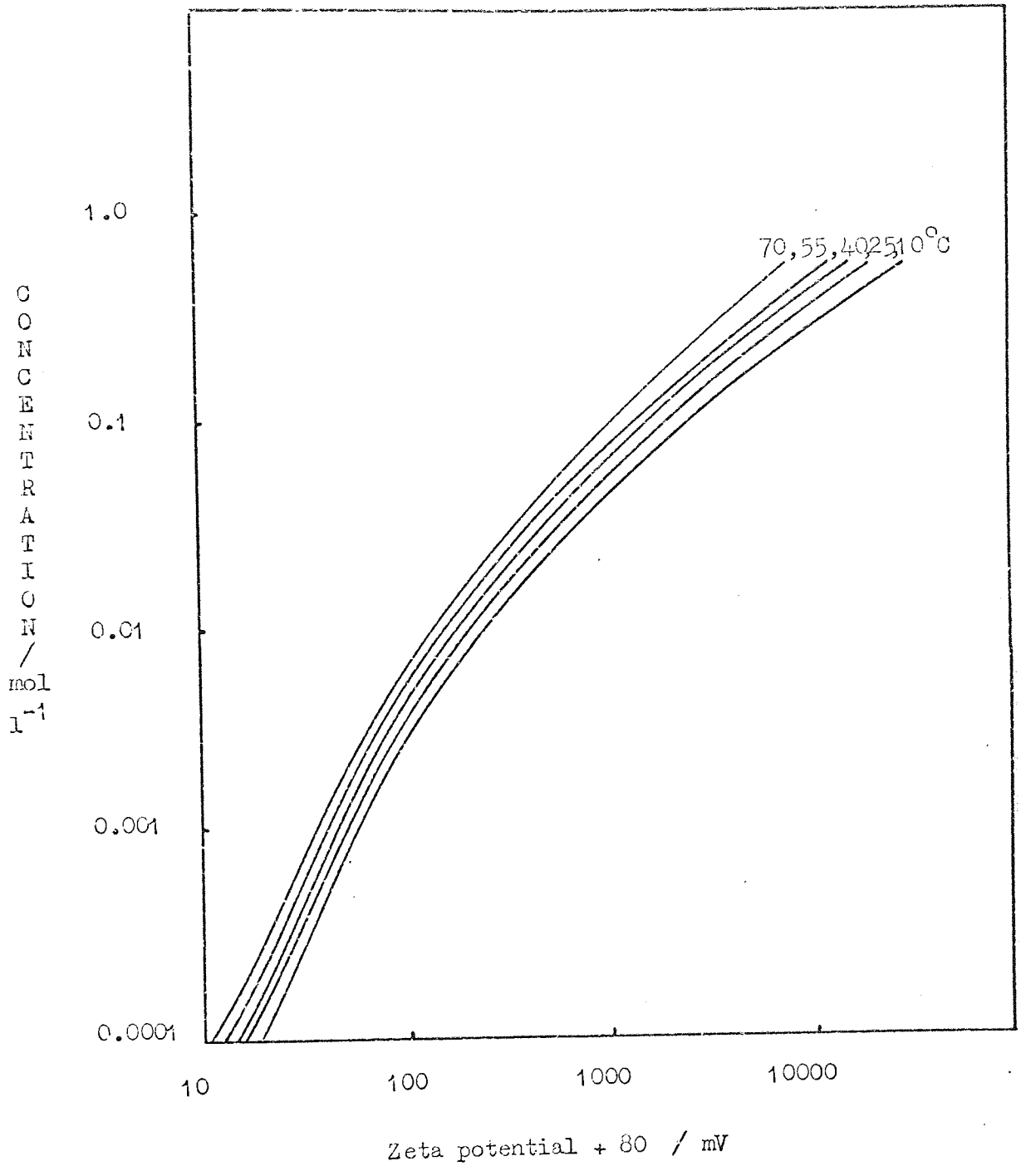

Fig. 4.6. Change of zeta potential with concentration and with temperature: quartz in copper sulphate/sulphuric acid solutions, from streaming current measurements.

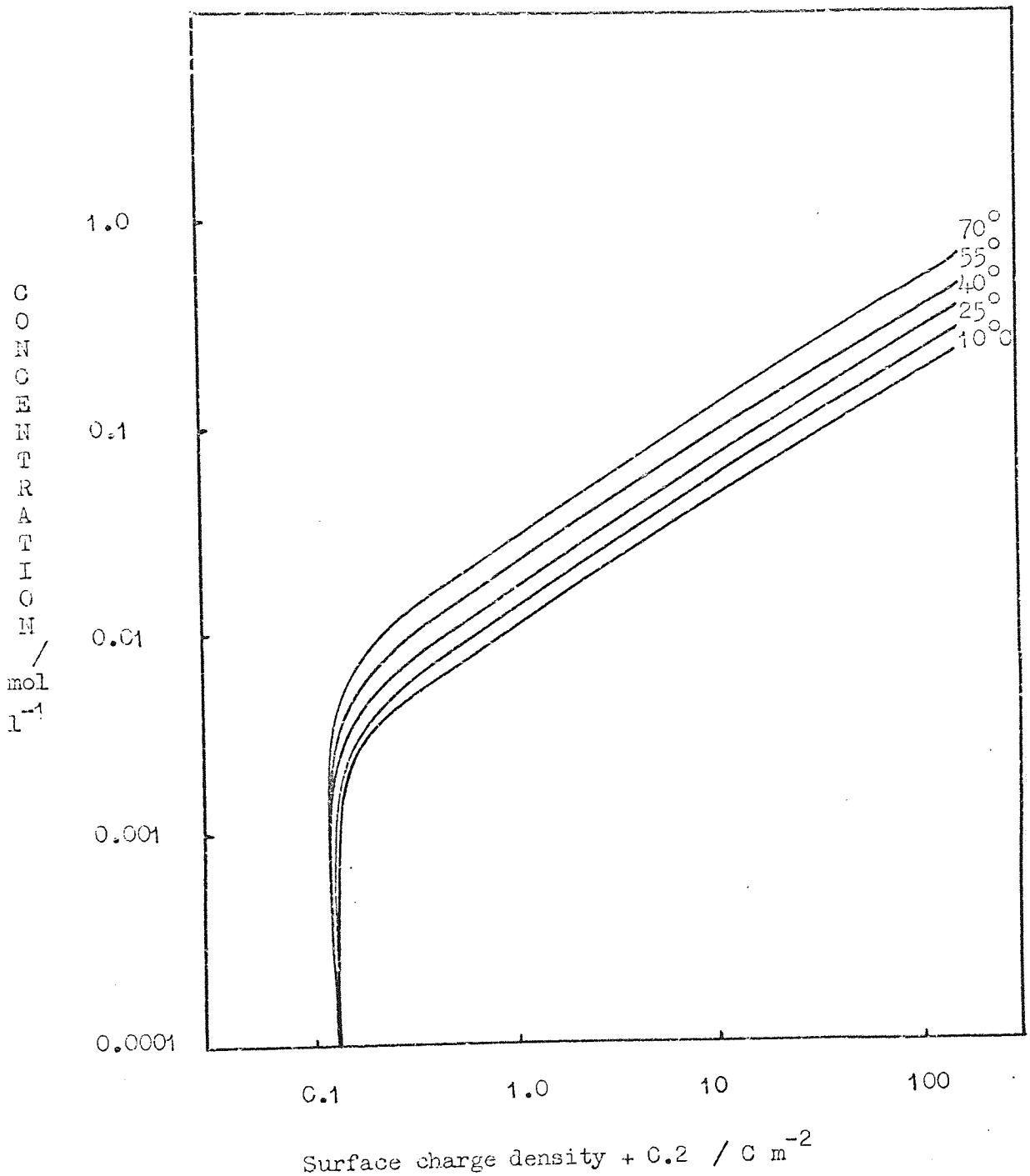

Fig. 4.7. Change of surface charge density with concentration and with temperature: quartz in copper sulphate/sulphuric acid solutions, from streaming potential measurements.

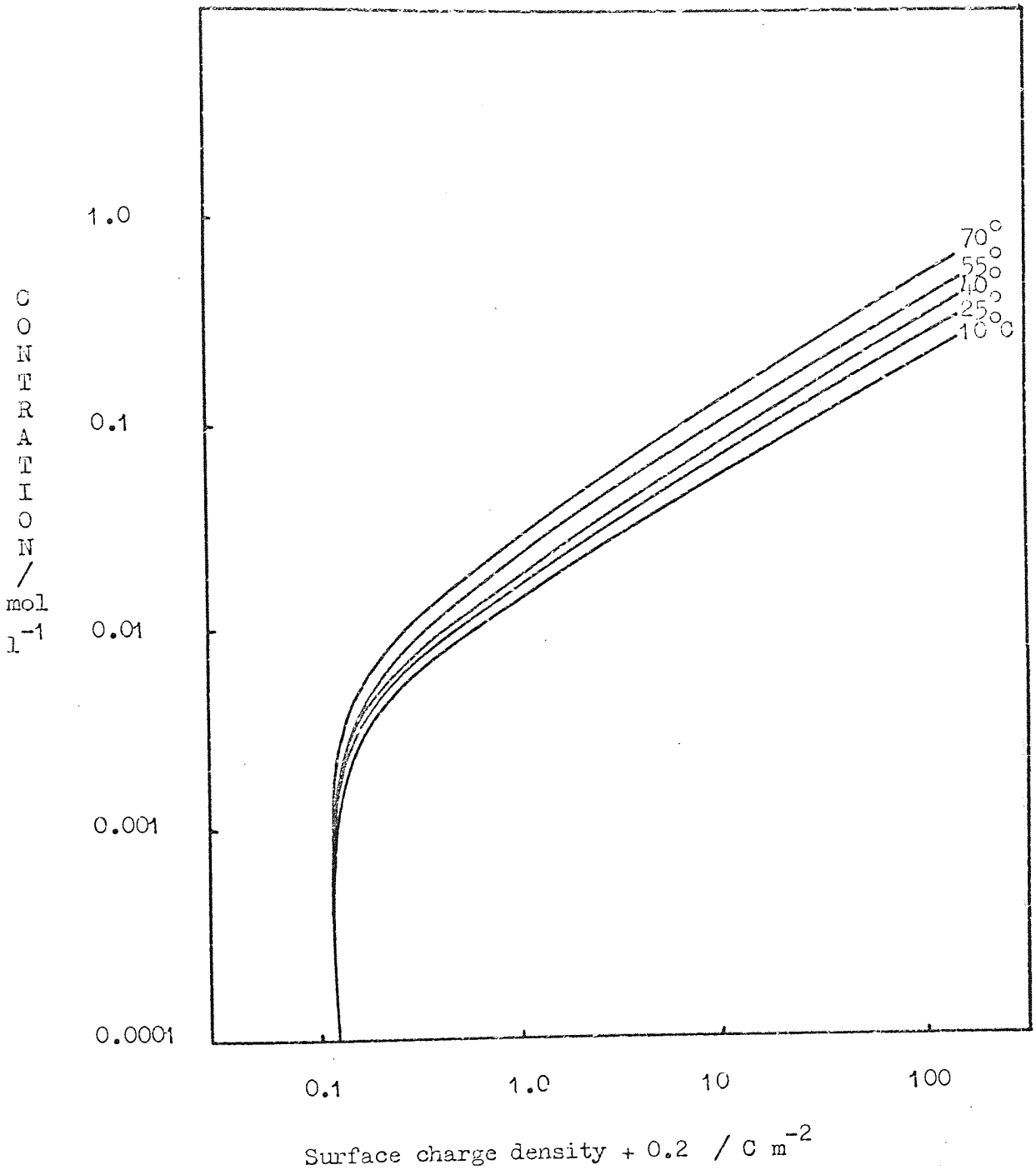

Fig. 4.8. Change of surface charge density with concentration and with temperature: quartz in copper sulphate/sulphuric acid solutions, from streaming current measurements.

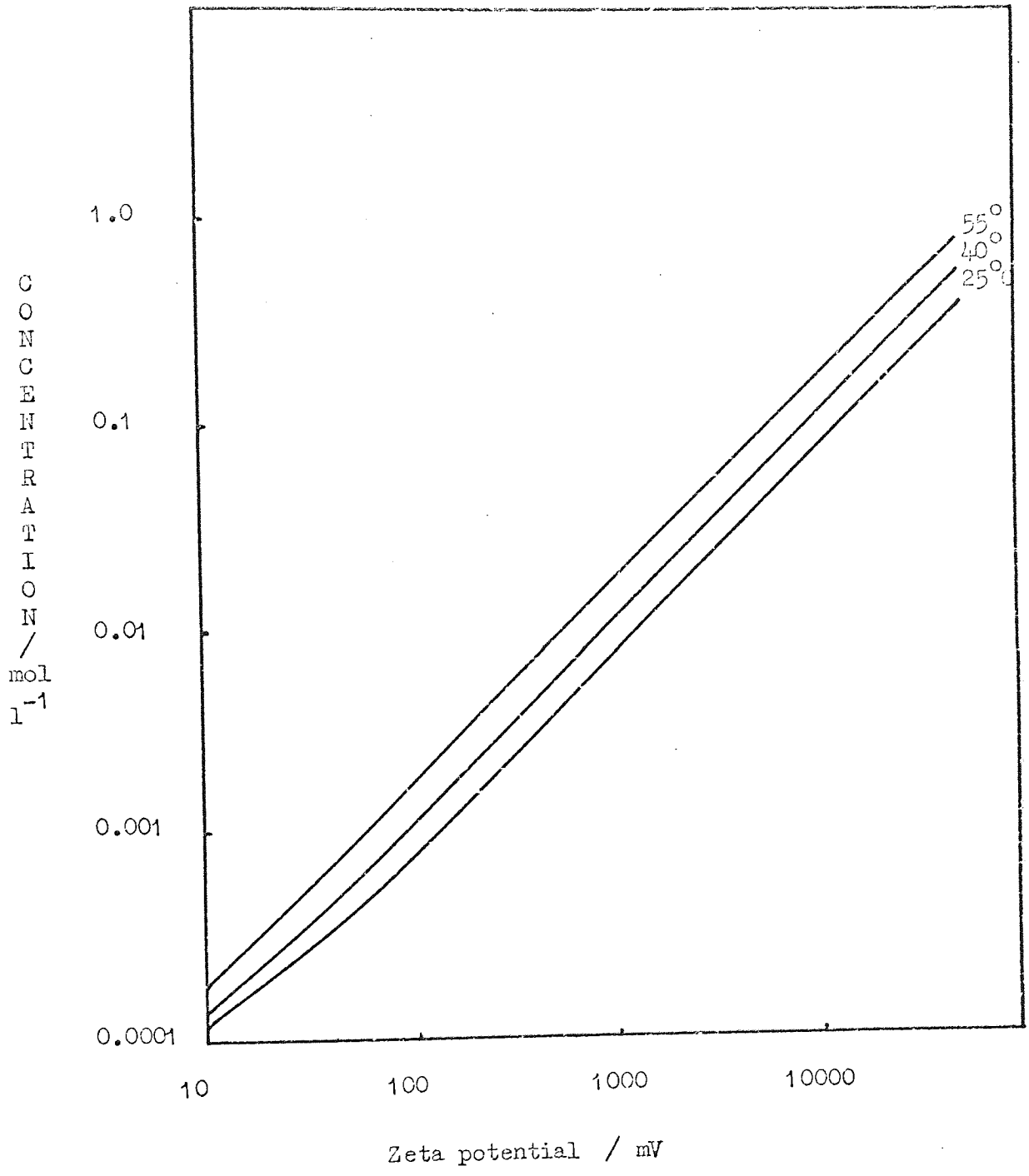

Fig. 4.9. Change of zeta potential with concentration and with temperature: chromium diboride in copper sulphate/sulphuric acid solutions, from streaming potential measurements.

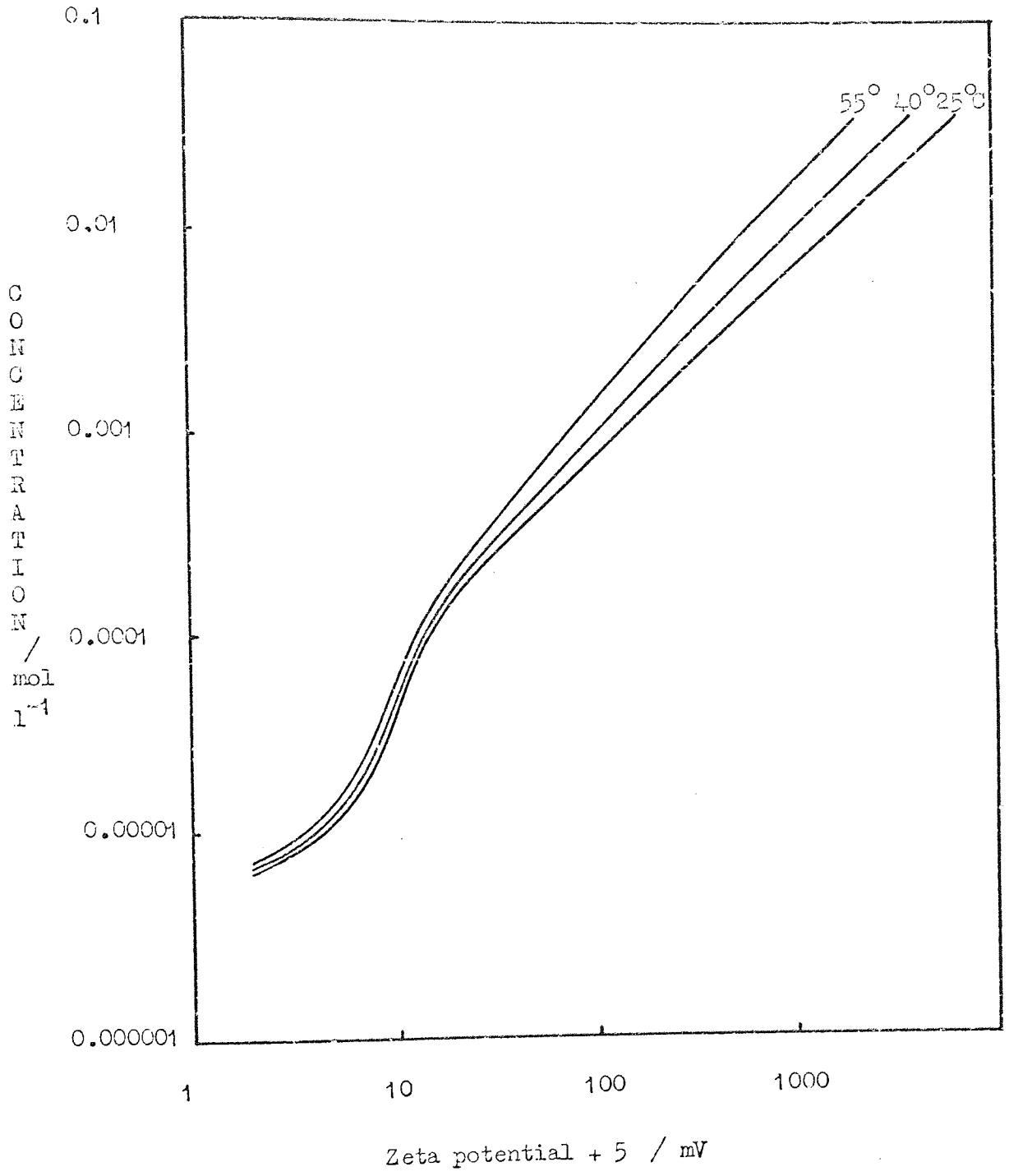

Fig. 4.10. Change of zeta potential with concentration and with temperature: chromium diboride in copper sulphate/sulphuric acid solutions, from streaming potential measurements and bulk conductivity measurements.

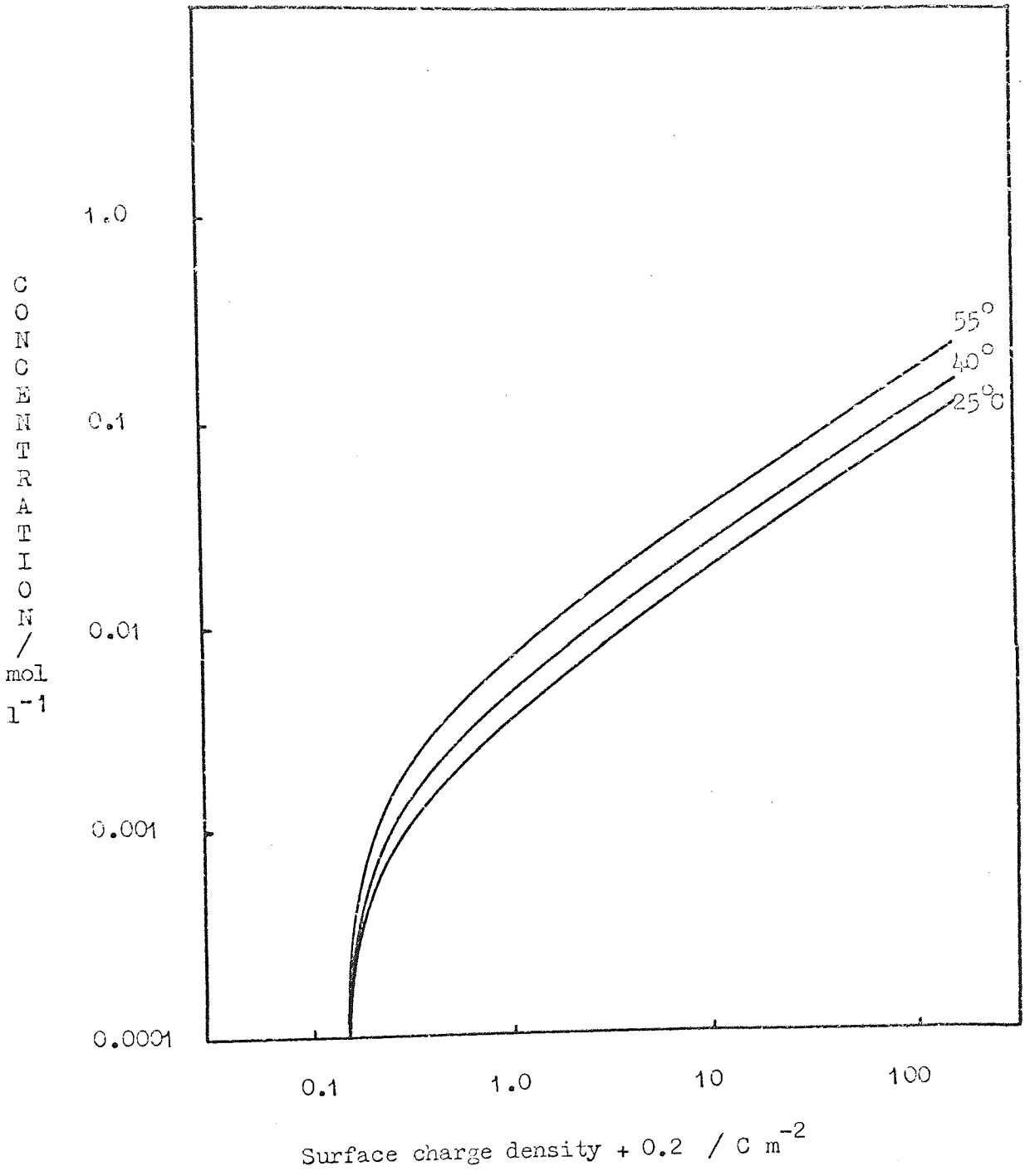

Fig. 4.11. Change of surface charge density with concentration and with temperature: chromium diboride in copper sulphate/sulphuric acid solutions, from streaming potential measurements.

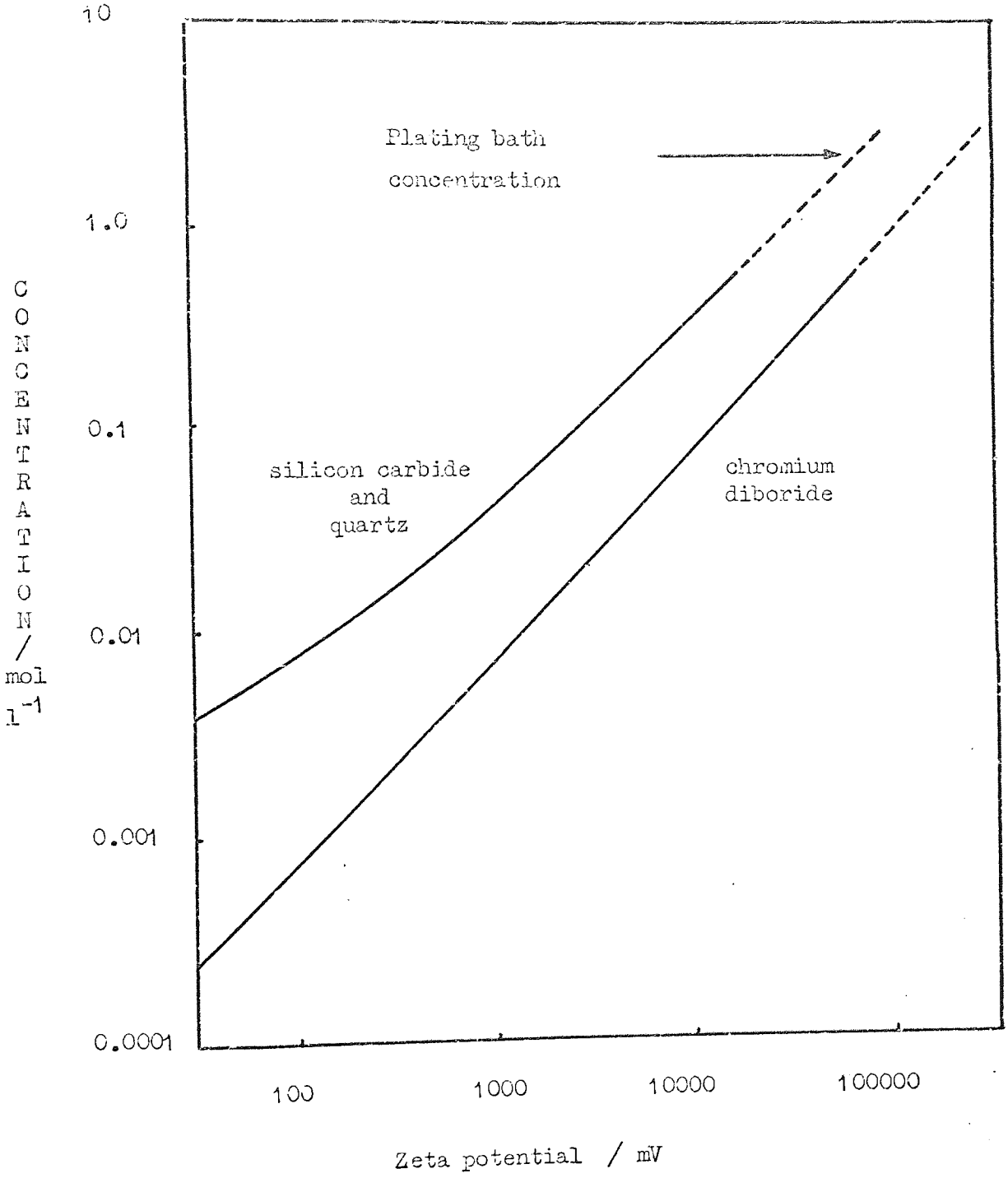

Fig. 4.12. Change of zeta potential with concentration at 25°C for silicon carbide, quartz and chromium diboride, extrapolated to plating bath concentration of 2 mol l^{-1}.

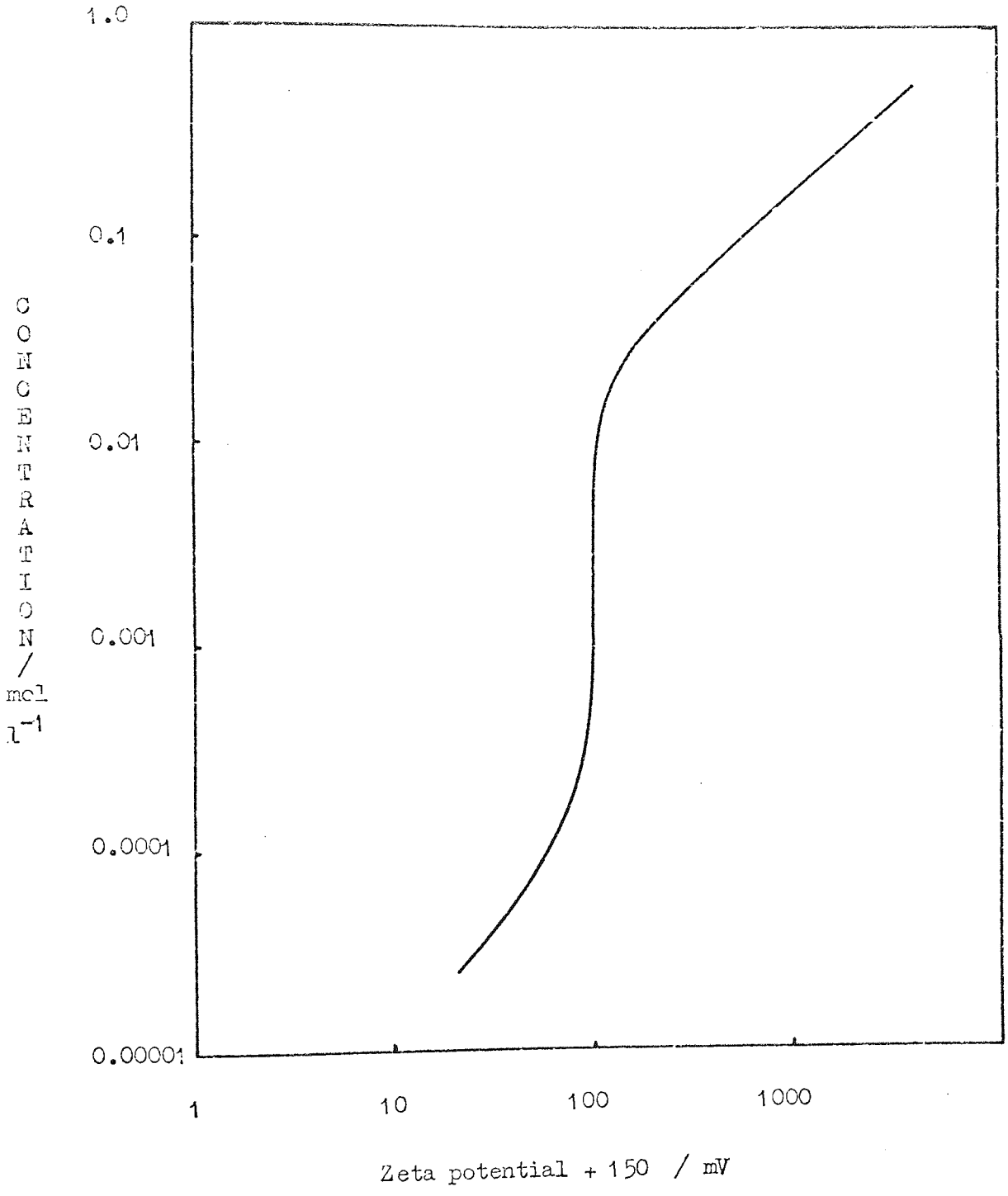

Fig. 4.13. Change of zeta potential with concentration at 25°C for quartz in potassium hydroxide solutions, from streaming potential measurements.

Results obtained with diaphragms Q1 and Q2 all fit this graph.

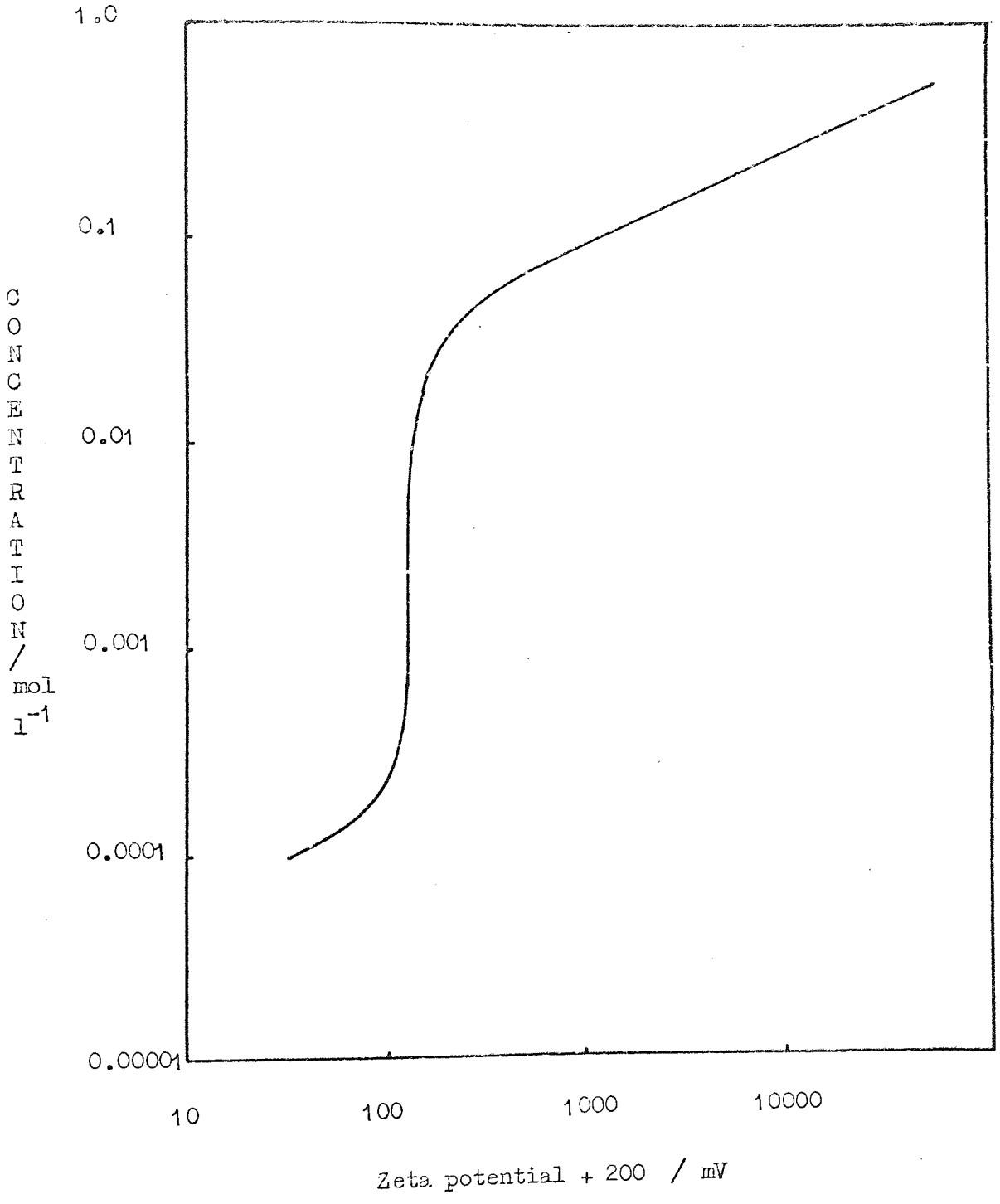

Fig. 4.14. Change of zeta potential with concentration at 25°C for silicon carbide in potassium hydroxide solutions, from streaming potential measurements.

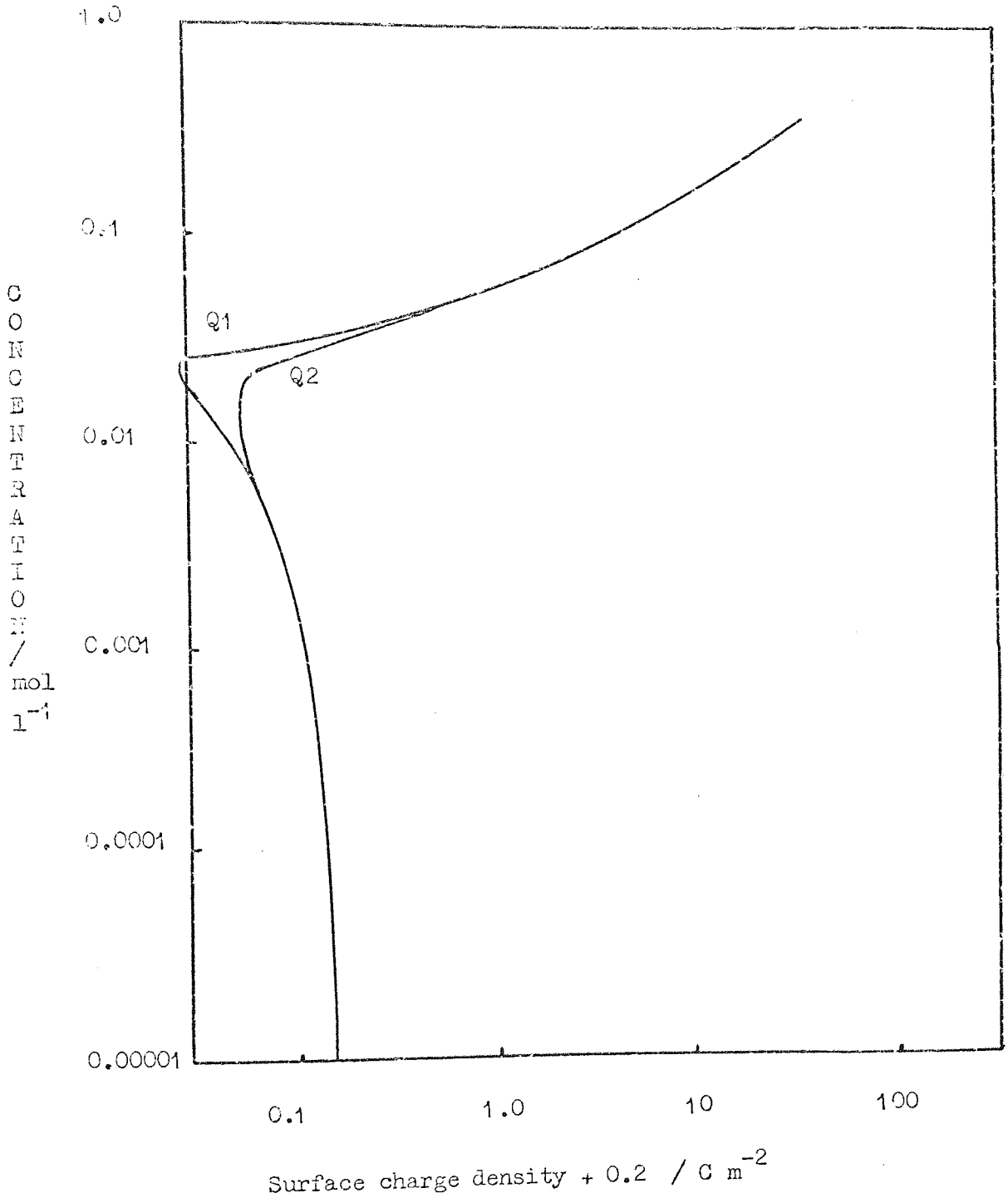

Fig. 4.15. Change of surface charge density with concentration at 25°C for quartz in potassium hydroxide solutions, from streaming potential measurements.
(Data from diaphragms Q1 and Q2.)

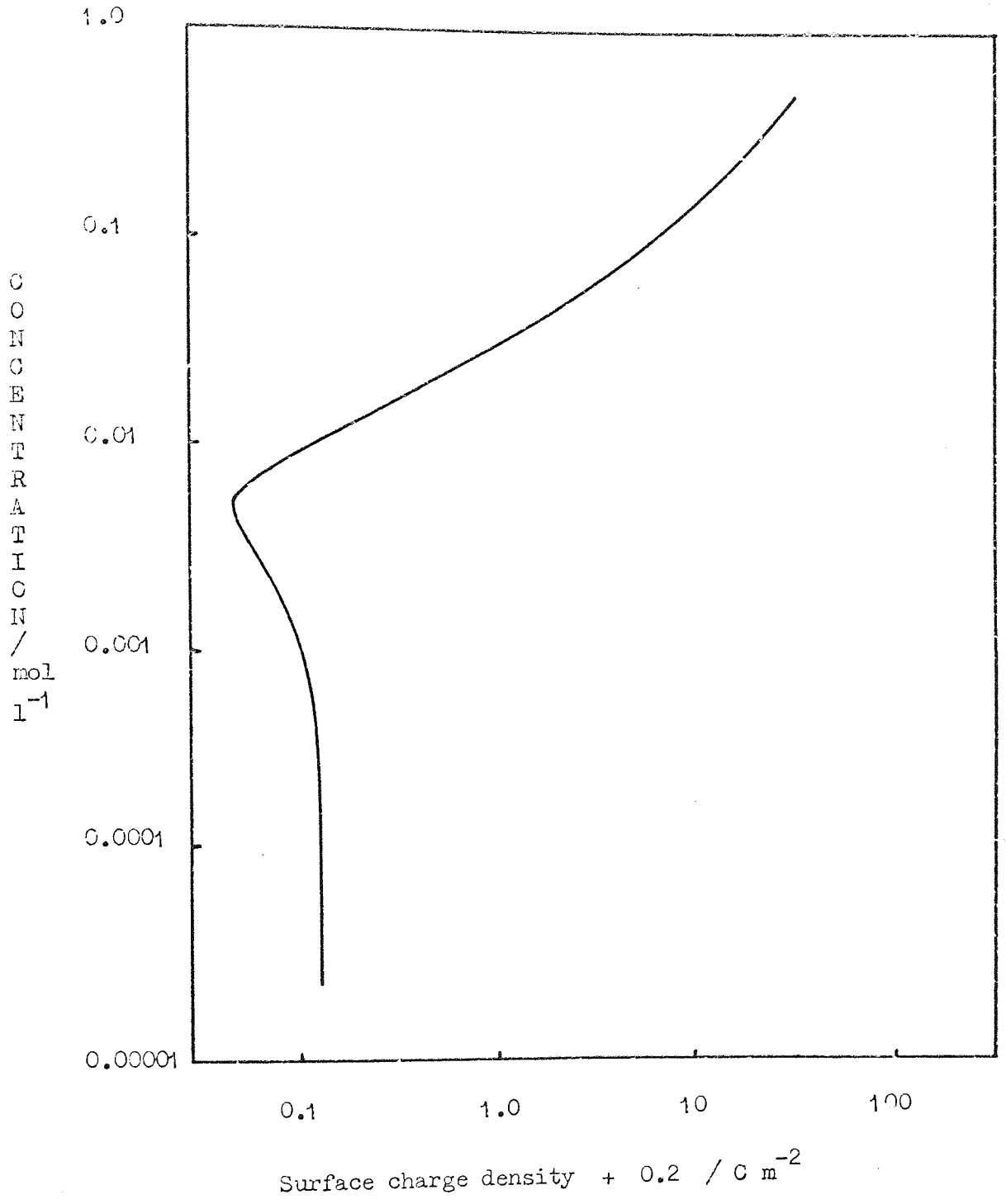

Fig. 4.16. Change of surface charge density with concentration at 25°C for silicon carbide in potassium hydroxide solutions, from streaming potential measurements.

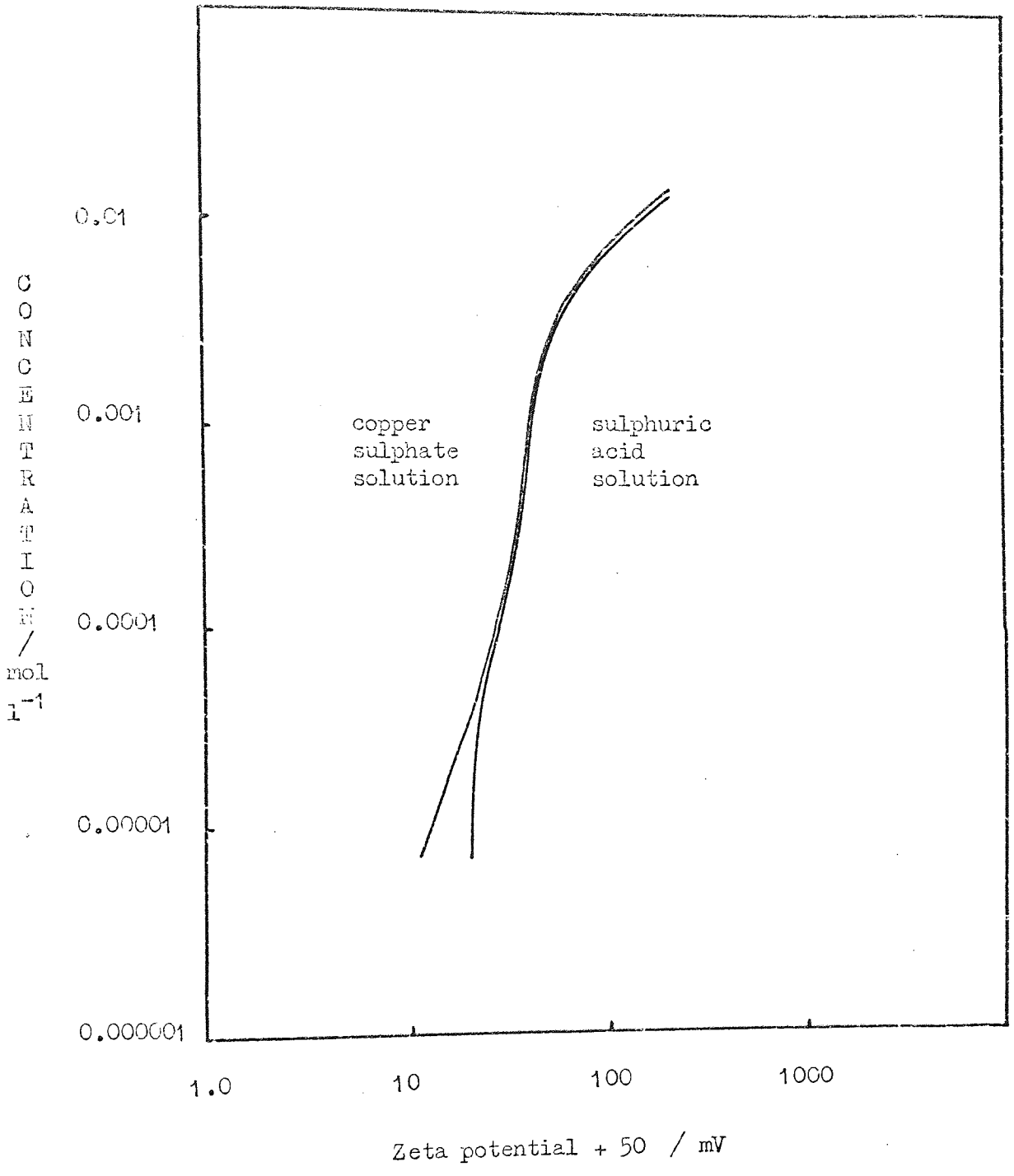

Fig. 4.17. Change of zeta potential with concentration at 25°C for silicon carbide in copper sulphate and in sulphuric acid solutions, from streaming potential measurements and bulk conductivity measurements.

CHAPTER 5. DISCUSSION OF RESULTS OF STREAMING

5.1 The effect of concentration.

Results obtained from streaming potential and streaming current measurements were very similar and showed that at concentrations below that required for charge reversal zeta potential and surface charge density increase less rapidly than concentration for all systems studied. In the absence of contact adsorption of ions onto the ceramic this is the result which would be expected as the diffuse, Gouy, layer of charge will contract with increasing concentration; more of the solution-side ions being concentrated into the outer Helmholtz plane (OHP). If this was the sole mechanism for variation of zeta potential and surface charge density with concentration then both would tend to zero as concentration increased.

Another mechanism which could have an effect on the change of charge with concentration is the contact adsorption of ions on the ceramic. If cations were adsorbed this would directly increase the positive charge on the ceramic. That such adsorption can occur has been demonstrated by Fuerstenau and Modi:[43] these workers showed that the reversal of sign of zeta potential was a sufficient criterion for contact adsorption on the Stern-Grahame model. That such adsorption can occur could be inferred from the results of another group of workers[44] who were able to alter the charge on alumina particles by addition of large monovalent ions such as Tl^+. Certainly readiness of adsorption of gases is increased if the pressure is increased[45] and an increased tendency for contact adsorption of cations as the ionic concentration is increased is not unexpected. There is considerable evidence that this does occur and furthermore that the logarithm of the amount adsorbed varies with the logarithm of the concentration of the electrolyte,[46,47,48,49]

i.e. $\frac{d \log x}{d \log C} = k$, where x is the amount adsorbed, C is the electrolyte concentration and k is a constant, for a "wide range" of electrolytes on glass and on suspended oil droplets. This log/log dependence is the same as was found in the present work, at concentrations above that for charge reversal, and gives support to the hypothesis that contact adsorption of ions is taking place at the surface of the ceramic. If contact adsorption does occur the effect of an increase in concentration of electrolyte will be twofold: not only will the Gouy layer contract but, as positive ion contact adsorbs on the ceramic the number of positive ions in the Gouy layer will be correspondingly reduced. Continued contact adsorption of cations will lead eventually to electrical neutrality between the particle and the solution, the Gouy layer disappearing. Any further contact adsorption of cations would increase the positive charge on the ceramic, giving a net positive charge, the solution-side Stern and Gouy regions being populated by negative ions. Ultimately it would be expected that the charge on the particle would no longer increase with increasing concentration but would become constant as available sites for ion adsorption all became occupied and the double layer thickness reached a minimum value, the distance from the surface of the solid to the OHP.

5.2. The effect of temperature.

Increase in temperature led to a decrease in the (positive) value of the zeta potential and of the surface charge density on the ceramic particle at all electrolyte concentrations for all of the systems studied.

According to Langmuir's theory of adsorption for both gaseous and condensed systems an increase in temperature will lead to a decrease in adsorption.[45] Assuming that this theory may be applied to aqueous electrolyte systems such are used in this work it would be expected that temperature increase would cause reduction

in the number of ions contact adsorbed on the ceramic surface. If cations were contact adsorbed the following effects would be expected upon raising the temperature of the system. Below the concentration for polarity reversal a smaller number of adsorbed positive ions would mean a greater net negative charge, double layer thickness being constant with temperature.[40] Above the concentration for charge reversal a reduction in adsorption would lead to a decrease in the magnitude of net positive charge. This postulate of contact adsorption of ions is supported by results obtained from the adsorption of alkali metal ions on silver iodide. It was shown that at room temperature the alkali metal ions are physically, rather than chemically, adsorbed on the surface of the silver iodide. As the temperature was raised a gradual desorption of ions took place, resulting in a marked decrease in the surface charge density on the solid.[36]

From the variation in surface charge density with temperature found in the present work it was possible to calculate the heat of adsorption of ions from solution, as is shown in the next section.

9.3. The effect of temperature on the adsorption energy of ions from solution.

The surfaces of some materials are inert in the sense that the valency requirements of their atoms are satisfied by bonding with adjacent atoms. On such surfaces adsorption tends to take place simply through forces of physical attraction. This kind of adsorption is called physical or van der Waals adsorption and is very similar in nature to the condensation of a vapour on the surface of its own liquid. Many surfaces, such as metals, are much more unsaturated and the valency requirements of their surface atoms can be considered as incompletely satisfied by bonding with adjacent atoms. In adsorption such a surface will tend to form chemical bonds with a nearby phase and this process is known as chemisorption.

The difference between chemical and physical adsorption is that electron transfer occurs between adsorbent and adsorbate in chemisorption but not in physical adsorption.

There is no single criterion which allows distinction to be made experimentally between the two types of adsorption in every case. Nevertheless there are few cases where it is uncertain which kind of adsorption is occurring. The best single criterion is the heat of adsorption. As chemical bonds are normally stronger than physical forces of attraction heats of chemisorption are generally large and heats of physical adsorption small. In fact although large heats always indicate chemisorption there may be uncertainty about the nature of a weak adsorption.[50] An example of this is the adsorption of hydrogen: chemisorption generally gave values of approximately 65 $kJmol^{-1}$,[51] although values of 12 $kJmol^{-1}$ [52,53] have been observed, whereas heats of physical adsorption were always less than about 8.5 $kJmol^{-1}$.[54] Similarly for carbon monoxide the heat of chemisorption is about 84 $kJmol^{-1}$ [55] whereas that for physical adsorption is always less than about 25 $kJmol^{-1}$.[56] Another criterion is the temperature at which the adsorption proceeds. Physical adsorption only tends to occur at temperatures near or below the boiling point of the adsorbate whereas chemisorption usually takes place at temperatures well above the boiling point. As chemisorption involves chemical reaction it may require appreciable activiation energy. Because of this it may only proceed at a reasonable rate above a certain temperature. Physical adsorption requires no activation energy and should occur as fast as adsorbate reaches the surface. Chemisorption will cease when the adsorbate can no longer make direct contact with the surface; it is therefore a single layer process. This is not the case with physical adsorption and under suitable conditions of temperature and pressure multilayers can be formed. As it involves chemical bond formation chemisorption possesses a certain specificity which

physical adsorption does not.

The results obtained from the streaming measurements have shown that the positive charge on the ceramic materials studied was reduced with increase in temperature in every case. This suggested that the adsorption of (positive) ions was reduced with increase of temperature. Using the values of surface charge density obtained at the various temperatures it was possible to calculate the heat of adsorption of cations from solutions of different concentration.

The heat of adsorption may be determined using an expression of the form

$q = A \exp \frac{-\Delta H}{RT}$ where q is the surface charge density, ΔH is the heat of adsorption, R is the gas constant, T the absolute temperature and A a constant.[57]

Hence $\ln q = \ln A - \frac{\Delta H}{RT}$ and

$$2.303 \log_{10} q = 2.303 \log_{10} A - \frac{\Delta H}{RT}$$

The heat of adsorption, ΔH, can be found from a graph of $\log_{10} q$ against $\frac{1}{T}$, the slope of which is

$$- \frac{\Delta H}{2.303\ R}$$

This was done for both silicon carbide and quartz. Solution concentrations of 0.01, 0.1 and 0.3 molar were chosen and for each concentration the value of q was obtained from the concentration vs. q graphs, figs 4.3 and 4.7, for each temperature used i.e. 10°, 25°, 40°, 55° and 70°C. The graphs of $\log_{10} q$ vs $\frac{1}{T}$ are shown in figs 5.3.1. and 5.3.2. For both silicon carbide and quartz acceptable straight lines could be drawn through the calculated points, particularly for the higher concentrations.

5.3.1. Calculation of ΔH (adsorption) on silicon carbide.

Within $\pm 5\%$ error the slopes of the $\log_{10} q$ vs $\frac{1}{T}$ graphs were the same at 1.1×10^{3}. Hence the heat of adsorption is given by

$$\frac{\Delta H}{2.303\ R} = -1.1 \times 10^{3}$$

$$\Delta H = -2.303 \times 8.314 \times 1.1$$

$$\Delta H = -21.1\ kJmol^{-1}$$

5.3.2. Calculation of ΔH (adsorption) on quartz.

All $\log_{10}\eta$ vs $\frac{1}{T}$ graphs gave the same slope of 1.17×10^{3}. Hence the heat of adsorption is

$$\Delta H = -2.303 \times 8.314 \times 1.17$$

$$\Delta H = -22.3\ kJmol^{-1}$$

The results for ΔH (adsorption) were therefore -21.1 and -22.3 $kJmol^{-1}$ on silicon carbide and quartz respectively irrespective of the concentration of the electrolyte at concentrations greater than 0.01M. The similarity between the results for the two ceramics suggested that the adsorption mechanism on each was the same. The value of approximately -22 $kJmol^{-1}$ indicated that the adsorption of ions by the ceramics from these solutions at concentrations greater than 0.01 molar was most likely to be physical in nature.

During the streaming experiments it was observed that if after an electrolyte of high concentration had been streamed it was replaced by water or a dilute solution the streaming potential (or current) immediately reverted to the magnitude and sign which had been obtained prior to the use of the concentrated solution. If adsorption had been chemical in nature this rapid desorption of ions would not have been expected. This observation therefore supports the conclusions, drawn from the heat of adsorption data, that the adsorption occurring on the ceramic is physical rather than chemical.

This model of the processes occurring with temperature change on the surface of the ceramic, i.e. adsorption and desorption of positive ions giving a change in zeta potential and surface charge density with temperature change, agrees very well with the observed changes for the systems studied.

x	⊙	+
0.01	0.1	0.3M
4.4	6.3	6.95
4.3	6.2	6.85
4.2	6.1	6.75
4.1	6.0	6.65
4.0	5.9	6.55
3.9	5.8	6.45
3.8	5.7	6.35
3.7	5.6	6.25
3.6	5.5	6.15
3.5	5.4	6.05
3.4	5.3	5.95

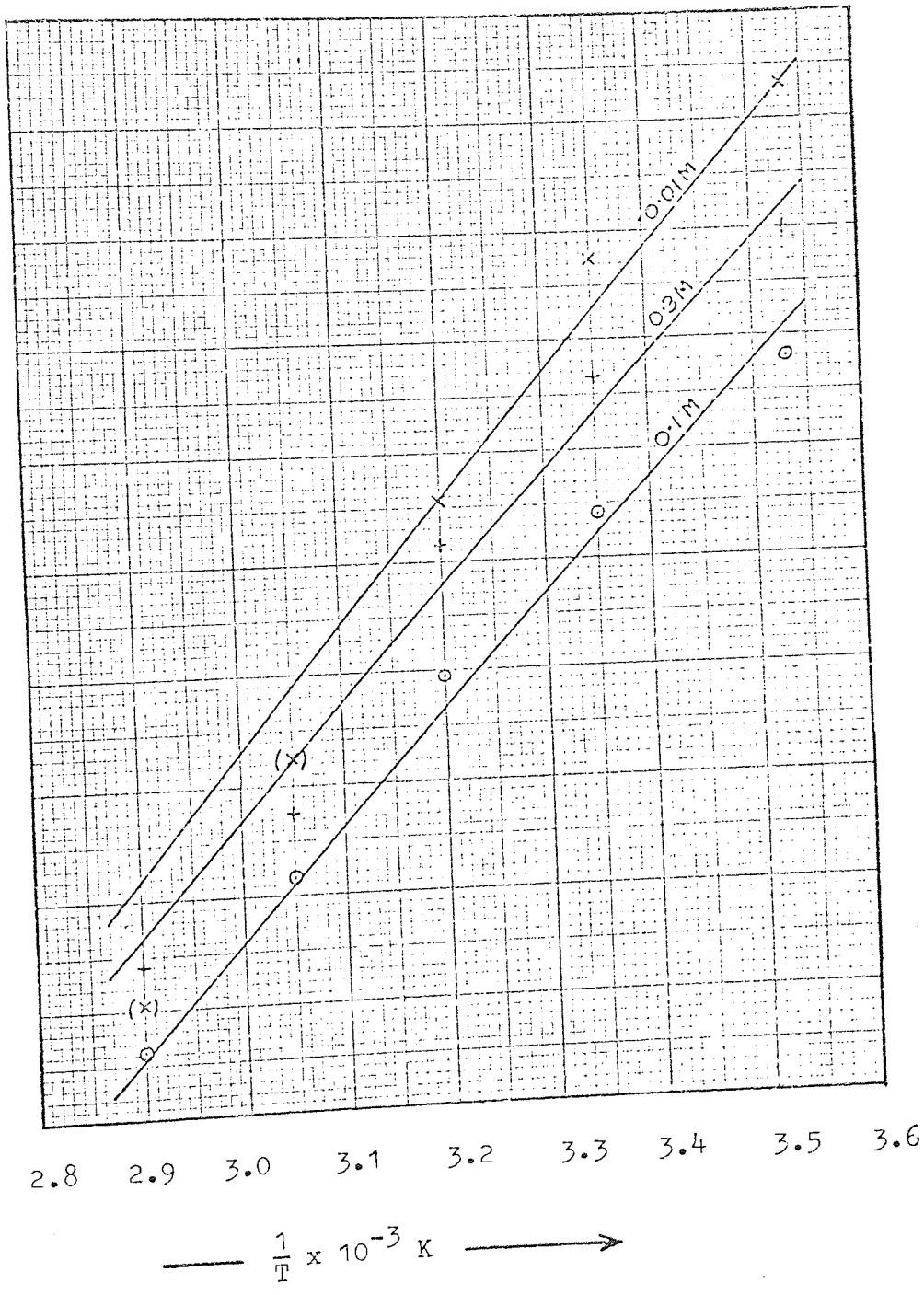

$\log_{10} q$

$\frac{1}{T} \times 10^{-3}$ K

Fig. 5.3.1. Change of $\log_{10}$ of surface charge density with reciprocal temperature for silicon carbide.

x	⊙	+
0.01	0.1	0.3M
4.45	6.3	7.0
4.35	6.2	6.9
4.25	6.1	6.8
4.15	6.0	6.7
4.05	5.9	6.6
3.95	5.8	6.5
3.85	5.7	6.4
3.75	5.6	6.3
3.65	5.5	6.2
3.55	5.4	6.1
3.45	5.3	6.0

$\log_{10} q$

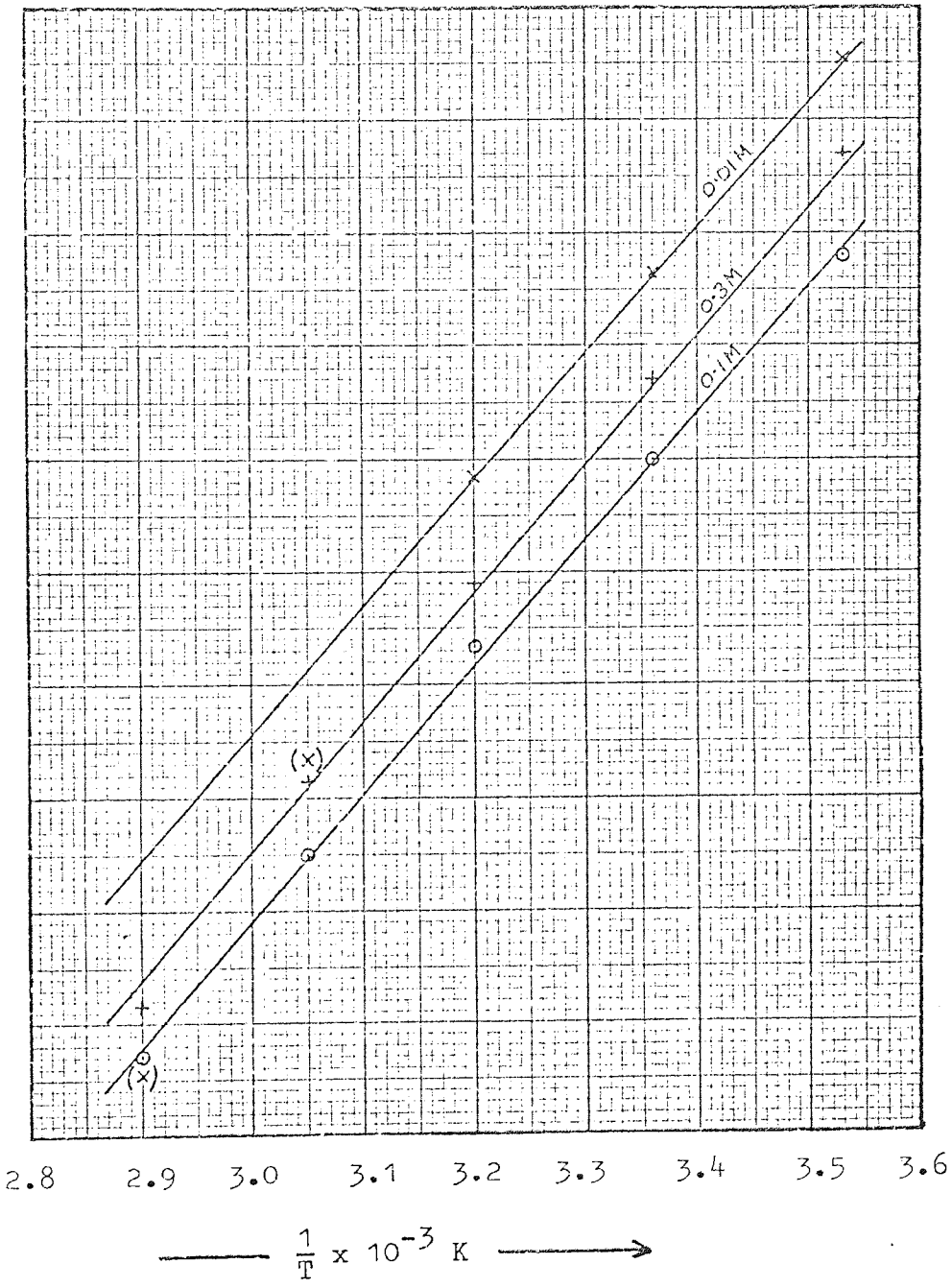

Fig. 5.3.2. Change of $\log_{10}$ of surface charge density with reciprocal temperature for quartz.

5.4. Comparison of the results obtained using acidic and alkaline solutions.

The results obtained were very similar, as can be seen from a comparison of figs 4.1-11 and 4.13-16., and this further confirms that changes in charge on a particle are determined largely by total ionic strength effects rather than effects due to the presence of specific ions unless those ions were particularly readily adsorbed. The greatest difference between the results obtained on silicon carbide and quartz for acidic and alkaline solutions was the difference in the concentration required to effect reversal of the sign of the charge. The great difference between the concentration of acid or salt solution required for charge reversal and that of alkali was not unexpected. It is readily explicable in terms of the silicic acid groups in the glass surface. These groups will ionise further in alkali but less in acid; the effect of such a reaction when working in alkaline solutions is that the charge on the glass will become more negative than it would be in neutral and much more so than in acid solution of equivalent concentration.[35] A larger number of cations must therefore be contact adsorbed on the glass surface before its negative charge is equalled in alkaline solution than would be necessary in acidic solution; the concentration of alkali required in order to give the condition of zero charge will thus be greater than the concentration of acid required. The same will apply to quartz as to glass surfaces and similarly to silicon carbide if surface reaction with the alkali is assumed.

CHAPTER 6. ELECTRODEPOSITION MECHANISM AT CATHODE SURFACE

The first step in the electrodeposition process is that in which an ion crosses the electrified interface, i.e. the charge-transfer reaction.

A metal electrode is a three-dimensional lattice consisting of ions held together by an electron gas; each ion in the lattice has associated electrons and can be regarded as a neutral atom, which is unhydrated. Ions in solution are both charged and hydrated. Consider a hydrated univalent metal ion at the outer Helmholtz plane. Before this ion can become part of a metal lattice it must gain an electron and shed its hydration sheath. Deposition of an ion thus consists of electronation, dehydration and finally incorporation into the lattice.

When an ion receives an electron two alternative subsequent steps are possible. The first is that when the neutralised ion lands on the metal surface it transfers this electron to the free-electron gas, becoming part of the metallic lattice and uncharged. However in this process the ion would have to shed all of its hydration sheath immediately and in one stage; calculations which assume the direct formation of charge-free surface atoms give values of the energy of activation so much higher than experimental figures that such formation is improbable.[58] The second alternative, thus favoured, is that when electrons have reached the ion the particles which are formed on the electrode surface are not of zero charge or completely dehydrated but are partially charged partially hydrated adsorbed ions, "adions".

6.1 Stepwise dehydration of an ion.

The surface of an electrode contains a variety of different types of site, all of which are presented to an ion crossing the interface; it will be considered initially as a single crystal

uninterrupted by grain boundaries. The surface will probably not be a perfect plane but will exhibit step sites, kink sites, edge vacancies and hole vacancies, fig. 6.1.1-4.

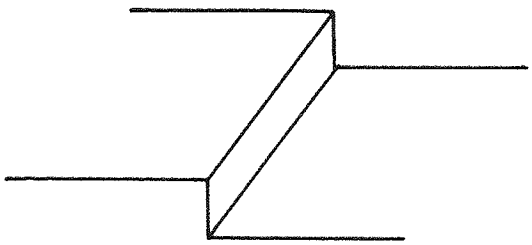

Fig. 6.1.1 Step site on a crystal-lattice plane.

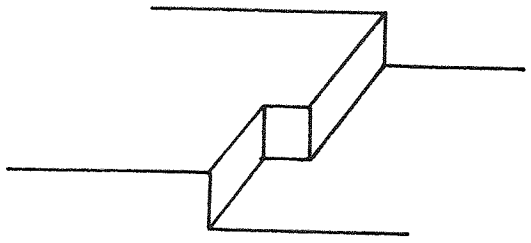

Fig. 6.1.2 Kink site on a crystal lattice plane.

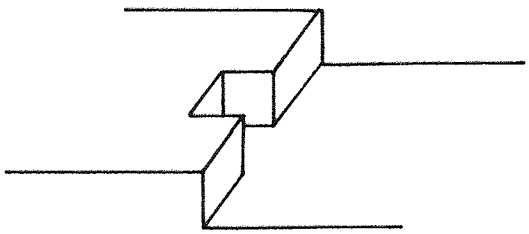

Fig. 6.1.3. Edge vacancy on a crystal-lattice plane.

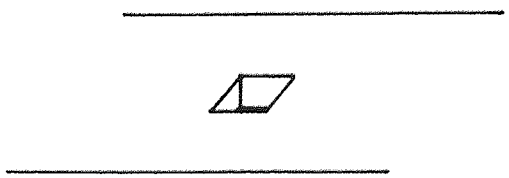

Fig. 6.1.4 Hole vacancy on a crystal-lattice plane.

When the electron transfer reaction takes place with the metal ion at the interface the ion is most likely to transfer onto a plane site. Such a move requires the minimum distortion in the ion-water complex and hence the minimum energy change from this source. Also there are a great many more plane sites than other sites. If an adion is in contact with a metal plane it will be partly in

contact with the metal atoms of the plane but can still accommodate water molecules in the remaining space around it. When on a plane the adion is associated with the largest possible number of water molecules and this number will decrease progressively as the adion moves from plane to step, kink, edge and finally hole. The adion loses a water molecule and gains a metal atom neighbour with each move until, in one of these steps, it is finally incorporated in the lattice. The deposition can thus be seen as a two-step reaction consisting of a charge transfer step followed by a rate determining surface diffision step.[59,60,61,62] It has recently been suggested, however, that in the electrodeposition of silver the contribution of surface diffusion is only about one third of that of direct transfer of ions from solution to step sites on a close packed plane.[63]

6.2. Nucleation and growth of electrodeposits.

The surfaces of perfect crystals may be classified as either close-packed (low index) surfaces or vicinal (high index) surfaces. A high index plane is always stepped on an atomic scale whereas a low index plane is generally considered as smooth. These steps on the high index surfaces are segments of close-packed planes and will always have a high concentration of kink sites.[64,65]

In a metal the atoms are arranged in a three dimensional close packed structure. The characteristic arrangements of atoms can be seen as planes in the crystal and if they are exposed in the surface they will be crystal faces. The atomic arrangement varies with the plane, as illustrated in fig. 6.2.1.: the planes shown (a), (b) and (c) have Miller indexes (111), (100) and (110) respectively.

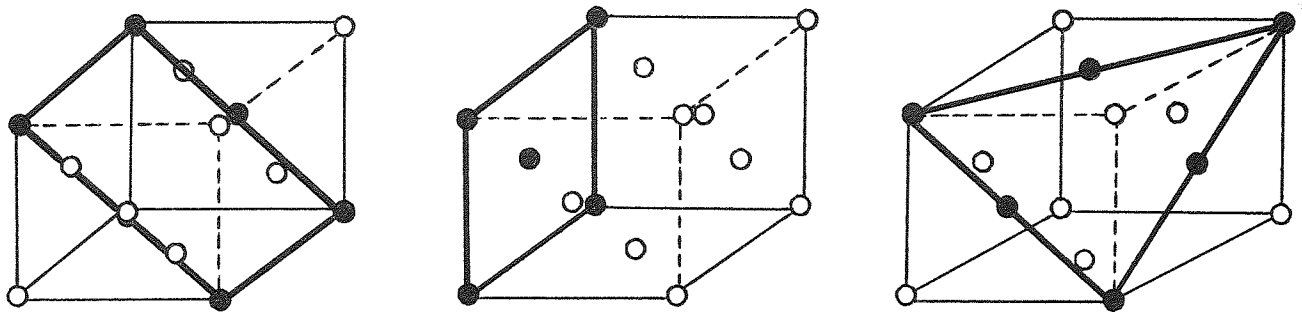

(a) (b) (c)

Fig 6.2.1. Variation of atomic arrangement with the direction of the plane chosen in a cubic lattice.

Each crystal face will contain all the microfeatures necessary for deposition to occur and deposition will occur on all of the faces. The rate of electrogrowth is different on different faces, [66] for copper deposition onto single crystals the rate of deposition increases in the order (111)<(100)<(110), similarly at low current density (~1 Adm^{-2}) the deposition overpotential increases (110)< (100)<(111). There are a number of explanations for the different rates of electrogrowth on different crystal faces. The energies of two-dimensional nucleation on different faces has been suggested [67] but this is not applicable to low current densities as nucleation is unlikely to be involved. [66] The most probable explanation is concerned with adion bonding energy on the various crystal planes. The number of underlying metal atoms which are in contact with an adion depends on the particular crystal plane: an adion on the (111), (100) and (110) planes would have 3, 4 and 5 nearest lattice atom neighbours respectively to which it will be bonded. The situation is similar to that in surface adion diffusion from one lattice site to another with successive gain in the number of nearest neighbours and increase in the strength of bonding.

When ions are transferred to a vicinal surface as adions the ions will first diffuse to a step and then along the step to a kink site. This diffusion occurs readily.[68] Assuming that the adion can be incorporated at a kink in the step the step will advance by addition of atoms at these sites until it disappears at the edge of the electrode, fig 6.2.2.

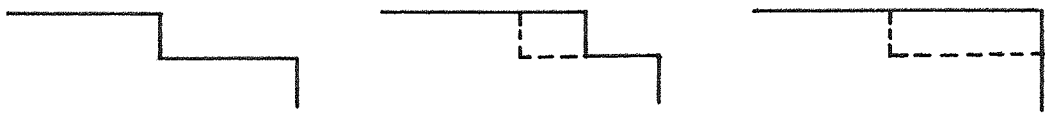

(a) (b) (c)

Fig 6.2.2. Stages in the advance of a step during electrogrowth.

The existence of steps is necessary for electrogrowth. Without steps the adion concentration on a plane will build up, the proportion of the surface covered by adions will increase and, as electronation of ions requires a bare surface, it will be more difficult for the charge-transfer reaction to occur and ultimately deposition will stop. This does not happen for two reasons. The first is that crystals are rarely perfect, the majority of crystals grown from a melt will grow with defects and imperfections in their atonic arrangements. The second is that at fairly high overpotentials, where concentration overpotential is comparable with activation overpotential, activation control is largely lost and two-dimensional nucleation can occur. This process requires current densities and hence deposition rates higher than are normally used. The presence of imperfections in the crystals is therefore important, the defects giving the property of self-perpetuating steps.

Such a defect is a "screw dislocation". A model of this would appear as if a perfect crystal had been cut partially through and the part on one side of the cut pushed up or down by one atomic distance relative to the other side as shown in fig 6.2.3.

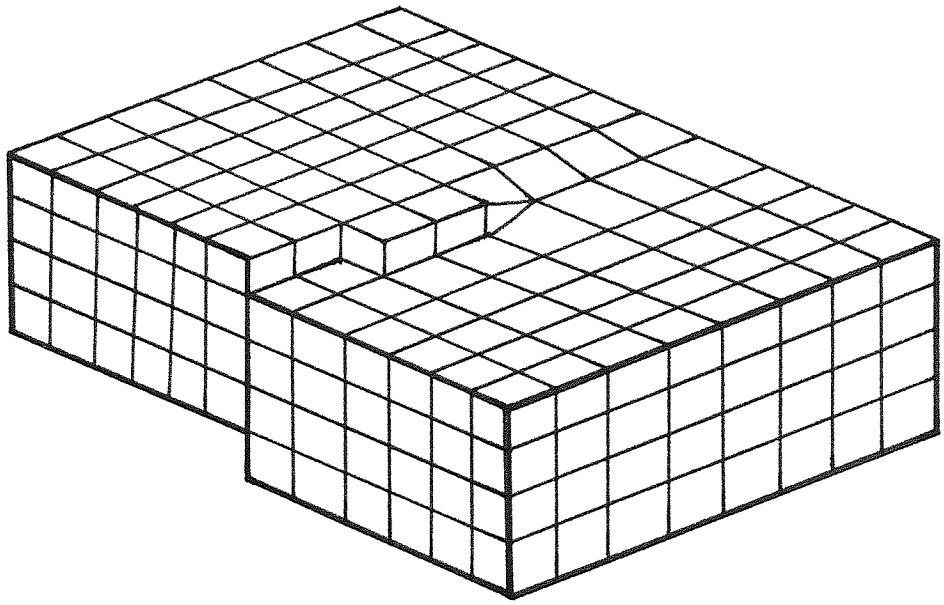

Fig 6.2.3. Model of a screw dislocation, showing a kink site in the growth edge.

The mismatch of the atomic layers has made a step emerge on the surface and adions will add to the step from its origin to the edge. The result is that the position of the origin will be unchanged but the step will advance to an angle from its initial position. However many rows of adions are added to the surface the step will remain: all that happens is that its orientation changes as shown in Fig 6.2.4.

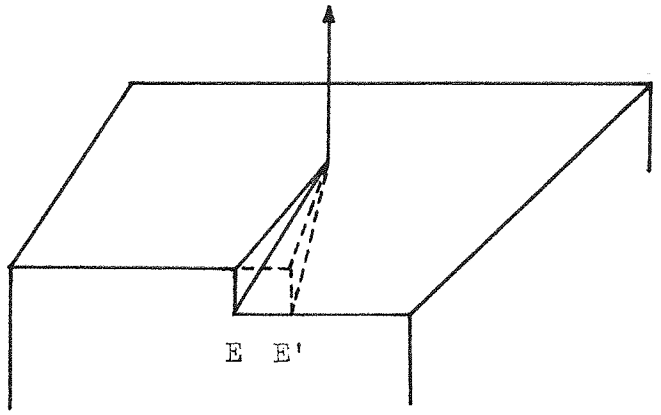

Fig 6.2.4. Initial stage in the addition of adions to a screw dislocation.

When the orientation has changed by one complete revolution the crystal will have added on one complete layer of atoms in its upward growth. If adions do not add on in complete rows all along the step from the screw axis another step will be formed, fig 6.2.5.

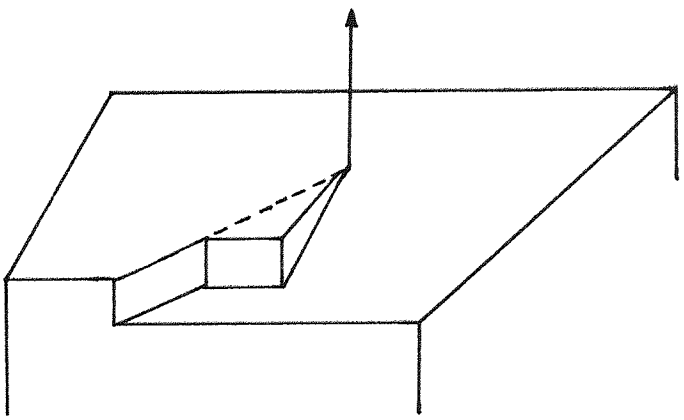

Fig 6.2.5. Formation of a second step in the growth face of a screw dislocation.

This step also can advance and if this process continues the growth obtained will look in plan like a spiral and in elevation like a terraced hilltop, fig 6.2.6. It is called microspiral growth.

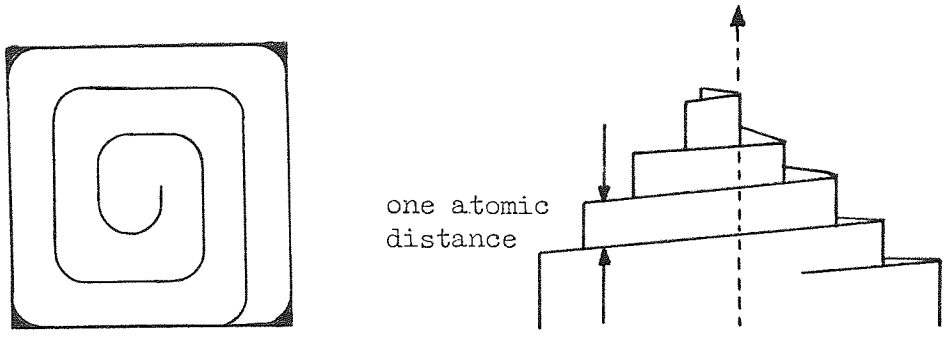

(a) (b)

Fig 6.2.6. Plan and elevation of microspiral growth.

These steps are microsteps, one atomic layer in height. Steps can sometimes be seen in the optical microscope and these must have a height of several hundred nm; they are known as macrosteps and numerous reasons have been suggested for their formation. [69-74]

On a high-index surface such as is shown in fig 6.2.7. the surface is made up of a series of low-index facets and the monatomic steps advance across these planes. A bunching process will occur as each successive step reaches the edge of the layer on which it is growing.

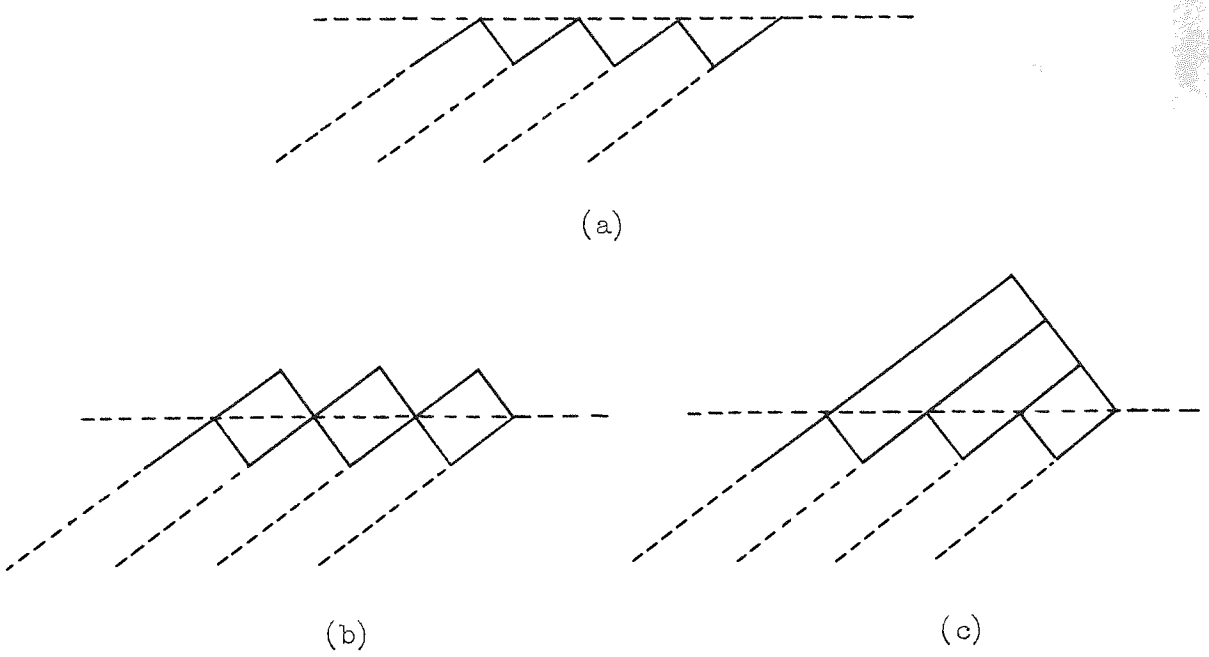

Fig. 6.2.7. Bunching of steps leading to macrostep formation on a high index plane.

On a less ideal surface microstep bunching depends on the fact that the rate of advance of a microstep is affected by the proximity of other microsteps following it and also by the presence of low concentrations of impurities which can adsorb at a step (where the free energy of adsorption is probably greater than on a plane) and either slow down or stop the advance of the step: in either case the rate of advance of the step will be less than that of the step following it. If an advancing microstep in a layer of atoms A is stopped then the layer B growing on top of it will continue advancing until reaching the point at which A was blocked. It will then stop as it has reached the edge of the crystal. If this process is continued as in fig. 6.2.8. the microsteps bunch into a macrostep.

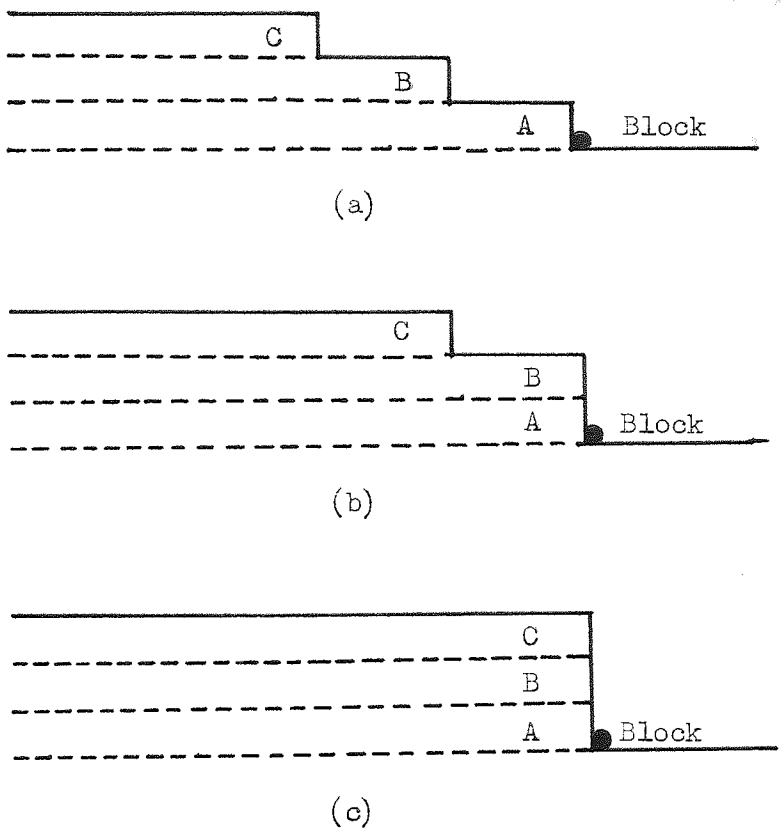

Fig 6.2.8. Successive stages in the formation of a macrostep by microstep bunching.

As deposition rates are different onto different crystal faces fast growing faces tend to grow out of existence while slow growing faces survive. This is shown in fig 6.2.9.

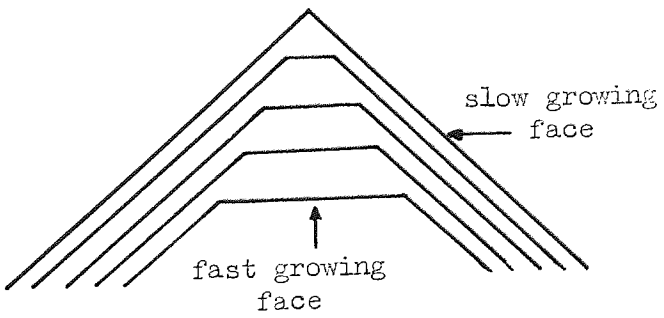

Fig 6.2.9. Survival of slow growing crystal faces and disappearance of fast growing ones.

6.3. The preparation of metal matrix composites by electro-deposition.

6.3.1. The effect of the nature of the electrolyte on the electro-forming process.

The ability to fill notches i.e. levelling or smoothing power is most important in the production of composites by electroforming and determines whether or not a continuous deposit can be obtained. This ability is related to the micro throwing power of the electrolyte which is ultimately related to the thickness of the cathode diffusion layer.[75] This is because on the cathode surface there are irregularities of the same order of size as the diffusion layer thickness. The diffusion layer will therefore vary in thickness with the result that the rate of mass transport of the depositing ions will be less in the recessed regions and greater on the protrusions. Thus the deposit will not reproduce the contours of the cathode surface satisfactorily. The thickness of the diffusion layer is determined largely by the mobility of the depositing ions, the current density and the agitation of the solution. If all other factors were equal the simple salt solution would thus be expected to be better than the complex solution and the latter should be improved by reducing the current density.

If ideal micro-throwing power is assumed, i.e. equal thicknesses of deposition on all surfaces, then levelling can only be of a geometric nature. The type of growth expected for deposition over conducting fibres is shown in fig 6.3.1.

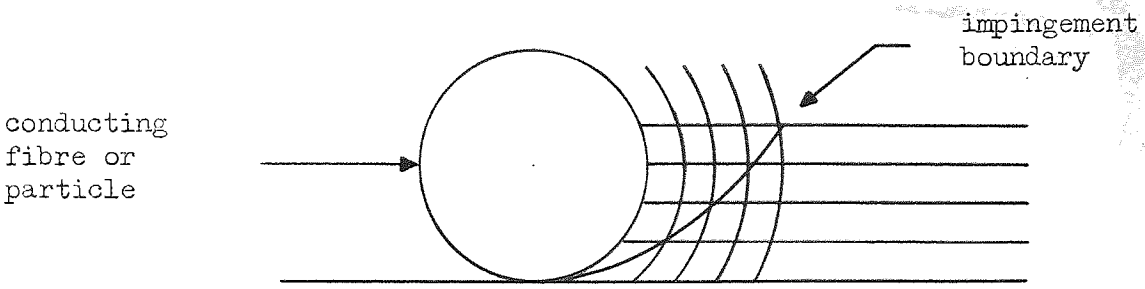

Fig 6.3.1. The geometric nature of levelling obtained from a solution of high micro throwing power.

The point of schematic cross-over of the growth front results in an impingement boundary representing the point of intersection of each "incremental layer". This behaviour obviously results in a continuous structure. The strength and nature of this boundary and the mechanism of its growth has been closely examined by a number of workers.[76-79] In the most recent work[79] plating was onto a surface having 90° notches and showed that the deposits grew out from the two faces, meeting in an impingement boundary plane which was clearly visible in an etched specimen. The strength of this boundary was not significantly different from that of the integral deposit.

In the case where micro throwing power is low and levelling is less than ideal the recessed regions will have less metal deposited on them than on the remainder of the surface. The result will be a crack of small angle emanating from the point of intersection and the resulting structure will be discontinuous as shown in fig 6.3.2.

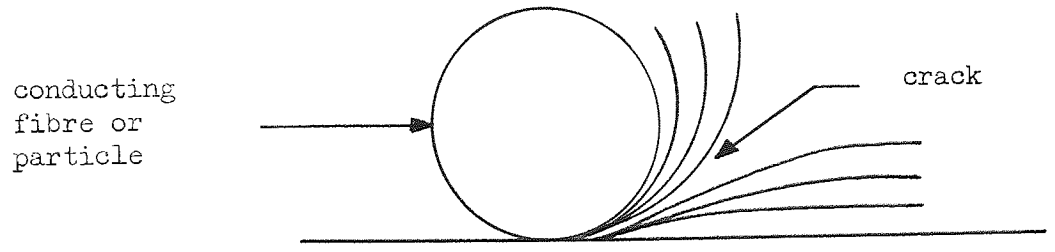

Fig 6.3.2. The formation of a crack in an electroform produced in an electrolyte of low micro throwing power.

N.B. The micro throwing power of a complex electrolyte, such as cyanide, can be improved by the use of periodic reversal of current.[75] The principle of this technique is that during the anodic part of the cycle the rate of dissolution is greatest in the peaks of the cathode profile where the diffusion layer is thinnest. On this basis the mode of deposition should revert from that of fig 6.3.2. to that of fig 6.3.1. That this does happen has been demonstrated.[13]

6.3.2. The effect of the nature of the ceramic on the electroforming process.

Ceramic materials, as they affect this process, fall into two classes: those that are electrical conductors and those that are not. When a ceramic material in fibre form is held in contact with a cathode surface while plating is carried out the process of keying the fibre into place will be quite different in the two cases. If ideal micro throwing power is assumed then for a conducting fibre the situation will be as described in 6.3.1. and metal will be deposited on the fibre as well as on the substrate. Fibre and substrate will thus be joined together by electrodeposited metal via an impingement boundary; the result is a permanent mechanical keying of the fibre after a short period of time, theoretically that for monolayer formation. In contrast for a non-conducting fibre

in contact with a cathode surface the keying process is quite different. The metal will be able to grow only from the cathode surface and must grow to a thickness of more than the fibre radius before the fibre is permanently keyed into the matrix, assuming fibres of circular cross section. This is shown diagramatically in fig 6.3.3.

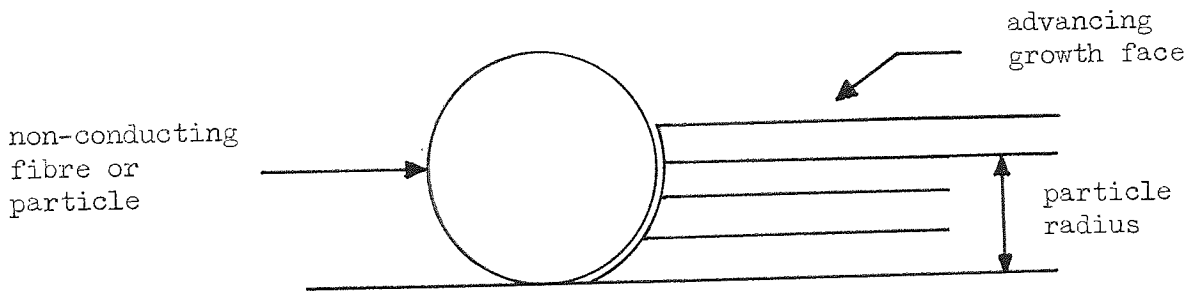

Fig 6.3.3. Keying of a non-conducting fibre into a metal matrix.

The time taken to achieve keying in this way can be considerable, for a fibre or particle of diameter 4/um it would require two minutes at 4 Adm^{-2} [1].

Work done using the technique of simultaneous electroforming and filament winding has given much useful information regarding the separation required to ensure void-free deposits. When the fibre is conducting voids are formed if the fibres are closer together than one diameter. This is a minimum distance assuming ideal throwing power and an equal growth rate on all surfaces;[13,14,80] it is shown in fig 6.3.4.

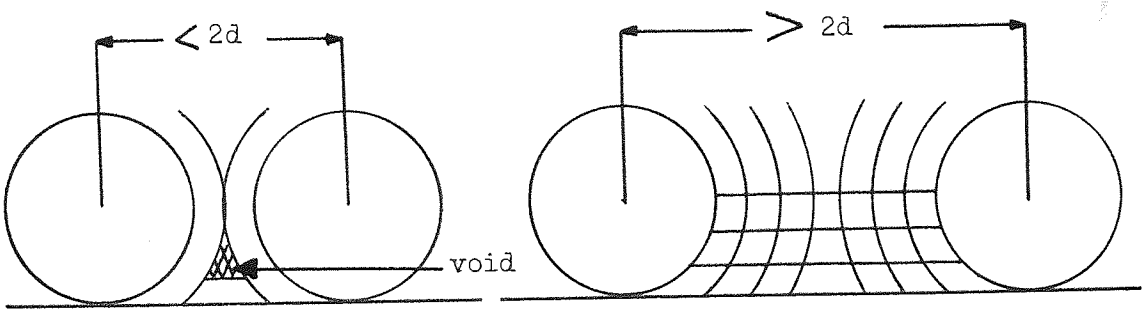

Fig 6.3.4. The effect of inter-fibre distance on void formation. Electroformed composite with conducting fibres: ideal throwing power assumed.

When the fibre is non-conducting the metal will grow between the fibres if they are separated by a minimum of 40% of a fibre diameter: when fibres are closer together than this large voids can be formed, [11] as shown in fig 6.3.5.

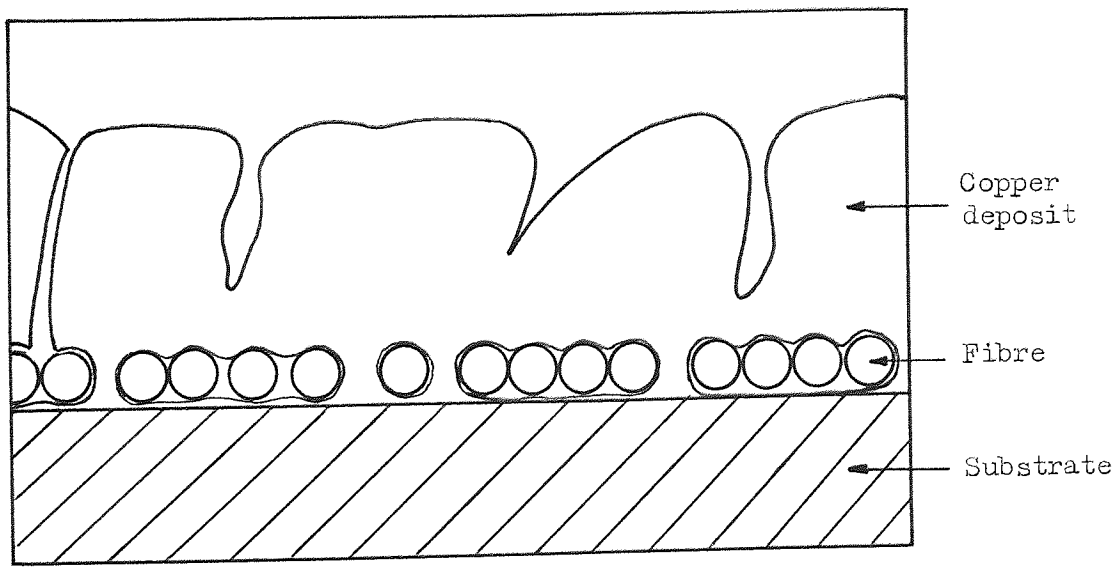

Fig 6.3.5. Copper deposited from an acid sulphate electrolyte over 50 /um glass fibres, X250. After G. A. Cooper "Electroformed composite materials" J.Mat.Sci.(1967),

Void-free composites have been produced using both conducting and non-conducting fibres.[14] The results suggest that a higher fibre density should be possible using non-conducting fibres.

The results, obtained using fibres which are effectively circular in cross-section, are very significant in the present work. This work involves the use of particles, which can be considered as spheres i.e. as having a circular cross-section. The growth mechanisms observed in the keying of fibres should be similar to those by which particles are keyed, the only difference being that a particle is not mechanically held against the cathode while keying by metal takes place but relies upon electrostatic, van der Waals and similar forces to hold it. The work with fibres has indicated that a dwell-time of particle on a smooth cathode surface before keying occurs is likely to be appreciable for non-conducting particles. Work by Foster[18] using periodic reversal of current has confirmed that a very short time only is required for keying conducting particles. As the dwell-time is longer for a non-conducing particle there is a much greater chance that the scouring and impacting action of the suspension will cause it to become dislodged before being keyed into the matrix.

CHAPTER 7. PREPARATION OF COPPER MATRIX CERMETS BY ELECTRODEPOSITION.

An extensive programme of electrodeposition was undertaken with the object of determining whether or not the magnitude of the zeta potential and surface charge density of a ceramic particle, suspended in a plating bath, had any direct bearing on the probability of inclusion of the particle under plating conditions. If the magnitude of the charge is of significance in deposition this could be demonstrated: the requirements would be a given formulation of plating bath and a number of particulate materials each of which has a different charge in that bath. Suspensions of these ceramics should be produced in plating baths such that each bath contained the same number of particles of the same size, irrespective of the density of the ceramic, per unit volume of solution. The results of plating from these solutions under controlled conditions of temperature, current density and agitation should show whether or not the inclusion density of ceramic obtained in the deposit depended upon the charge carried by the ceramic particles. That the number of particles of each ceramic material per unit volume, the "bath loading", should be constant is very important, (see section 7.1.).

7.1. Plating equipment and electrolyte.

The electrolyte was the common acidic copper sulphate solution as used previously: it was of composition

$CuSO_4 \cdot 5H_2O$	250g
H_2SO_4	50g
water	to one litre

The plating tank was a parallel sided glass tank of dimensions 200 x 125 x 125 mm. Agitation of the solution was by a centrally located electrically driven paddle stirrer which also served to maintain the ceramic powder in suspension. The anode (Canning "Rolled Copper Anode") of dimensions 125 x 135 x 6 mm occupied one

end of the tank. Plating was carried out onto brass strip specimens of dimensions 50 x 25 x 2 mm: the specimen to be plated was suspended 30 mm from the end of the tank opposite to and with its face parallel to that of the anode. The D.C. supply used for plating was an unsmoothed full wave rectified mains supply controlled, as before, by means of a rehostat.

It is known that particle inclusion density varies with the bath loading of ceramic [81-85] and this indicates that the number of impacts between particle and cathode is significant in determing the final inclusion density. Use of a bath loading of powder which gives a constant number of particles irrespective of their density and a constant rate of agitation should give a constant number of impacts per second between particles and cathode.

There is considerable disagreement in the literature regarding the effect of cathode current density on particle inclusion density obtained from a given plating bath. [1] It is claimed variously that the current density is not significant, [86,87] not significant at current densities above 10 Adm^{-2}, [83] that lower current densities give higher inclusion densities [84,88] and that for some materials an increase in current density gives a higher inclusion density and for others a lower. [85]

The present electroplating studies were carried out using apparatus similar to that used in the earlier part of this work. [1] So that the distribution of ceramic particles in the deposit could be seen relative to physical features in the metal structure a considerable thickness of metal was deposited, usually approximately 1.5 mm.

7.2. Ceramic materials.

The ceramic materials used were silicon carbide, quartz and chromium diboride, the same materials as were used in the streaming work.

For electrodeposition it was required that each ceramic material should be of the same particle size and that in every case the number of particles in suspension should be the same per unit volume. The particle size chosen was 4.5 /um, which was the size used in earlier plating work. This was separated from the commercially available material (-300 mesh to dust in the cases of quartz and chromium diboride) by water elutriation using the elutriator used in 3.2. and described in appendix VI. The size distribution in the powder collected was determined using a metallurgical microscope with a suitable eyepiece graticule in conjunction with a stage micrometer.

The three materials were of widely differing densities, quartz 2.65, silicon carbide 3.2, chromium diboride 5.1. To ensure that the same number of particles per unit volume of electrolyte were used in each case a loading of 100 gl^{-1} of silicon carbide was taken as a standard and the weights of all other materials were calculated accordingly.

The ceramic powder was dispersed in the electrolyte by simple addition of the powder to the electrolyte with vigorous stirring by paddle stirrer. Before use the bath was stirred for approximately six hours to ensure complete dispersion. When this system was used no agglomerates of particles could be detected in codeposits produced from the bath and the method was considered completely satisfactory.

7.3. Conditions used for electroplating.

7.3.1. Cathode current density.

Current densities of 4 and 2 Adm^{-2} were used. The majority of the work was carried out at 4 Adm^{-2} but in order to investigate the effect of current density on the inclusion density an additional investigation using silicon carbide was carried out at 2 Adm^{-2}.

7.3.2. Temperature.

Electroplating was carried out at 25° and 55°C. Control of the temperature was achieved by immersion of the plating bath in a thermostat bath at the required temperature, which could be controlled $\pm 1^{\circ}C$ between 20° and 100°C.

7.3.3. Agitation.

Just sufficient agitation was used to maintain all of the ceramic in suspension; inevitably a greater degree of agitation was required for the ceramics of greater density. Speeds of rotation required for the materials used were 280, 360 and 700 RPM for quartz, silicon carbide and chromium diboride respectively. This ratio between the rotation speeds is what would be expected for suspensions of these materials in water: the ratio of the densities in water is

$$(2.65-1) : (3.2-1) : (5.1-1)$$

i.e. $1 : 1.33 : 2.48$ and the ratio of speeds of rotation of the stirrer

$$280 : 360 : 700$$

i.e. $1 : 1.29 : 2.5$ This was considered to be very good agreement between particle density and degree of agitation.

To determine the effects, if any, of a change in the stirring rate on the inclusion process an investigation was carried out using silicon carbide and also chromium diboride. This investigation was carried out at 25°C and involved preparation of specimens at a current density of 4 Adm^{-2} with a number of stirring rates. The rates of stirring chosen were based on the rate required to just maintain all of the ceramic in suspension and were 0.75, 1.5 and 2 times this rate.

7.3.4. Preparation of specimens for plating.

Deposition was carried out using brass strip cathodes. These were prepared from 25 mm strip by filing off corners, mechanical abrasion with 320 grade corborundum paper, vapour degreasing then 30 seconds immersion in 1:1 nitric acid followed by washing in distilled water. The prepared specimens were transferred wet to the plating bath, electrical connection being made immediately after immersion.

Early in the course of the work it was realised that there is some variation, in the results obtained for inclusion density, between specimens prepared under nominally identical conditions. Because of this it was considered necessary to produce a large number of specimens under each set of conditions; a minimum of eight were prepared.

N.B. Some of the variations in inclusion density with current density reported in the literature could possibly be accounted for by variations between specimens plated under nominally identical conditions.

CHAPTER 8. RESULTS OF ELECTRODEPOSITION EXPERIMENTS.

At the conclusion of the electroplating period a typical specimen containing ceramic inclusions had a greater surface roughness and a larger edge build-up than a specimen plated under the same conditions but in the absence of ceramic. This was true for all the ceramic materials used.

All specimens were sectioned both parallel to and transverse to their surface, polished to a 1 /um diamond finish and examined microscopically. The distribution of ceramic particles throughout the deposit could be clearly seen. Following this examination the specimens were etched in ferric chloride reagent so that such physical features as grains and nodules in the deposit could be distinguished and the distribution of ceramic relative to them could be determined.

A number of specimens were plated with copper in the absence of ceramic particles. The structure of the electrodeposit produced is shown, after etching in ferric chloride reagent, in figs. 8.1-4.

8.1. Silicon carbide.

8.1.1. Specimens prepared at 25°C with current density 4 Adm^{-2}.

The surface was slightly rough and nodular with some build-up at the edges. Examination parallel to surface showed that there was a high inclusion density. Initially, and up to a deposit thickness of the order of 500 /um the particle distribution was fairly even across the specimen. As the thickness increased and the metal structure became more coarse and columnar a concentration of ceramic particles could be seen in the boundaries between the (approximately hexagonal) columnar growths. These effects can be seen in figs. 8.5-7.

Examination transverse to surface showed a high inclusion

content within and between the columnar growths as can be seen in fig. 8.8. The effect on the structure of the metal of the silicon carbide inclusions can be seen in fig. 8.9.: the inclusions are both within and between the grains.

8.1.2. $25^{\circ}C$ and current density of 2 Adm^{-2}.

The superficial appearance of the specimens was similar to those prepared at the higher current density; microexamination showed no observable difference in inclusion density or distribution.

8.1.3. $55^{\circ}C$ and current density of 4 Adm^{-2}.

The superficial appearance of the specimens was similar to those produced at $25^{\circ}C$ and 4 Adm^{-2}. The distribution of ceramic material was similar but the inclusion density was noticeably less. This can be seen in figs. 8.10-11. No detailed study was carried out into the change of inclusion density with temperature for silicon carbide or for the other ceramics used.

8.1.4. The effect of variation in stirring rate: $25^{\circ}C$ and 4 Adm^{-2}.

The stirring rate used for preparing cermet specimens was just sufficient to maintain the particular ceramic in suspension; this was 360 r.p.m. for silicon carbide. When the stirring rate was increased from this no change in inclusion density was detected for a rate increase of 50%. When the stirring rate was doubled the inclusion density fell to about one tenth of its previous value, which suggested that the increased scouring action of the suspension was dislodging particles from the surface of the cathode before they could become keyed by metal. When the stirring rate was reduced to 75% the inclusion density again fell sharply. This was not surprising as a large proportion of the ceramic could be seen to settle out of suspension, reducing the effective bath loading considerably. The effect of this was evidently greater than the reduced scouring effect resulting from reduced agitation.

8.2. Chromium diboride.

Specimens were prepared at 25°C with current densities of 4 Adm^{-2}.

The superficial appearance of the specimens was similar to those containing silicon carbide: the surface was more rough and there was a rather greater edge build-up. The structure in the edge build-up was distinctly dendritic. Micro-examination showed a high inclusion density and a distribution similar to that obtained for silicon carbide, as can be seen in figs. 8.12 and 8.13. Etching again showed that ceramic particles were both within and between grains, as shown in fig. 8.14. When the stirring rate was considerably increased the inclusion density of chromium diboride was reduced noticeably: unfortunately it was not possible to double the stirring rate without causing unacceptable solution losses through splashing. As for the case of silicon carbide a reduction in stirring rate caused settling out of the ceramic and a considerable fall in inclusion density.

8.3. Quartz.

Specimens were prepared at 25°C with current densities of 4 Adm^{-2} and 2 Adm^{-2}.

In appearance the specimens were superficially similar to those prepared using silicon carbide or chromium diboride. When removed from the plating bath they were coated in quartz powder, which had formed a thick layer on the side facing the anode and stirrer. This layer of quartz powder was so dense and thick near to the centre in one area of the specimens that it had prevented electrodeposition of metal except for a number of fairly large nodules; this is shown in fig. 8.15.

When the specimens were sectioned for examination the whole deposit was found to be extremely porous to an extent which made it largely fall to pieces during hacksawing. Microexamination after sectioning showed that there was virtually no quartz powder included in any part of the deposit. The structure of the deposit, after etching, is shown in figs. 8.16 and 8.17; it can be seen to be similar to that of those specimens plated in the absence of ceramic and shown in figs. 8.1-4.

8.4. Silicon carbide and quartz mixture.

The bath used contained 100g l^{-1} of silicon carbide and the corresponding weight of quartz. The intention was to determine whether or not the difference in charge carried by the two materials caused a difference in inclusion density. In the event, as stated in 8.3., it was not found possible to obtain inclusions of quartz in copper from the plating bath used, hence the results obtained from the mixture were of no value.

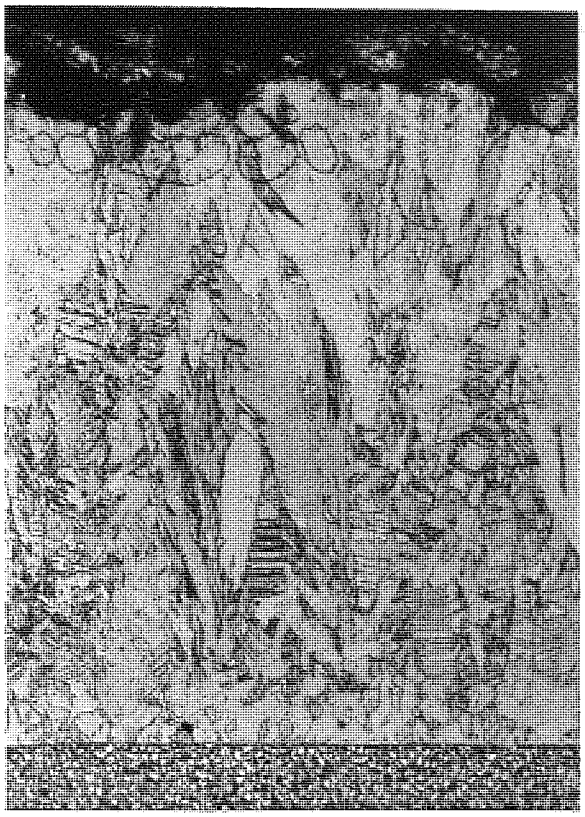

Fig. 8.1. Electrodeposited copper, transverse section etched in ferric chloride reagent.
x 24, enlarged x 3.

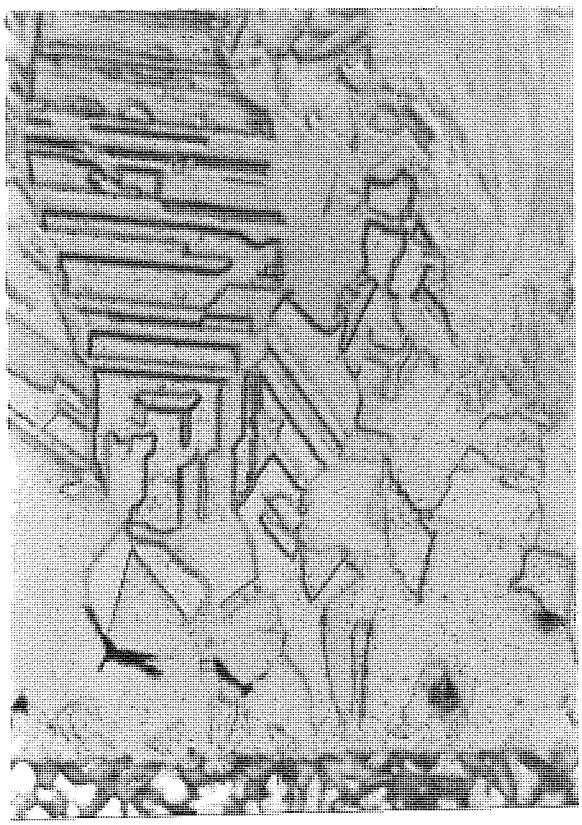

Fig. 8.2. Electrodeposited copper, transverse section etched in ferric chloride reagent.
x 150, enlarged x 3.

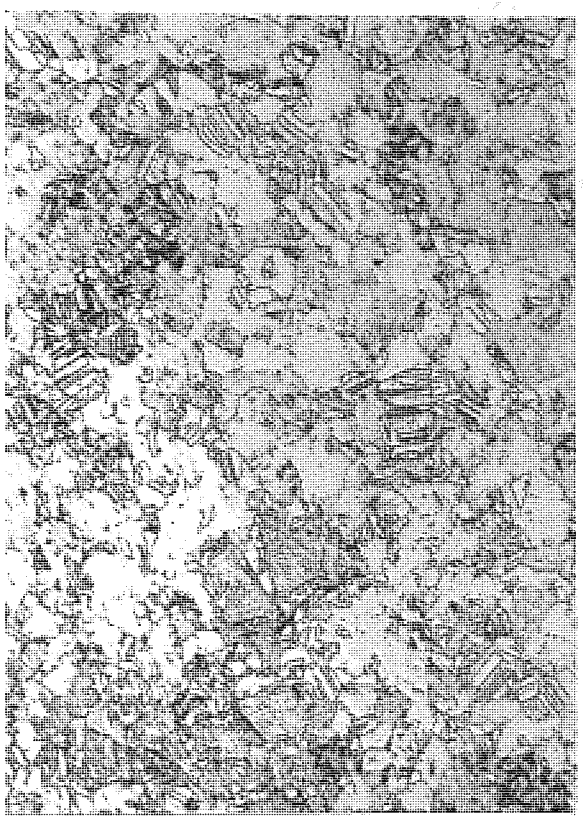

Fig. 8.3. Electrodeposited copper, parallel to surface, etched in ferric chloride reagent.
x 24, enlarged x 3.

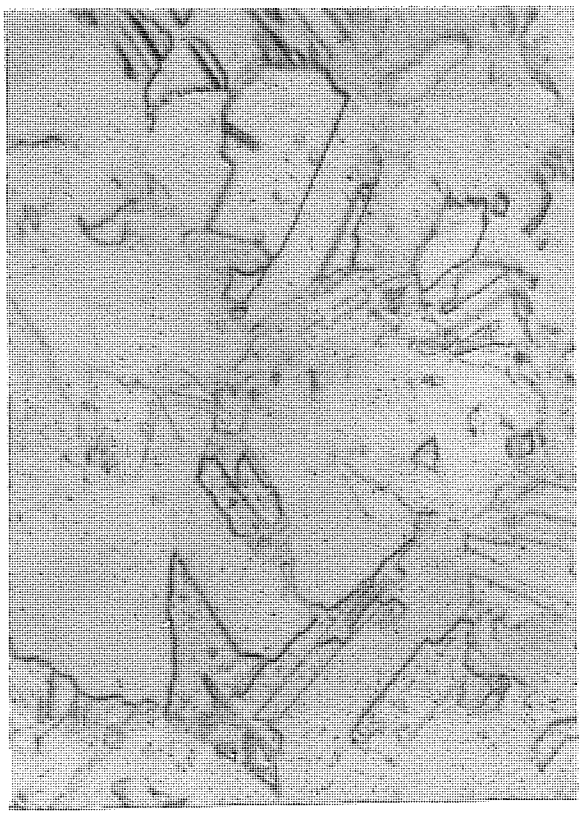

Fig. 8.4. Electrodeposited copper, parallel to surface, etched in ferric chloride reagent.
x 150, enlarged x 3.

Fig. 8.5. Silicon carbide, 25°C, 4 A dm^{-2}, parallel to surface at thickness of 500 µm.
x 24, enlarged x 3.

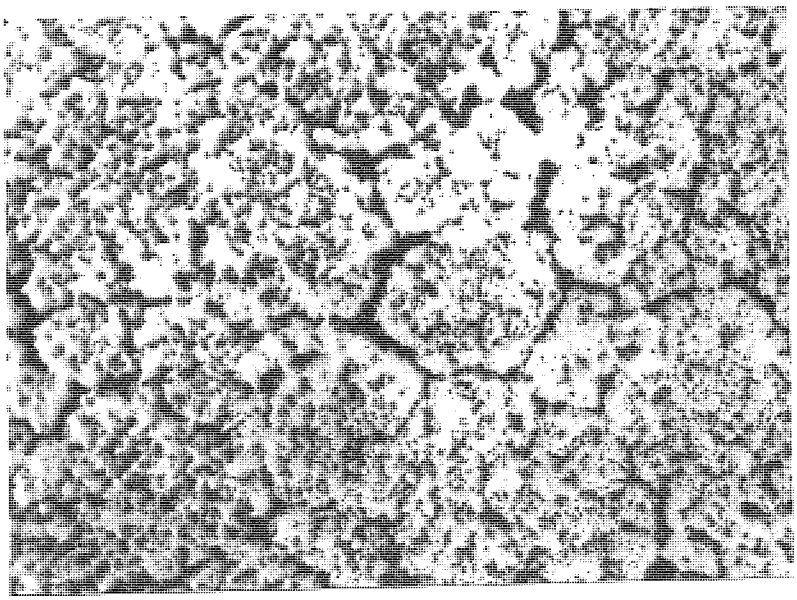

Fig. 8.6. Silicon carbide, 25°C, 4 A dm^{-2}, parallel to surface at thickness of 1000 µm.
x 25, enlarged x 3.

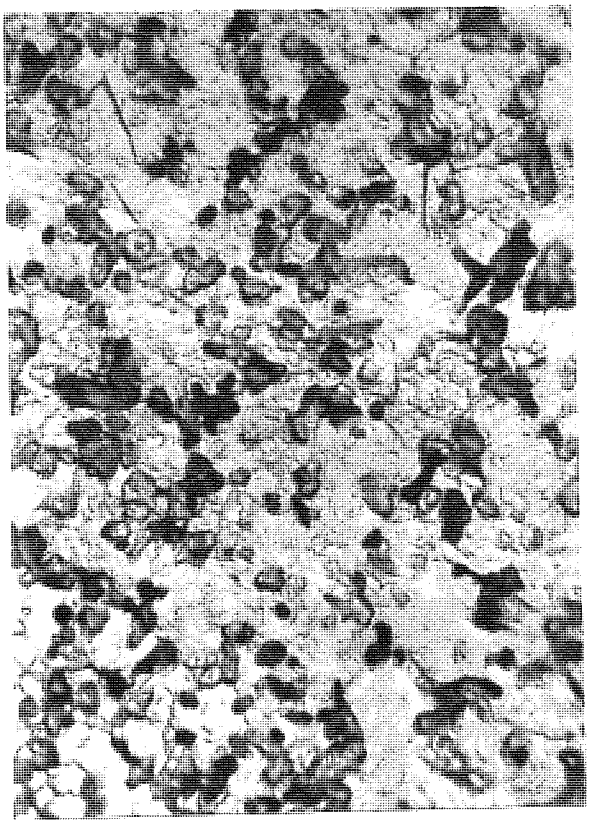

Fig. 8.7. Silicon carbide, 25°C, 4 Adm^{-2}. Parallel to surface at thickness of 1000/um, etched in ferric chloride reagent.
x 150, enlarged x 3.

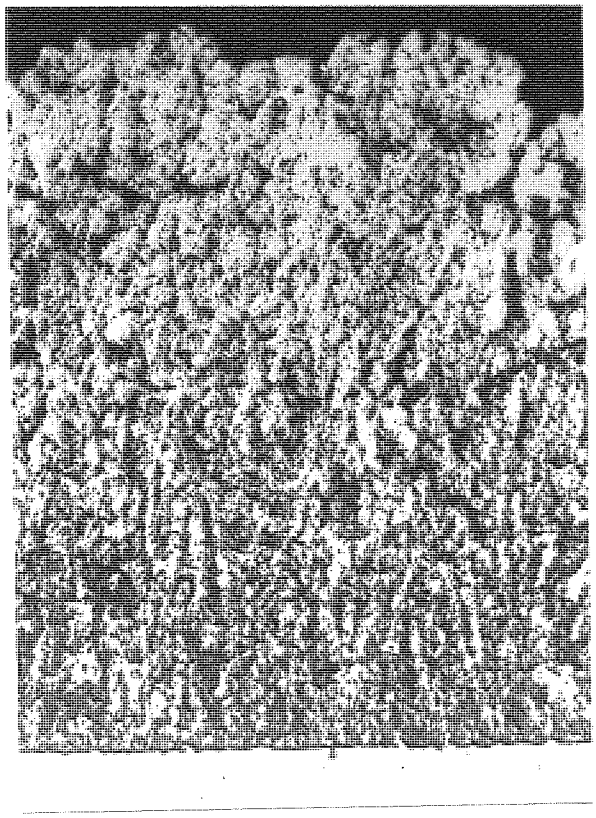

Fig. 8.8. Silicon carbide, 25°C, 4 Adm^{-2}, transverse section.
x 24, enlarged x 3.

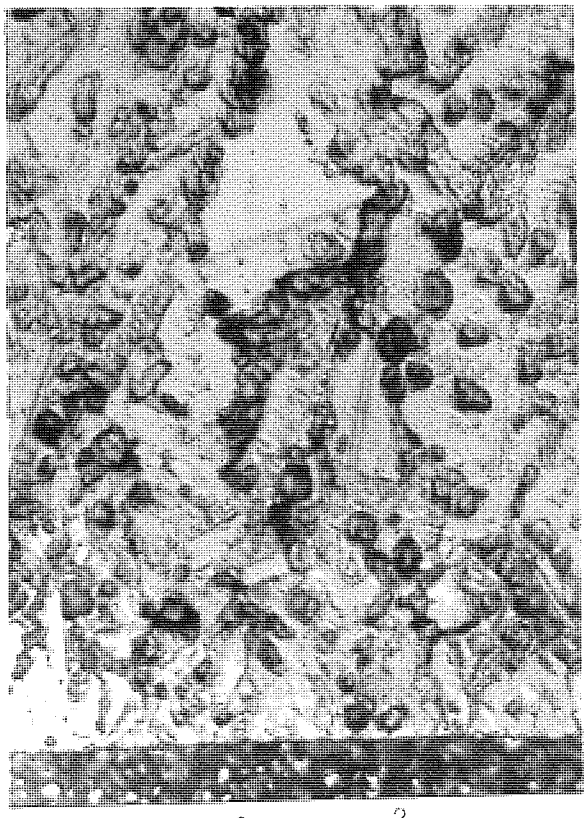

Fig. 8.9. Silicon carbide, 25°C, 4 Adm^{-2}, transverse section etched in ferric chloride reagent.
x 150, enlarged x 3.

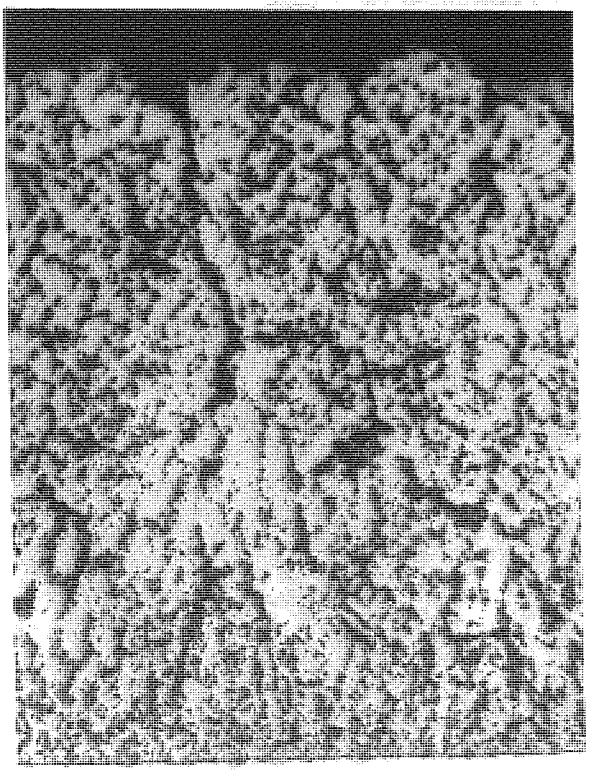

Fig. 8.10. Silicon carbide, 55°C, 4 Adm^{-2}. Transverse section.
x 24, enlarged x 3.

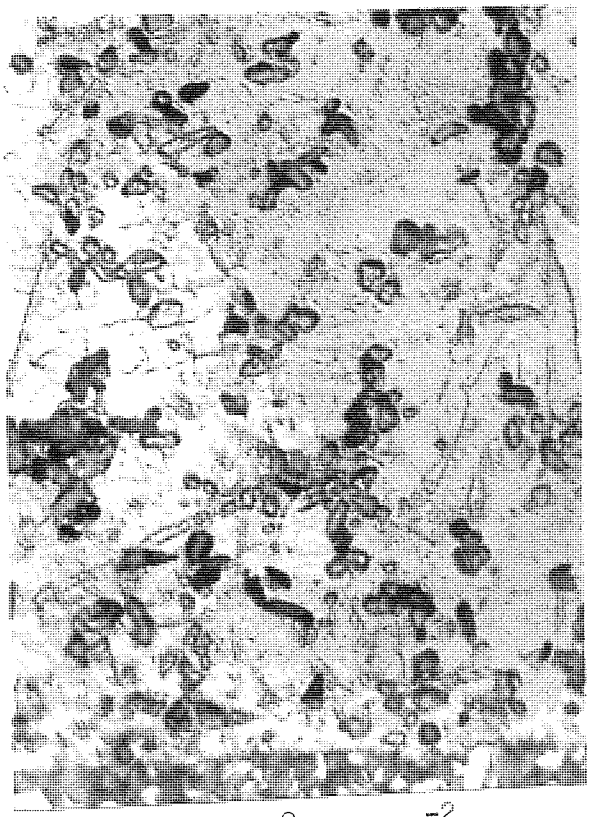

Fig. 8.11. Silicon carbide, 55°C, 4 Adm^{-2}. Transverse section etched in ferric chloride reagent.
x 150, enlarged x 3.

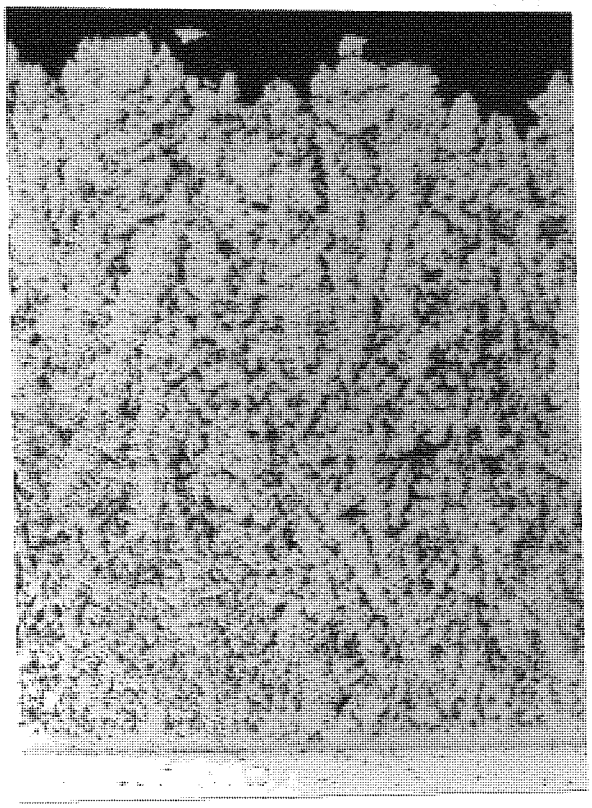

Fig. 8.12. Chromium diboride, 25°C, 4 Adm^{-2}. Transverse section.
x 24, enlarged x 3.

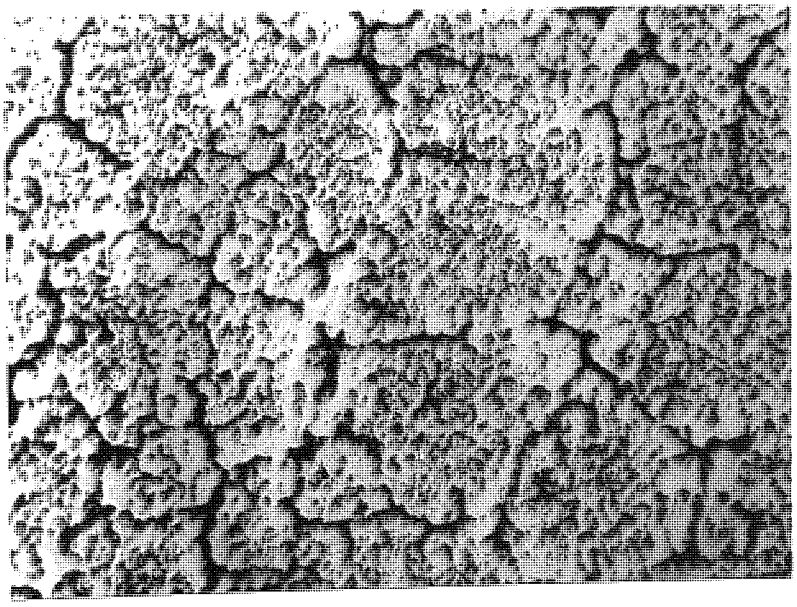

Fig 8.13. Chromium diboride, 25°C, 4 Adm^{-2}. Parallel to surface at thickness of 1000/um.
x 24, enlarged x 3.

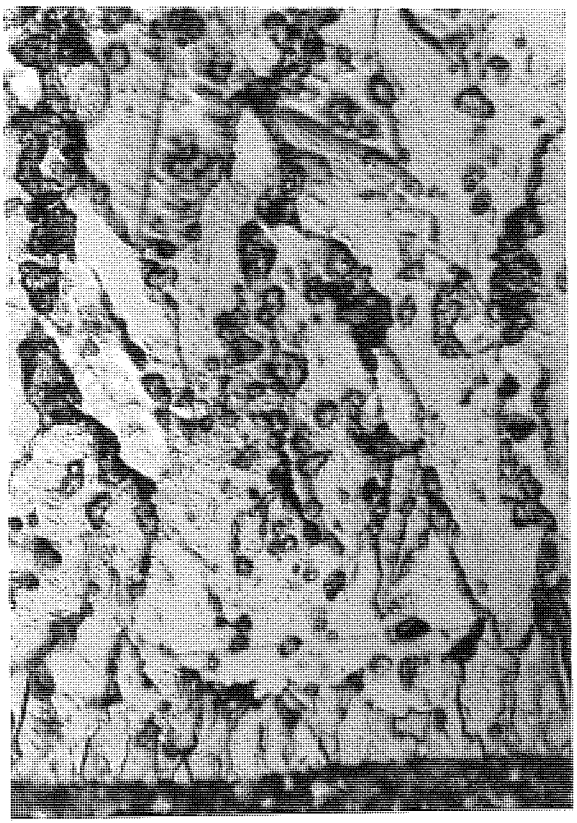

Fig. 8.14. Chromium diboride, 25°C, 4 Adm^{-2}. Transverse section etched in ferric chloride reagent. x 150, enlarged x 3.

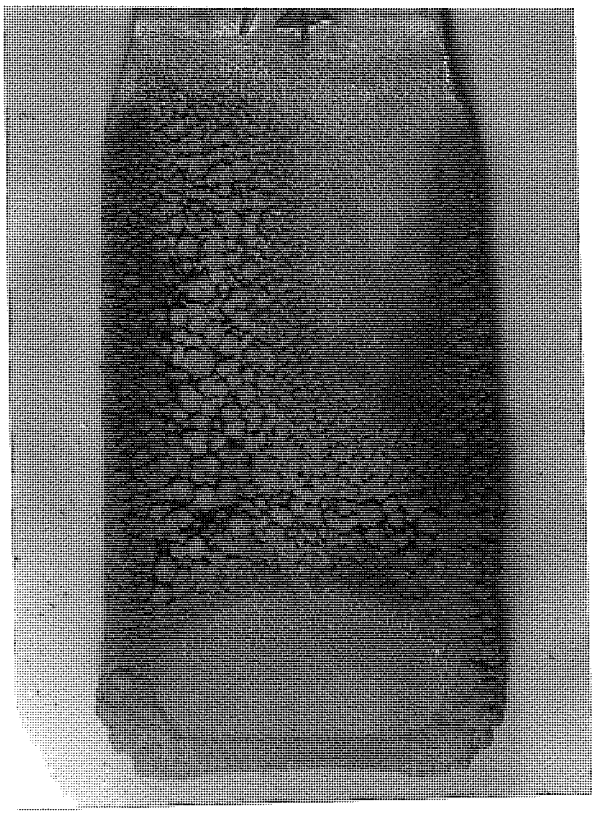

Fig. 8.15. Quartz: appearance of the specimen as removed from the plating bath.
x 2 actual size.

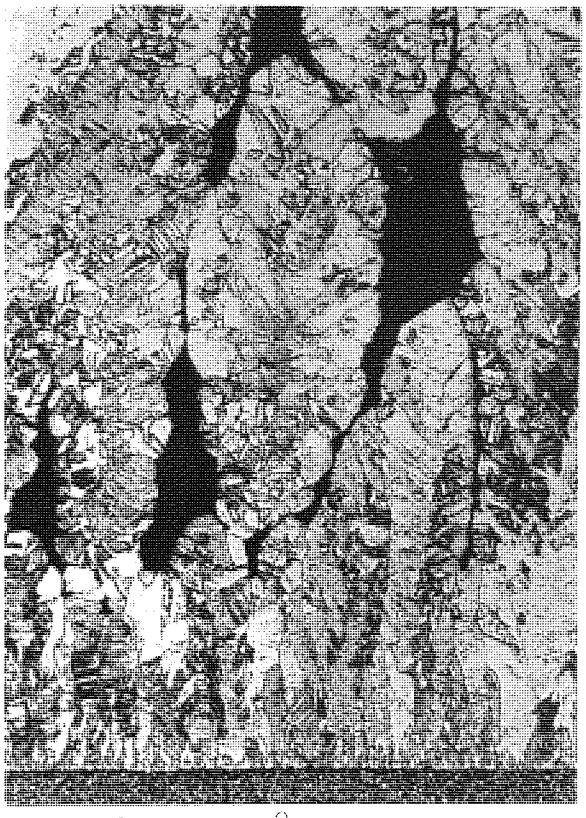

Fig. 8.16. Quartz, 25°C, 4 Adm^{-2}. Transverse section etched in ferric chloride reagent.
x 24, enlarged x 3.

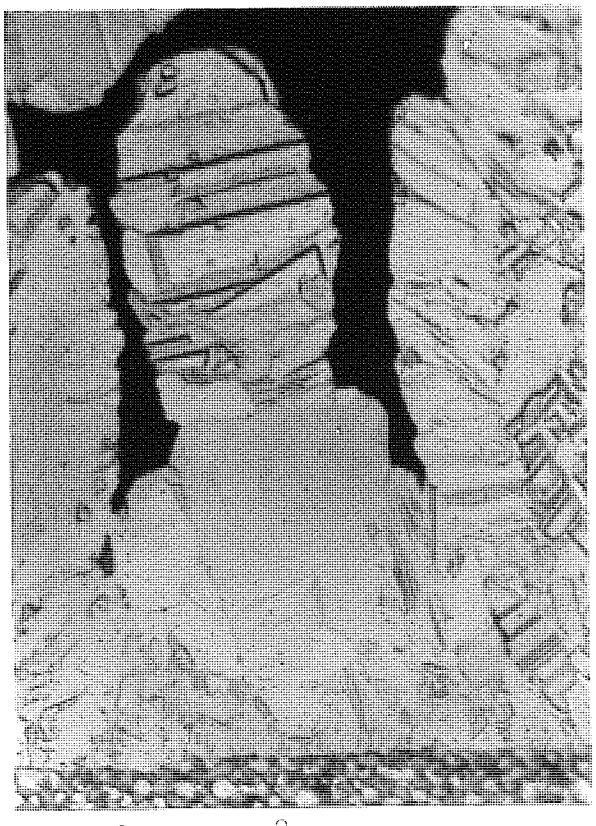

Fig. 8.17. Quartz, 25°C, 4 Adm^{-2}. Transverse section etched in ferric chloride reagent.
x 150, enlarged x 3.

CHAPTER 9. DISCUSSION OF THE MECHANISM OF PARTICLE ENTRAPMENT AND THE RESULTS OF ELECTRODEPOSITION.

Specimens prepared from solutions containing suspensions of silicon carbide or chromium diboride were found to have high inclusion densities of ceramic particles. The inclusion density did not appear to be significantly changed when the cathode current density was decreased by half but it was reduced when the temperature was increased from 25° to 55°C. The distribution of ceramic particles in the metal deposit was apparently completely random. Particles were within grains and between both grains and nodules; they were not confined either to grain boundaries or to any particular physical features. Similar results have been reported for the distribution of alumina[89] and also silicon carbide particles[90] deposited from a Watts nickel bath. The presence of inclusions did not, in the present work, appear to have caused changes in the microstructure of the electrodeposited copper except that, with the exception of the specimens plated from the bath containing suspended quartz particles, there is a much reduced proportion of stacking faults. These effects can be clearly seen in figs. 8.2 and 8.9. Specimens prepared from solutions containing suspensions of quartz particles contained virtually no inclusions. However it was evident that quartz powder had been transported to and, moreover, had become firmly attached to the surface as it could be clearly seen adhering to the surface and had prevented electrogrowth from occuring evenly.

9.1. The mechanism of particle entrapment.

When a particle is suspended in a stirred electrolyte solution it is rapidly transported by the hydrodynamic motion of the electrolyte. In addition, if the particle is charged it will undergo

electrophoretic transport owing to the electrical field present under electroplating conditions. It has been established that in the bulk of the electrolyte electrophoretic transport is negligible compared with hydrodynamic transport[1] but that once a particle has reached the double layer on the cathode the very high field within the double layer would cause a very rapid movement of the particle through the double layer to the cathode surface.

Particle entrapment may be by one of two principal mechanisms; the discussion of them assumes that the particles are spherical, all of one size and are deposited on a smooth plane surface. The first, hereafter referred to as "mechanical", assumes that the charge carried by the particle is of no significance in the process and that particles are incorporated by a simple mechanical process. The particles are transported to the cathode by the hydrodynamic motion of the stirred suspension and once in contact with the cathode surface "cling" until mechanically keyed by metal. The second, known hereafter as "electrochemical" differs in that part of the process which occurs when the particle arrives in the vicinity of the cathode surface. If the charge carried by the particle is significant then the effect of the field on a positively charged particle will be attraction towards the cathode. In a field of given strength an increase in the magnitude of the charge on a particle will increase the rate at which particles are transported through the double layer on the cathode[1] and also the tenacity with which they are held onto the surface. Similarly for a given particle an increase in field strength would increase both the transport rate and the tenacity with which it was held onto the cathode surface.

9.2. The effect of increased cathode current density on particle inclusion density.

An increase in the cathode current density will increase the rate at which metal is deposited. For a particle of a given size the time required for keying into the matrix will therefore be reduced. There will be an increase in the amount of metal deposited per particle impact on the cathode surface. If it is assumed that every impact led to an inclusion then this increase in metal deposited would result in a lowering of particle inclusion density as the cathode current density was increased. If alternatively (and this is much more likely) a significant proportion of particles which impact on the cathode are subsequently removed before keying the situation is slightly different; the result will be a fractional change in inclusion density which can be calculated as follows.

Let: x be the initial relative current density, proportional to the mass of metal deposited in a given time

y be the increased relative current density

a be the percentage of particles striking the cathode which are finally keyed, for current density x

b be the percentage of particles striking the cathode which are finally keyed, for current density y

f be a proportionality factor equal to the fractional change in inclusion density. Then

$$\frac{a}{x} \times \text{fractional change in inclusion density} = \frac{b}{y}$$

$$\text{or } f = \frac{x}{y} \times \frac{b}{a} \quad . \quad . \quad . \quad . \quad . \quad . \quad . \quad . \quad 9.1$$

When higher current densities are used the electrical field strength in the electrolyte is also increased. This increased field strength may, if the mechanism of deposition is "electrochemical", give rise to a greater rate of transport of particles in the region of the double layer on the cathode. This will result in more impacts between particles and the cathode and a greater tenacity between

particle and cathode. If every particle/cathode impact led to inclusion of the particle an increased field strength would lead to an increase in the number of particles included in a given time. The change in the number of impacts may, of course, be proportional to, greater than or less than the increase in field strength. To enable an estimate to be made of the effect of increased field strength on the proportion of impacts resulting in inclusion equation 9.1 can be extended. If the increase in the number of impacts is directly proportional to the increase in current density then for an increase from x to y the number of impacts per unit time will be increased by the ratio $\left(\frac{x + (y - x)}{x} \right)$ the inclusion density being correspondingly increased. When this factor is introduced equation 9.1 becomes

$$f = \frac{x}{y} \times \frac{b}{a} \times \left(\frac{x + (y - x)}{x} \right) \quad . \quad . \quad . \quad . \quad . \quad 9.2$$

which reduces to

$$f = \frac{b}{a}$$

If the increase in the number of impacts is different from that of the current density a multiplying factor m must be introduced hence

$$f = \frac{x}{y} \times \frac{b}{a} \times \left(\frac{x + (y - x)\, m}{x} \right) \quad . \quad . \quad . \quad . \quad 9.3$$

The equation in this form can be applied generally and used to gain an estimate of the effect of increased cathode current density on the particle inclusion density for the "mechanical" and "electrochemical" mechanisms.

9.2.1. The effect for the mechanism of "mechanical" entrapment.

As stated above an increase in the cathode current density will increase the rate at which metal is deposited thus reducing the time required to key a particle of a given size into the matrix. Also it is probable that a significant proportion of particles that strike the cathode are subsequently removed before they can become keyed. This is most easily illustrated by an example. If, of the particles which strike the cathode, 50% are removed before they

can be keyed into place; if the current density is doubled then the time for keying will be halved. If, further, halving of the time required for keying a particle results in removal of only 25% of the particles which strike the cathode then, using equation 9.3 (which with m = o reduces to the form of equation 9.1)

$$f = \frac{1}{2} \times \frac{(100 - 25)}{(100 - 50)}$$

$$f = 0.75 \text{ or } 75\%$$

The result of doubling the current density would thus be to decrease the inclusion density to 75% of its previous value.

N.B. In the unlikely event of doubling of the current density resulting in the inclusion of all particles which strike the cathode the change in inclusion density would be given by

$$f = \frac{1}{2} \times \frac{(100)}{(100 - 50)}$$

$f = 1.0$ indicating that the inclusion density would be unchanged. In the similarly unlikely event of doubling of the current density resulting in inclusion of exactly the same proportion as before of the particles which strike the cathode the change in inclusion density would be given by

$$f = \frac{1}{2} \times \frac{(100 - 50)}{(100 - 50)}$$

$f = 0.5$ indicating that the inclusion density would be halved.

For the "mechanical" mechanism an increase in current density could, if other conditions are maintained constant, result in an unchanged inclusion density but is most likely to lead to a reduced inclusion density.

9.2.2. The effect for the "electrochemical" mechanism.

An increase in the cathode current density will give an increase in the rate of metal deposition and, as before, this will reduce the time required to key a particle. When higher current

densities are used the field strength in the electrolyte is also increased and may lead to a greater rate of transport of particles in the region of the double layer on the cathode. However, the increase in the amount of metal deposited per unit time will, as described in 9.2.1., lead to a decrease in inclusion density. If as before it is assumed that a significant proportion of the particles which strike the cathode are removed before keying can occur then an argument similar to that used for the "mechanical" mechanism can be applied. Assume that under a given current density, 50% of the particles were removed before keying. If the current density was doubled the time for keying a particle would be halved and also the tenacity with which a particle was held on to the cathode would be increased. If under these conditions the number of particles which were removed before keying was reduced to 10% of those striking the cathode (compared with 25% for the "mechanical" mechanism) then by doubling the rate of metal deposition an increase of inclusion from 50% to 90% of all impacts has been achieved. The fractional change in inclusion density will be given by

$$f = \frac{x}{y} \times \frac{b}{a} \text{ from which } f = 0.9.$$ The symbols have the same meaning as previously used. The effect on the f value of the increased number of impacts on the cathode caused by the higher field strength can now be illustrated.

9.2.2.1. Increase in the number of impacts is directly proportional to the increase in the current density.

If the same theoretical conditions are used as above application of equation 9.3. with m = 1 gives

$$f = \frac{1}{2} \times \frac{90}{50} \times (1 + 1) \quad \text{hence}$$

$f = 1.8$ i.e. the inclusion density is increased by a factor of 1.8 for a doubling of current density.

9.2.2.2. Increase in the number of impacts is different from the increase in current density.

Using the same conditions as before if it is assumed that the number of impacts is increased by 1.5 times the increase in current density application of equation 9.3. with m = 1.5 gives

$$f = \frac{1}{2} \times \frac{90}{50} \times (1 + (1 \times 1.5)) \qquad \text{hence}$$

$$f = 2.25$$

Similarly if the number of impacts is increased by 0.5 times the increase in current density application of equation 9.3. with m = 0.5 gives $f = \frac{1}{2} \times \frac{90}{50} \times (1 + (1 \times 0.5))$ hence

$$f = 1.35$$

The results of the calculations in 9.2.1. and 9.2.2. show that for a "mechanical" mechanism an increase in current density would give a reduced inclusion density and for an "electrochemical" mechanism an increase in current density would result in an increased or significantly unchanged inclusion density.

The results quoted in the literature[83-87] show that an increase in current density was seen to give either no change in or an increase in inclusion density except in the cases of alumina[84] and titania[84,85] in sulphamate nickel which showed a decrease. No electrokinetic data for titania in nickel solutions was available but values of zeta potential in nickel sulphate are quoted[44,91] which, on extrapolation, gives values of approximately + 15 mV and -8 mV respectively for solution concentrations of 1 molar nickel ion. From these very low values, one positive and one negative it must be assumed that alumina in nickel solution of plating concentration will be virtually uncharged. For an uncharged particle the inclusion mechanism can only be "mechanical" hence the fall in inclusion density with increase of current density is to be expected.

The results obtained in the present work show the inclusion density to be significantly unchanged at approximately 700 000 cm^{-2},

for silicon carbide particles at 25°C, with current density increase, i.e. $f \triangleq 1$ (see section 8.1.). This suggests that the mechanism is more likely to be "electrochemical" than "mechanical".

9.3. The effect of temperature on particle inclusion density.

An increase in temperature of an electroplating solution causes a decrease in resistance hence a given cathode current density can be obtained by using a lower emf. As a result the electric field strength in the plating bath will be lower at higher operating temperatures.

Increase in temperature causes a decrease in the zeta potential and the surface charge density of all the ceramic materials studied. For a temperature increase from 25° to 55°C the decrease in surface charge density was to approximately 0.4 of its value at 25°C for all materials studied.

An increase in temperature should not cause any change in the inclusion density if a "mechanical" mechanism is responsible for the process. If, however the mechanism is "electrochemical" the marked decrease in surface charge density on the particle and also the reduced field strength should cause a decrease in the inclusion density. This was in fact the result obtained: a marked decrease in inclusion density, from about 700 000 to about 400 000 cm^{-2} (see figs. 8.8-8.11), resulted from a temperature increase from 25° to 55°C. A similar fall in inclusion density with temperature increase has been reported[92] for work using an acid sulphate bath containing barium sulphate, particle size 1-5 /um, in the presence of Tl^+ as a "promoter". This result gave further evidence for the mechanism being "electrochemical", i.e. depending on the charge on the particle and the field strength.

9.4. The effect of agitation of the electrolyte.

A particle, having reached the cathode surface, has to be held on the surface until keyed by electrodeposited metal. The time

for which a particle has to be held on the surface may be critical because of the scouring action of the electrolyte and the bombarding action of particles in suspension tending to dislodge it. As the degree of agitation was increased the resulting inclusion density increased to a maximum and then fell. The reason for this is that when the degree of agitation is low not all of the ceramic particles are kept in suspension and the effective bath loading is reduced. As agitation is increased a higher proportion of the particles are kept in suspension and the inclusion density increases. Once all the particles are in suspension further increase in agitation simply increases the scouring action of the suspension on the cathode surface before they can be keyed by metal.

(N.B. It has been shown that for particles of chromium[83] and sub-micron particles of alumina and titania in sulphamate nickel[84] an increase in stirring rate gives an increased inclusion density. This can readily be explained: for very fine particles the degree of agitation required to maintain them in suspension is small and gives rise to very little solution movement. Before particles can be included into the metal matrix they have to be brought to it by movement of the solution: increase in agitation will increase the number of particles brought to the cathode per unit time. Eventually the degree of agitation would become so high that the scouring action would prevent further increase in inclusion density with increased agitation. The authors of these papers did not use any very high agitation rates so it is likely that they had not reached the maximum value of inclusion density possible.)

When particles of a high density material are being used more agitation is required to keep them in suspension than is required for lower density materials: the stirring rate required is approximately proportional to the relative densities of the particles when in the electrolyte (section 7.3.1.). Such a particle on the cathode surface must thus undergo much more violent scouring and

bombarding while it is being keyed into the matrix than does a less dense particle which requires a lower degree of agitation to keep it in suspension. If the inclusion density obtained with the two materials is similar then the more dense material must be much more tightly held onto the cathode surface than the less dense one. For silicon carbide and chromium diboride the rate of stirring required to keep all the ceramic in suspension was very different: that for chromium diboride being almost double that for silicon carbide. When this higher rate was used with suspensions of silicon carbide virtually no ceramic was included in the matrix. As high inclusion densities of chromium diboride were obtained using this degree of agitation it was evident that the chromium diboride particles must be held on the cathode surface more tightly than silicon carbide particles. The only mechanism by which a particle of one material can be held on the cathode more tightly than that of another is if it carries a higher charge, in which case it will be held by a greater electrostatic force. The positive charge carried by a chromium diboride particle in the plating solution is four times greater than that of silicon carbide and the rate of agitation required is twice as great. The ratio of the increased charge to increased agitation is thus approximately 2:1. Agitation of this vigour, if used with silicon carbide, would have resulted in a deposit with an extremely low inclusion density: that a high inclusion density was obtained indicated that the particles of chromium diboride were more strongly held at the cathode surface than were particles of silicon carbide. This is very strong evidence that the deposition of ceramic particles depends upon the charge which they carry.

9.5. Electrical conductance of the particles.

The results obtained in experiments on concurrent filament winding and electroplating, already described, are very significant.

The simple copper sulphate electrolyte used in the current work has a high microthrowing power and it was shown that solutions of this type when used with conducting or non-conducting fibres could give a void-free deposit provided that the fibres were separated by at least one fibre diameter in the former case and by at least 40% of a fibre diameter in the latter. A non-conducting fibre will be keyed into the matrix when it is submerged to greater than half of its diameter; a conducting fibre will be keyed, via an impingement boundary, in a very much shorter time. The same mechanism of metal growth would be expected to take place around a particle as a fibre, as discussed in section 6.3.2.

9.5.1. Non-conducting particles, mechanism of entrapment

When a non-conducting particle arrives at the cathode surface having passed through the double layer it must remain in position on the cathode surface until sufficient metal has grown around it to key it into place. Under the conditions currently used this would take approximately two minutes for a 4 /um particle on a plane surface. During this time the particle must remain stationary: if the surface was rough the time would be reduced[1]. In the case under consideration where the microthrowing power of the solution is high the advancing growth face of metal, growing up from the substrate, would come up against the lower surface of the particle and be deflected by it. It has been suggested[93] that the growing metal face can in fact dislodge the particle completely, carrying it forward as the metal surface advances. (These authors used as a basis for this hypothesis the mechanism of the zone refining process in which an insoluble solid impurity can be carried before the advancing recrystallisation front[94]). If this is so it might be expected that to produce codeposits containing non-conducting particles, even if they had a high positive charge, from solutions of high microthrowing power would be difficult. The results obtained in the present work using quartz suspensions confirm this.

Similarly it has been observed by other workers[18,44,86,91,93] that alumina cannot be satisfactorily deposited from the copper sulphate bath.

9.5.2. Conducting particles, mechanism of entrapment.

When a conducting particle arrives at the cathode surface, having passed through the double layer, it will make electrical contact with it and, even if the particle is a poor conductor, metal will be deposited upon it. If the plating bath is one which has a high microthrowing power then the growth faces advancing from the substrate and from the particle will meet in an impingement boundary, permanently trapping the particle in a very much shorter time than would be required to submerge it to half of its diameter. (This has been confirmed by Foster[18] using periodic reversal of current, see section 6.3.2.). As the dwell-time of the particle before keying is short it is much more likely to be keyed into the matrix before being dislodged from the cathode surface than is a non-conducting particle. It has been claimed that for satisfactory deposition of conducting (chromium) particles a plating solution having a high microthrowing power should be used,[83] in contrast to the case of non-conducting particles[93].

9.6. The roughness of the cathode surface.

The effects of roughness were discussed in detail in the earlier work[1]. If the cathode surface is rough the high points are able to give some shelter from the scouring effects of the electrolyte to particles in troughs in the surface. This is likely to be of greater significance in the case of non-conducting particles, for which the dwell time can be minutes long. Any very rough surface can trap particles: once in deep trough or crack a particle can very rapidly be trapped by growth of metal closing the top of the trough as shown in fig. 9.6.1.

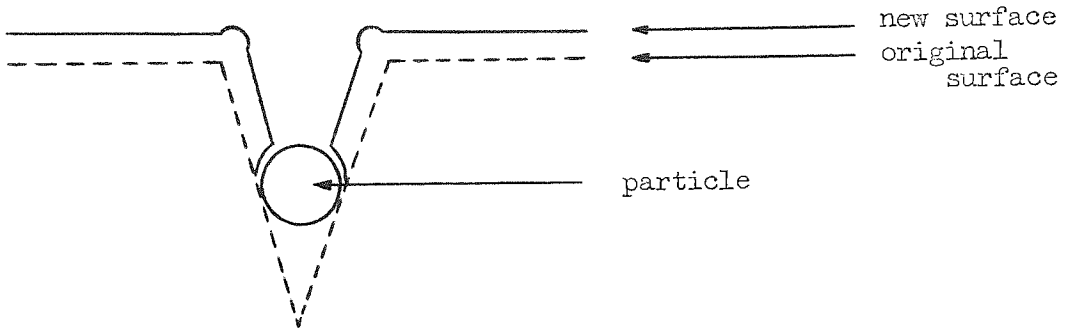

Fig. 9.6.1. The effect of a trough in the surface of an electrodeposit.

Adjacent to the brass substrate the inclusion density was very low, as can be seen in figs. 8.9 and 8.14 particularly clearly. The increased inclusion density as the electrodeposit becomes thicker and rougher gave further evidence that a rough cathode surface aided particle entrapment and/or retention. The surface roughness is not in itself, of course, a part of the fundamental mechanism of particle deposition but can significantly assist in the process.

Recent papers describing work on the mechanism of this process are broadly in agreement with these results, although there are some disagreements between authors. That a particle requires a positive charge before it can be readily codeposited has been demonstrated: powdered materials which were uncharged[95] or carried a negative charge[44,91] when immersed in a plating solution were studied, in the former case P.V.C. particles in Watts nickel and in the latter alumina particles in acid copper sulphate solutions. These materials could not be deposited satisfactorily from the stated baths. In each case it was shown that addition of a cationic surfactant to the solution caused the charge on the particle to become positive. it was also shown that in the presence of the surfactant the particulate materials could be satisfactorily codeposited. It was

shown[44] that the surfactant did not alter the micro throwing power of the plating solution as measured by its ability to deposit in shallow notches: no evidence was offered regarding other possible effects due to the presence of the surfactant, such as selective adsorption on the cathode. It has been shown by adsorption analysis that positive adsorption will take place on silicon carbide in copper sulphate solution at concentrations above 0.01M[44]. This compares fairly well with the results in this thesis which show that the sign of the charge on silicon carbide will reverse at a concentration of approximately 2.5×10^{-3}N for solutions of copper sulphate, sulphuric acid and mixtures of the two (see section 4.3.1.) It has been claimed that in solutions containing monovalent ions an increase in concentration will cause the -ve charge on alumina to tend to zero and not to reverse and become increasingly positive in the manner that it did with divalent ions[21]. This is in direct contrast to the results shown in this thesis for all materials studied.

N.B. It should be pointed out that these workers also stated that particle deposition from acid sulphate copper baths cannot be achieved without the presence of addition agents and this is not confirmed by the present work or by work published in 1970[1] and 1970'[1] by the present writer. That the behaviour of a particle in a plating solution depends strictly on the structure of the layer of ions and molecules adsorbed on its surface was suggested by Guglielmi[63] using an elegant mathematical treatment. This postulated that the behaviour of the particle and the likelihood of its codeposition must depend upon the nature of the solution with which it is in contact. He states, without quoting any evidence, that there is a fundamental objection to any electrophoretic effect and suggests a two-stage mechanism for the process: firstly a loose physical adsorption of the particle, with its adsorbed layer of ions and molecules, then a field-assisted adsorption

resulting in removal of the ion/solvent sheath. He suggests that these two adsorption processes take place at the inner and outer Helmholtz planes respectively. Finally the particle, held at the inner Helmholtz plane, is submerged by metal. This two-stage process, the second of which involves field assisted transport of the particle through the outer Helmholtz plane, is similar to that proposed previously[1,42] by the present writer.

Summary of results and proposed mechanism for the process.

The effect on the particle inclusion density of variation of a number of factors was as follows. The effect of increasing the temperature of the plating bath was to reduce the inclusion density: change of current density made no noticeable difference to the inclusion density. Agitation in excess of that required to maintain all of the ceramic powder in suspension caused a decrease in inclusion density; increased zeta potential and surface charge density on the ceramic caused an increase. Increased surface roughness of the cathode gives an increased inclusion density, inclusion being to some extent concentrated at troughs and crevices in the surface but not being confined to any obvious physical features such as grain boundaries. If a particle is an electrical conductor it is more likely to be keyed into the matrix before being dislodged from the surface than is a non-conducting particle. Conducting particles form dense codeposits when produced from solutions having a high micro throwing power. Non-conducting particles in solutions of high micro throwing power and in the absence of surfactants can be transported to the cathode surface but not keyed into place by metal.

CHAPTER 10. CONCLUSIONS.

When this section of the work was undertaken it had already been established[1] that the change of zeta potential on silicon carbide with electrolyte concentration was not dependent upon the particular electrolyte or combination of electrolytes present but was a total ionic strength effect. It had also been shown that the zeta potential on silicon carbide, initially negative in water, became increasingly less so and tended towards zero as the electrolyte concentration was raised. One of the factors which it was wished to investigate was the effect of very high concentrations of electrolyte on silicon carbide and also upon other materials. Another factor was the effect of temperature change upon the zeta potential on a particle.

The results of streaming measurements made on silicon carbide, quartz and chromium diboride using a range of concentration of electrolyte from 8×10^{-6} to 5.28×10^{-1} molar and a range of temperature from 10° to 70°C show that for all the materials studied an increase in electrolyte concentration made the zeta potential and surface charge density more positive and an increase in temperature made it less so. These two effects are explained by contact adsorption of cations onto the ceramic, adsorption increasing with electrolyte concentration increase and decreasing with temperature increase. Calculations of heats of adsorption showed that this adsorption was most probably physical in nature.

Electrodeposition from suspensions of silicon carbide, quartz and chromium diboride in acid copper sulphate plating solutions of constant composition showed that particles were readily included from suspensions of silicon carbide and chromium diboride but not from suspensions of quartz powder. The particle inclusion density in the deposit was reduced by an increase in temperature and was

significantly unchanged by a change in current density.

The effects on the particle inclusion density of the temperature, current density and stirring rate/density of material ratio are good evidence that the mechanism of the process of particle inclusion is "electrochemical". It is suggested that the process takes place in three main stages: firstly hydrodynamic transport of the particle to the outer Helmholtz plane on the cathode; secondly an electrophoretic transportation of the particle, under the high field within the double layer, through the double layer on the cathode to the cathode surface. As the particle passes through the outer to the inner Helmholtz plane its sheath of ions and water molecules will become distorted, as would happen to a solvated ion arriving at a plane surface (see section 6.1.). Finally the particle, now at the cathode surface, will be held against it by electrostatic attraction until keyed by metal. Conducting particles are likely to be more readily keyed into the metal matrix than are non-conductors; quartz particles are not readily included in copper deposits produced from acid baths having high micro throwing power, certainly not in the absence of cationic surfactants, even although the particles are transported to the cathode surface.

The results of this work have gone some way towards allowing prediction, from simple streaming measurements, of whether a particular ceramic/electrolyte combination should give good co-deposits or not. They have helped considerably in elucidating the mechanism of the process for a solution of high micro throwing power.

SUGGESTIONS FOR FUTURE WORK

Further knowledge, or confirmation, of the relationship between the following variables would be of value in the more complete understanding of the codeposition process.

1. The effect of other plating electrolytes of high micro-throwing power on the ceramics studied in this work

2. Current density effects

3. Variation in deposition characteristics of particles having similar electrical conductivities and densities but appreciable differences in zeta potential.

APPENDIX I

A1.1. Calculation of zeta potential from experimental results.

The zeta potential was calculated, as described in section 2.4. by means of the Helmholtz-Smoluchowski equation: for calculations from streaming potential this was

$$\zeta = \frac{I}{P} \times \frac{4\pi\eta K}{D}$$

K was measured, as described in section 3.1.5., in units of Ω^{-1} cm^{-1} and P was measured in cm of mercury. As the computer program, details of which are at the end of this appendix, was originally written for equations expressed in electrostatic units the following conversion factors were included:

$$1\ \Omega^{-1}\ cm^{-1} = 8.9816 \times 10^{11}\ esu$$

$$1\ cm\ mercury = 1.3332 \times 10^{4}\ dynes\ cm^{-2}$$

It was required that zeta potentials from streaming current data should be expressed in milivolts as were results from streaming potential data. The equation for calculation of zeta potential from streaming current measurements is

$$\zeta = \frac{I}{P} \times \left(\frac{r}{R} + 1\right) \times \frac{4\pi\eta}{D} \times \square \quad \text{as shown in section 2.4.2.}$$

Streaming current measurements are made in microamperes; it was required to use the same computer program to make the calculations as was used for calculations using potential data. The conversion factors used in the change from potential to current measurements were as follows

$$\zeta\ (mV) = \frac{I}{P}\ (mV) \times \frac{4\pi\eta}{D} \times K\ (\Omega^{-1} cm^{-1} \times 10^{-6}) \quad . \quad A1$$

$$\zeta\ (mV) = \frac{I}{P}\ (\mu A) \times \frac{4\pi\eta}{D} \times \square \times \Big(3.0 \times 10^{2} \times \underbrace{\quad}_{\text{(remove E}}$$

$$\underbrace{3.0 \times 10^{9}}_{\text{I to esu}} \times \underbrace{10^{-6}}_{\text{A to } \mu\text{A}} \times \underbrace{10^{3}}_{\substack{\text{V to mV} \\ \text{for } \zeta}} \times$$

$$\underbrace{\mu\Omega^{-1}\ 10^{6}\ \text{to}\ \Omega^{-1}}_{} \times \left.\begin{array}{l} \dfrac{10^{-11}}{9.0} \\ \text{removal} \\ \text{of K} \end{array}\right)$$

$$\zeta\ (mV) = \frac{I}{P}\ (\mu A) \times \frac{4\pi\eta}{D} \times \square \times 10^{3} \quad . \quad . \quad . \quad . \quad A2$$

Comparison of equations A1 and A2 shows that A1 has the form

$$\zeta = \frac{E}{P} \times C \times K \qquad \text{and that A2 has the form}$$

$$\zeta = \frac{I}{P} \times C \times \square \times 10^{3} \qquad \text{where C is a constant having}$$

the same value in each case and the other symbols have their usual meanings. Thus the computer program which is used for calculation of zeta potentials from streaming potential measurements can be used for the determination of zeta potentials directly from streaming current measurements by inserting, in place of the solution conductivity term, the value of $\square \times 10^{3}$ in the data fed into the computer.

A1.2. Variable terms in the Helmholtz-Smoluchowski equation.

A1.2.1. Viscosity.

The viscosity of water changes with addition of electrolyte and also with temperature change. As a very wide concentration range was used and also an appreciable temperature range the viscosities of the solutions used were measured using a simple viscometer. In practice they were not very different from the "literature" values for water at the same temperature.

A1.2.2. Dielectric coefficient

The dielectric coefficient of water changes with addition of electrolyte and with temperature. As it proved to be extremely difficult to obtain reliable and consistent results from dielectric coefficient measurements it was decided to use the bulk value for water at each of the temperatures used (see section 2.2. and ref. 1) This decision was justified by the fact that in the calculation for surface charge density the dielectric coefficient is eliminated.

A1.2.3. Conductivity.

The conductivity of the solutions used was determined as described in section 3.1.5.

```
      PROGRAM(WATT)
      INPUT2=CRO
      OUTPUT3,(MONITOR)=LPO
      TRACE
      END
      MASTERSHIP
      DIMENSION X(50),Y(50),R(50),W(50),A(9),P(150)
      WRITE(3,11)
11    FORMAT(49X,23HIPSWICH  CIVIC  COLLEGE//52X,16HCOMPUTER  CENTRE///
     146X,32HCALCULATION OF ZETA POTENTIAL OF)
      READ(2,14)
14    FORMAT(1H ,49X,30H                              )
      WRITE(3,14)
      READ (2,1)ETA, APPA,D
1     FORMAT(F0.0,F0.0,F0.0)
      READ (2,12) M
12    FORMAT(I2)
      NMAX=2
      MM=5*NMAX+2*M+3
      IF(M-50)10,10,90
10    WRITE(3,13) M,ETA,APPA,D
13    FORMAT(33X,5HFROM ,I2,46H STREAMING POTENTIAL AND PRESSURE MEASURE
     1MENTS///48X,16HFOR   ETA    =    ,F7.3//54X,10HKAPPA =    ,F7.3//54X,
     210HD      =    ,F7.3////58X,7HRESULTS///)
      DO 20 I=1,M
20    READ(2,2) X(I),Y(I)
2     FORMAT(F0.0,F0.0)
      P(1)= -1
      P(3)=  0
      P(4)=  1
      P(5)=  0
      DO 3 N=1,50
3     W(N)= 1.
      CALL F4CFORPL (M,NMAX,MM,X,Y,R,W,A,P)
      CALL F4CFORPL (M,NMAX,MM,X,Y,R,W,A,P)
      FACTOR=4*3.1416*8.9816E+11/1.3332E+4
      ZETA= A(2)*ETA* APPA*FACTOR/D
      ZETA= ZETA*1E-3*1E-6
      WRITE(3,30) ZETA,A(2),A(1)
30    FORMAT(33X,7HZETA =  , F11.7,15H MV     SLOPE =  ,   F7.3,16H     INTE
     1RCEPT =  ,F7.3/////////)
      STOP
90    WRITE(3,91)
91    FORMAT(///45X,20HTOO MANY DATA POINTS/////////)
      STOP
      END
      LIBRARY
      READ FROM (MT,-.FSCE)
      FINISH
```

Computer program used in the calculation of zeta potentials from streaming data.

APPENDIX II

DATA LAYOUT FOR CALCULATION OF ZETA POTENTIAL FROM STREAMING DATA.

When using the program shown in Appendix I the data was fed into the computer on cards using a data layout, with a separate card for each item, as follows

heading

viscosity of solution, conductivity, dielectric coefficient — on one card, in this order

number of readings in the set

corresponding values of P and E (or I), one card for each pair of readings.

The heading for each set of data was chosen such that it gave a "finger print" description of the particular diaphragm and solution, solution concentration, temperature and date.

A2.1. The diaphragm.

This was identified according to its composition and to which diaphragm of that composition it was e.g. the second diaphragm of quartz was given the "label" Q2 and the first silicon carbide diaphragm SICI.

A2.2. The solution composition.

The components of the solution were given in terms of chemical symbols e.g. a copper sulphate and sulphuric acid solution was distinguished by CUH.

N.B. The relative concentrations were constant at 1:1 molar.

A2.3. The solution concentration.

This was identified by a number between 1 and 9; total molar

concentrations were identified as follows.

8×10^{-6}	by 1
3.2×10^{-5}	by 2
1.28×10^{-4}	by 3
5.12×10^{-4}	by 4
2.05×10^{-3}	by 5
8.19×10^{-3}	by 6
3.28×10^{-2}	by 7
1.32×10^{-1}	by 8
5.28×10^{-1}	by 9

A2.4. The temperature.

This was simply stated as 25DEG for a solution used at 25°C.

A2.5. The date.

This was simply written in in full if required.

A particular heading could therefore be readily interpreted without need for further reference e.g. SIC2CUHI-910DEG refers to the second diaphragm of silicon carbide being streamed for the first time with a solution of copper sulphate and sulphuric acid of concentration 0.528 molar at a temperature 10°C.

APPENDIX III

STATISTICAL TREATMENT OF EXPERIMENTAL RESULTS

Example of a calculation of confidence limits.

Consider a sample of three points 12, 16, 20.

The unbiased estimate of the population mean in this case

$$= \frac{12 + 16 + 20}{3}$$ which is the Sample Mean

$$= 16$$

Range of the sample $20 - 12 = 8$

Estimate of the standard deviation of the whole population

$$= \text{Range of the sample} \times a_3$$

$$= 8 \times 0.5908$$

$$= 4.73$$

Estimate of standard deviation of sample means

$$= \frac{4.73}{\sqrt{3}}$$

$$= 2.72$$

95% confidence limits for the population mean:

Sample Mean $\pm$ t_2 x standard deviation of sample mean

$$= 16 \pm 4.3 \times 2.72$$

$$= 16 \pm 11.6$$

a_3 is a factor relating the range to the standard deviation as a function of the number of items in the sample.

t_2 is "Student's" t variate with two degrees of freedom

Factors a_3 and t_2 were obtained from "Cambridge Elementary Statistical Tables".

APPENDIX IV

EXPERIMENTAL RESULTS

A4.1. Zeta potential on silicon carbide.

A4.1.1. Zeta potential from streaming potential measurements.

Title	K_c	ζ	ζ_{mean}	Range	Limits of variation for 95% confidence
S1C2CUH1 -10DEG					
3	33.3	-18.8	-18.9	0.5	0.4
		-19.0			
		-18.7			
		-19.2			
4	93.3	- 5.7	- 5.9	1.7	1.3
		- 5.2			
		- 6.9			
		- 5.9			
5	374	0.65	0.67	0.05	0.04
		0.68			
		0.70			
		0.65			
6	1251	148	158	11	16
		168			
		159			
7	4654	942	949	12	17.6
		951			
		954			
8	12660	3592	3592	0	0
		3592			
9	42500	16500	16920	920	1350
		17420			
		16750			

Missing page(s) from the bound copy

Title	K_c	δ	δ_{mean}	Range	Limits of variation for 95% confidence.
S1C1CUH4 -25DEG					
3	19.2	-24.5	-24.5	0	0
		-24.5			
4	129	- 7.89	- 7.93	0.08	0.1
		- 7.97			
		- 7.94			
6	1570	132	132	1	8
		131			
7	4980	720	755	55	81
		775			
		769			
8	15170	3177	2962	446	654
		2977			
		2731			
9	45830	11850	11414	740	572
		11260			
		11110			
		11440			

Title	K_c	δ	δ mean	Range	Limits of variation for 95% confidence.
S1C1CUH1 -25DEG					
3	33.7	-18.7	-18.7	0.7	1.0
		-18.3			
		-19.0			
4	130	- 7.2	- 7.2	0	0
		- 7.2			
5	476	- 2.2	- 1.96	0.5	0.15
		- 1.7			
		- 2.1			
		- 1.7			
		- 2.2			
		- 2.1			
		- 1.7			
		- 2.1			
S1C1CUH3 -25DEG					
3	34	-19.7	-18.8	1.5	1.2
		-19.0			
		-18.2			
		-18.3			
4	132	- 7.7	- 7.7	0.3	0.23
		- 7.5			
		- 7.6			
		- 7.8			
5	474	- 2.1	- 2.03	0.5	0.15
		- 1.8			
		- 2.1			
		- 1.8			
		- 2.2			
		- 1.7			
		- 2.2			
		- 2.2			

Title	K_c	δ	δ_{mean}	Range	Limits of variation for 95% confidence.
S1C1CUH2 -4.0DEG					
3	42.9	-19.6	-20.2	1.1	0.84
		-20.5			
		-20.0			
		-20.7			
4	164	- 9.2	- 9.2	0.7	0.54
		- 8.9			
		- 9.3			
		- 9.6			
5	550	- 2.8	- 3.02	0.4	0.1
		- 3.2			
		- 2.9			
		- 2.8			
		- 3.0			
		- 3.3			
		- 3.2			
		- 2.8			
6	1750	63	70.2	19	10
		63			
		63			
		71			
		78			
		82			
7	5333	548	550	4	32
		552			
8	16670	2830	2793	60	88
		2770			
		2780			

Title	K_c	ζ	ζ_{mean}	Range	Limits of variation for 95% confidence.
S1C1CUH1 -4.0DEG					
3	43.2	-20.7	-20.8	0.5	0.7
		-20.6			
		-21.1			
4	163	- 9.2	- 9.0	0.6	0.9
		- 9.2			
		- 8.6			
5	536	- 3.3	- 3.31	0.9	0.3
		- 3.3			
		- 3.3			
		- 3.6			
		- 3.2			
		- 3.2			
		- 2.7			
		- 3.4			

Title	K_c	δ	δ_{mean}	Range	Limits of variation for 95% confidence.
S1C1CUH3 -55DEG					
3	39	-24.7	-25.6	1.2	0.9
		-25.9			
		-25.8			
		-25.9			
4	187	-11.7	-11.9	0.4	0.6
		-12.1			
		-11.9			
5	642	- 5.2	- 5.35	0.9	0.5
		- 4.8			
		- 5.7			
		- 5.4			
		- 5.7			
6	1933	27.2	29.3	5.0	3.9
		32.2			
		29.6			
		28.0			
7	5670	370	382	23	18
		380			
		393			
		380			
8	17670	2228	2198	91	70
		2189			
		2233			
		2142			

Title	K_c	δ	δ_{mean}	Range	Limits of variation for 95% confidence.
S1C1CUH4 -55DEG					
3	51.7	-25.0	-25.1	1.9	1.5
		-24.2			
		-26.1			
		-25.1			
4	178	-13.3	-13.35	0.1	0.8
		-13.4			
5	630	- 6.9	- 6.97	0.6	0.3
		- 7.3			
		- 6.7			
		- 6.9			
		- 6.9			
6	1930	57.0	48.9	25.3	19.5
		60.3			
		35.0			
		43.3			
7	5500	377	351	102	79
		375			
		325			
		326			
9	52080	7680	7694	50	39
		7690			
		7675			
		7725			

Title	K_c	δ	δ_{mean}	Range	Limits of variation for 95% confidence.
S162CUH1 -7ODEG					
3	59.3	-25.3	-25.5	0.4	3.2
		-25.7			
4	187.5	-19.8	-19.1	1.4	2.1
		-18.4			
		-19.1			
5	717	-11.5	-11.0	0.9	0.37
		-11.5			
		-11.5			
		-10.6			
		-10.6			
		-10.6			
6	2117	22.7	21.7	1.7	0.7
		22.1			
		21.6			
		21.0			
		21.6			
		21.0			
7	5917	269	275	16	23
		295			
		269			
8	19170	1133	1157	50	73
		1193			
		1153			
9	55170	5500	5429	33	48
		5500			
		5467			

4.1.2. Zeta potential from streaming current measurements.

Title	Cell constant	K_c	ζ	ζ_{mean}	Range	Limits of variation for 95% confidence.
C1C2CUH1 -1ODRG 3	14.8	33.3	-48.1 -53.3 -49.4	-50.3	5.2	7.6
4		93.3	-28.9 -26.8 -27.6	-27.8	2.1	3.1
5		374	2.3 2.2 2.2	2.2	0.1	0.15
6		1251	232 241 235	236	9	13
7		4654	1118 1114 1120	1117	6	8.8
8		12660	4810 4720 4850	4813	70	103

Title	Cell constant	K_c	δ	δ_{mean}	Range	Limits of variation for 95% confidence.
S1C2CUH -7CDEG						
3	14.8	59.3	-51.3	-50.9	0.5	0.75
			-49.9			
			-51.4			
4	14.8	188	-30.2	-30.2	0.5	0.75
			-29.9			
			-30.4			
5	14.8	718	-12.5	-12.3	0.6	0.9
			-11.9			
			-12.4			
6	14.8	2116	24.3	23.9	0.6	0.9
			23.6			
			23.8			
7	14.8	5930	275	269	13	19
			262			
			270			
8	14.8	19160	1240	1245	31	45
			1263			
			1232			

4.2 Surface charge density on silicon carbide

Title	Double-layer thickness d in cm.	ζ in mV within 95% confidence		Charge density $-2q$ in coulombs m	
		potential	current	potential	current
S1C2CUH -10DEG					
3	135	-19.2	-42.9	-0.00769	-0.0172
4	91.9	- 5.8	-24.5	-0.00466	-0.0197
5	46.0	0.7	2.4	0.00113	0.00386
6	23.0	154	226	0.496	0.727
7	11.6	932	1111	5.95	7.09
8	5.74	3590	4870	46.3	62.8
9	2.86	15750	-	408	-

Title	Double-layer thickness d in cm.	ζ in mV within 95% confidence potential	Charge density $y_2 q$ in coulombs m potential
S1C1CUH1 -25DEG			
3	185	-19.7	-0.00736
	91.9	- 7.2	-0.00543
	46.0	- 2	-0.0030
S1C1CUH3 -25DEG			
3	185	-20	-0.00749
4	91.9	- 8	-0.00603
5	46.0	- 2	-0.0030
S1C1CUH4 -25DEG			
3	185	-24.5	-0.00916
4	91.9	- 8	-0.00603
6	23.0	139	0.418
7	11.6	730	4.31
8	5.74	3210	38.3
9	2.86	11670	257
S1C1CUH3 -40DEG			
3	185	-20.8	-0.00726
4	91.9	- 9.8	-0.00689
5	46.0	- 3.1	-0.00436

Title	Double-layer thickness d in cm.	ζ in mV within 95% confidence potential	Charge density $y_2 q$ in coulombs m potential
S1C1CUH2 -40DEG			
3	185	-20.8	-0.00726
4	91.9	- 9.8	-0.00689
5	46.0	- 3.1	-0.00436
6	23.0	70.8	0.199
7	11.6	544	3.0
8	5.74	2750	29.7
S1C1CUH3 -55DEG			
3	185	-25.0	-0.00816
4	91.9	-12.5	-0.00819
5	46.0	- 5.8	-0.00792
6	23.0	45.8	0.119
7	11.6	398	2.05
8	5.74	2130	21.7
S1C1CUH4 -55DEG			
3	185	-25.0	-0.00816
4	91.9	-12.6	-0.00826
5	46.0	- 6.7	-0.00879
6	23.0	29.3	0.0761
7	11.6	398	2.05
9	2.86	7730	145

Title	Double-layer thickness d in cm.	ζ in mV within 95% confidence		Charge density $-2q$ in coulombs m	
		potential	current	potential	current
S1C2CUH1 -70DEG					
3	185	-28.3	-50.9	-0.00862	-0.0155
4	91.9	-20.0	-30.2	-0.0123	-0.0185
5	46.0	-11.2	-12.3	-0.0137	-0.0151
6	23.0	22.4	23.9	0.0549	0.0586
7	11.6	260	269	1.27	1.31
8	5.74	1230	1245	11.6	11.7
9	2.86	5500	-	97.6	-

A4.3 Zeta potential on quartz.

A4.3.1. Zeta potential from streaming potential measurements.

Title	K_c	ζ	ζ_{mean}	Range	Limits of variation for 95% confidence.
Q1CUH1 -1CDEG					
3	27	-19.3 -19.5	-19.4	0.2	1.6
4	93.3	-12.0 -12.0	-12.0	0	0
5	374	- 1.62 - 1.62 - 1.62	- 1.62	0	0
6	1334	158 162 160	160	4	5.9
7	4580	1125 1125 1125	1125	0	0
8	13660	4620 4660 4640	4640	40	59
9	42640	22500 22500	22500	0	0

Title	K_c	δ	δ_{mean}	Range	Limits of variation for 95% confidence.
Q1CUH1 -25DEG					
3	35.6	-21.4 -21.4 -21.4	-21.4	0	0
4	133	-13.9 -13.9 -14.0	-13.9	0.1	0.147
5	460	- 6.6 - 6.4 - 7.2	- 6.7	0.8	1.32
6	1542	125 125 125 125	125	0	0
7	4990	910 922	916	12	96
8	14920	3430 3500 3400	3460	70	102
9	32500	18400 18150 18300	18280	250	370

Title	K_c	δ	δ_{mean}	Range	Limits of variation for 95% confidence.
21CUH1 -40DEG					
3	44.5	-23.5 -23.2 -24.3 -23.5	-23.6	1.1	0.85
4	165	-15.7 -16.6 -16.5	-16.2	0.9	1.32
5	546	- 9.8 - 9.7 - 9.8 -10.0	- 9.8	0.3	0.23
6	1750	82.3 83.2 82.3	82.6	0.9	1.32
7	5510	662 647 654	654	15	22
8	16330	2650 2730 2690	2690	80	117
9	49140	13750 14080 13150	13660	930	1360

Title	K_c	δ	δ_{mean}	Range	Limits of variation for 95% confidence.
91CUH1 -55DEG					
3	53.3	-27.6 -27.7	-27.7	0.2	1.59
4	195	-20.7 -20.1 -20.2 -20.3	-20.3	0.6	0.5
5	629	-16.2 -17.7 -17.7	-17.2	1.5	2.2
6	1958	48.3 50.8 50 50.8	50.2	2.5	1.9
7	5590	394 380 392 387	388	14	11
8	17650	2033 1983 2007	2008	50	73
9	52260	9092 9125 9104	9107	33	48

Title	K_c	δ	δ_{mean}	Range	Limits of variation for 95% confidence.
01CUH1 -70DEG					
3	65	-29.3 -29.3 -29.3	-29.3	0	0
4	228	-23.5 -24.1 -23.5 -24.0	-23.7	0.5	0.4
5	718	-20.8 -20.9 -19.9	-20.6	1.0	1.5
6	1875	20.8 20.7 20.9	20.8	0.2	0.29
7	5928	225 227	226	2	16
8	19010	1417 1417	1417	0	0
9	55120	5950 5953 5962	5958	9	13

A4.3.2. Zeta potential from streaming current measurement

Title	Cell constant	K_c	ζ	ζ_{mean}	Range	Limits of variation for 95% confidence.
21CUH1 -10DEG						
3	18.2	27.0	-58.5 -59.0 -58.8	-58.8	0.5	0.7
4		93.3	-37.4 -38.7 -36.7	-37.6	2.0	2.9
5		374.4	- 5.54 - 4.99 - 5.82	- 5.45	0.83	1.2
6		1334	119.6 118 119.6	119	1.6	2.3
7		4580	681 676	679	5	7.3
8		13660	3510 3510 3480	3500	30	44
9		42640	21970 21870 22060	21970	190	279

Title	Cell constant	K_c	δ	δ_{mean}	Range	Limits of variation for 95% confidence.
Q1CUH1 -25DEG						
3	18.2	35.6	-61.6 -61.1 -60.6	-61.1	1.0	1.5
4		133	-37.3 -37.2 -38.2 -38.5 -39.3	-38.1	2.1	1.1
5		460	-10.9 -10.4 -11.4	-10.9	0.5	0.73
6		1542	104 107 103 101	104	6	4.6
7		4990	532 504 520	519	28	41
8		14920	2780 2704 2730 2652	2718	128	99
9		32500	15470 15600 15760	15610	290	425

Title	Cell constant	K_c	δ	δ_{mean}	Range	Limits of variation for 95% confidence
31CUH1 -40DEG						
3	18.2	44.5	-63.7 -66.3 -64.2	-64.7	2.6	3.8
4		165.1	-44.2 -45.5 -43.2	-44.3	3.3	4.8
5		546	-18.2 -16.9 -17.7	-17.6	1.3	1.9
6		1750	88.4 86.1 90.5	88.3	4.4	6.5
7		5510	429 421 434	428	13	19
8		16330	2160 2110 2200	2157	90	132
9		49140	12740 12550 13000	12760	450	660

Title	Cell constant	K_c	δ	δ_{mean}	Range	Limits of variation for 95% confidence.
Q1CUH1 -55DEG						
3	18.2	53.3	-67.6 -66.6 -65.8	-66.7	1.8	2.6
4		195	-47.3 -51.2 -49.4	-49.3	3.9	5.7
5		629	-23.4 -23.4 -25.5	-24.1	2.1	3.1
6		1958	62.4 63.7 61.9	62.7	1.8	2.6
7		5590	351 361 360	357	10	14.7
8		17650	1794 1790 1801	1795	11	16
9		52260	11180 11140 11210	11180	70	103

Title	Cell constant	K_c	δ	δ_{mean}	Range	Limits of variation for 95% confidence
C1CUH1 -70DEG						
3	18.2	65	-65 -66.8 -64.2	-65.3	2.6	3.8
4		228	-46.9 -51.2 -51.5	-49.7	5.0	7.3
5		718	-30.9 -30.2 -31.5	-30.9	1.3	1.9
6		1875	46.8 49.4 44.5	46.9	4.9	7.2
7		5928	265 273 268	269	8	11.7
8		19010	1430 1420 1430	1427	10	14.7
9		55120	6236 6236 6236	6236	0	0

4.4. Surface charge density on quartz.

Title	Double-layer thickness d in cm.	ζ in mV within 95% confidence		Charge density $_2$q in coulombs m	
		potential	current	potential	current
21CUH1 -10DEG					
3	185	-18.3	-58.7	-0.00733	-0.0236
4	91.9	-12.0	-34.8	-0.00966	-0.0280
5	46.0	- 1.62	- 5.2	-0.00260	-0.00836
6	23.0	158	121	0.508	0.39
7	11.6	1125	681	7.18	4.35
8	5.74	4698	3540	60.4	45.7
9	2.86	22500	22200	582	314
21CUH1 -25DEG					
3	185	- 21.4	-59.8	-0.00799	-0.0223
4	91.9	-14.0	-39.0	-0.0105	-0.0293
5	46.0	- 7.6	-10.2	-0.0114	-0.0151
6	23.0	125	108	0.376	0.323
7	11.6	820	535	4.84	3.16
8	5.74	3390	2805	41.4	34.9
9	2.86	17900	16030	394	353
21CUH1 -40DEG					
3	185	-24.1	-67.6	-0.00842	-0.0236
4	91.9	-17.2	-48.0	-0.0241	-0.0336
5	46.0	-10.0	-17.8	-0.0141	-0.0250
6	23.0	83.9	83.9	0.236	0.236
7	11.6	635	447	3.5	2.46
8	5.74	2750	2280	29.7	24.6
9	2.86	12800	13200	257	265

Title	Double-layer thickness d in cm.	ζ in mV within 95% confidence		Charge density q_2 in coulombs m	
		potential	current	potential	current
21CUH1 -55DEG					
3	185	-27.5	-68.7	-0.00896	-0.0224
4	91.9	-20.8	-52.0	-0.0137	-0.0341
5	46.0	-15.0	-26.0	-0.0197	-0.0341
6	23.0	48.3	64.2	0.126	0.167
7	11.6	375	351	1.93	1.81
8	5.74	1980	1801	20.2	18.4
9	2.86	9107	11280	171	212
21CUH1 -70DEG					
3	185	-29.3	-68.9	-0.00892	-0.0210
4	91.9	-24.0	-57.0	-0.0147	-0.0350
5	46	-20.4	-32.1	-0.0250	-0.0394
6	23	21.1	44.2	0.0517	0.108
7	11.6	242	266	1.17	1.28
8	5.74	1417	1425	13.4	13.4
9	2.86	5945	6236	106	111

A.5 Zeta potential on chromium diboride from streaming potential measurements.

Title	K_c	ζ	ζ_{mean}	Range	Limits of variation for 95% confidence.
CRB1CUH2 -25DEG					
3	35.0	10.1	10.1	0.1	.08
		10.1			
		10.1			
		10.2			
5	450	321	314	11	16
		312			
		310			
6	1500	1008	1027	81	63
		1068			
		987			
		1045			
7	4917	4647	4714	135	198
		4714			
		4782			
8	14580	17360	17510	310	455
		17670			
		17490			
9	49330	71210	70370	1460	2140
		69750			
		70170			

Title	K_c	δ	δ_{mean}	Range	Limits of variation for 95% confidence.
CRB1 CUH1 -40DEG					
3	43.9	10	9.79	0.7	0.5
		10			
		9.3			
		9.8			
5	533	205	203	0.3	0.23
		203			
		203			
		202			
6	1750	751	753	6	8.8
		757			
		751			
7	5167	2767	2742	42	32
		2742			
		2725			
		2733			
8	16670	12580	12640	170	250
		12580			
		12750			
9	54670	43330	43970	1170	1720
		44500			
		44080			

Title	K_c	δ	δ_{mean}	Range	Limits of variation for 95% confidence.
CRB1CUH1 -55DEG					
3	52.5	9.1 9.3 7.2 7.8	8.4	2.1	1.6
4	200	23.6 23.6 25.0	24.2	1.4	2.1
5	617	116 116 116	116	0	0
6	1930	483 476 450 483	475	25	19
7	5500	1325 1375 1375	1358	50	73
8	18330	9000 9167 8830	9000	337	495
9	58670	37080 36920 36830	36940	150	220

Title	K_b	δ	δ_{mean}	Range	Limits of variation for 95% confidence.
CRB1CUH2 -25DEG					
1	3.92	-1.9 -2.3 -2.2 -2.3	-2.18	0.4	0.31
2	11	4.4 4.7 4.6 4.6	4.6	0.3	0.23
3	42	12.1 12.1 12.1 12.2	12.1	0.1	0.077
4	160	88 85 86	86	3	4.4
5	540	385 374 372	377	13	19.1
6	1800	1210 1282 1184 1254	1233	98	75.7
7	5800	5576 5657 5738	5657	162	125
8	17500	20230 21200 20990	21007	370	543
9	59200	85450 83700	84450	1700	1352

Title	K_b	ζ	ζ_{mean}	Range	Limits of variation for 95% confidence
CRB1CUH1 -40DEG					
1	5.2	-2.55	-2.62	0.25	0.37
		-2.75			
		-2.55			
2	14	4.25	4.25	0.1	0.08
		4.3			
		4.2			
		4.25			
3	52.8	12	11.75	0.8	0.62
		12			
		11.2			
		11.8			
4	200	62	60	4	3.1
		60			
		57			
		59			
5	640	246	244	4	3.1
		244			
		244			
		242			
6	2100	901	904	8	6.2
		909			
		901			
7	6200	3320	3290	50	38.6
		3290			
		3270			
		3260			
8	20000	15100	15170	200	154
		15100			
		15300			

Title	K_b	δ	δ_{mean}	Range	Limits of variation for 95% confidence
CRB1CUH1 -4CDEG					
9	65600	52000	52770	1400	1080
		53400			
		52900			

Title	K_b	δ	δ_{mean}	Range	Limits of variation for 95% confidence
CRB1CUH1 -55DEG					
1	6.2	-2.4 -2.5 -2.6	-2.5	0.2	0.29
2	17	3.5 3.45 3.3 3.45 3.35 3.35	3.4	0.2	0.083
3	63	10.9 11.2 8.7 9.4	10.1	2.5	1.9
4	240	38.3 38.3 40.0	39.0	1.7	2.49
5	740	139 139 139	139	0	0
6	2320	580 571 550 580	570	30	23.2
7	6600	1590 1650 1650	1630	60	88
8	22000	10800 11000 10600	10800	400	587
9	70400	44500	44330	300	440

A4.6 Surface charge density on chromium diboride from streaming potential measurements.

Title	Double-layer thickness d in cm.	ζ in mV within 95% confidence	Charge density $_2$q in coulombs m
CRB1CUH2 -25DEG			
3	185	10.2	0.00381
5	46.0	298	0.448
6	23.0	1085	3.26
7	11.6	4670	27.8
8	5.74	17170	207
9	2.86	71700	1578
CRB1CUH1 -40DEG			
3	185	9.29	0.00324
5	46.0	203	0.285
6	23.0	761	2.14
7	11.6	2750	15.3
8	5.74	12490	135
9	2.86	45690	918
CRB1CUH1 -55DEG			
3	185	6.8	0.00222
4	91.9	26.3	0.0173
5	46.0	116	0.152
6	23.0	456	1.18
7	11.6	1430	7.36
8	5.74	8510	56.8
9	2.86	36820	691

A4.7 Zeta potential on silicon carbide in alkaline solution from streaming potential measurements.

Title	K_c	ζ	ζ_{mean}	Range	Limits of variation for 95% confidence
S1C3KCL1 -25DEG					
2	12.6	-122 -121 -121	-121	1	1.5
3	24.8	-179 -175 -161 -129 -123	-153	56	30
4	57.7	-76.2 -75.9 -75.9	- 76	0.3	0.4
5	252	-80.6 -80.3 -79.8 -79.0	-79.9	1.6	2.4
6	1050	-67.1 -67.1 -64.5 -63.4	-65.5	3.7	2.9
7	4290	Indeterminable owing to violent fluctuation from +ve to -ve			
8	13600	884.0 902.0 951.0	905.7	31.0	45.5
9	53170	25800 17920 18430	20650	7880	1130

A4.8 Surface charge density on silicon carbide in alkaline solution from streaming potential measurements.

Title	Double-layer thickness d in cm.	ζ in mV within 95% confidence	Charge density σ_2 in coulombs m^{-2}
SIC3KOH1 -25DEC			
3	34.8	-153	-0.0304
4	175	-76.4	-0.0302
5	87	-77.4	-0.0615
6	43.7	-66.5	-0.104
8	10.9	906	5.75
9	5.43	2065	26.3

A.9. Zeta potential on quartz in alkaline solution from streaming potential measurements.

Title	K_c	ζ	ζ_{mean}	Range	Limits of variation for 95% confidence.
21AUG1 -25DEC					
2	13.0	-127 -126	-127	1	8
3	27.0	-101 -102 -102	-102	1	1.5
4	84.5	-64.2 -64.2 -64.0	-64.1	0.2	0.3
5	343.2	-62.7 -63.7 -64.2	-63.5	1.5	2.2
6	1420	-62.4 -62.4 -62.4	-62.4	0	0
7	5460	-46.0 -47.3 -48.6	-47.3	2.6	3.8
8	20200	506 509 474	496	35	52
9	79260	2260 2675 2260 2260	2366	415	321

Title	K_c	$\mathcal{E}$	$\mathcal{E}_{mean}$	Range	Limits of variation for 95% confidence
92KOH1 -25DEG					
2	13.0	-127 -121 -127 -120	-124	7	5.4
3	28.3	-101 -101 -102	-101	1	1.5
4	85.3	-64.7 -65.3 -67.3	-65.8	2.6	3.8
5	347	-62.7 -63.4 -64.0	-63.4	1.3	1.9
6	1420	-63.2 -62.7 -63.7 -63.4	-63.0	1.3	1.0
7	5480	-28.3 -27.6 -30.9 -25.7	-28.1	5.2	4.0
8	20267	509 475 450 433	497	119	92
9	73550	2515 2310 2230 2736 2311	2562	550	294

4.10 Surface charge density on quartz in alkaline solution from streaming potential measurements.

Title	Double-layer thickness δ in cm.	ζ in mV within 95% confidence	Charge density σ_2 in coulombs m^{-2}
01KOH1 -25DEG			
2	697	-129	-0.0128
3	348	-103	-0.0205
4	175	-64.2	-0.0254
5	87	-63.5	-0.0505
6	43.7	-62.4	-0.0988
7	21.8	-43.5	-0.138
8	10.9	444	2.82
9	5.43	2690	343
02KOH1 -25DEG			
2	697	-129	-0.0128
3	348	-102.5	-0.0204
4	175	-64.2	-0.0254
5	87	-63.5	-0.0505
6	43.7	-63.2	-0.0988
7	21.8	-39.1	-0.102
8	10.9	444	2.82
9	5.43	2700	344

A4.11 Zeta potential on silicon carbide in copper sulphate solution from streaming potential measurements.

Title	K_b	ζ	ζ_{mean}	Range	Limits of variation for 95% confidence.
31C1CUL -25DEG					
1	4.9	-40.4 -40.4 -40.4	-40.4	0	0
2	10.2	-30.6 -30.6 -30.6	-30.6	0	0
3	31.8	-21.1 -21.3 -21.1 -21.2	-21.2	0.2	0.15
4	110.4	-11.0 -11.3 -11.6 -11.7 -11.5	-11.4	0.7	0.37
5	328	- 6.0 - 6.1 - 6.3 - 6.3	- 6.2	0.3	0.24
6	1051	53.1 53.3 52.7 52.9	53	0.6	0.5

A4.12. Zeta potential on silicon carbide in sulphuric acid solutions from streaming potential measurements.

Title	K_b	ζ	ζ_{mean}	Range	Limits of variation for 95% confidence
S1C1H1 -25DEG					
1	3.44	-29.4 -29.8 -29.2 -29.5	-29.5	0.6	0.5
2	12.8	-29.5 -28.1 -26.2 -24.0	-27.0	9.5	7.5
3	51.6	-19.5 -19.7 -19.5 -19.6	-19.7	0.4	0.3
4	200	-11.0 -10.5 -11.5 -10.3	-10.8	1.2	0.9
5	798	- 3.5 - 3.8 - 3.2 - 3.4	- 3.5	0.6	0.46
6	3103	61 66 65 63 68	65	8	4

A4.13 Temperature and surface charge density values, for quartz and silicon carbide, used in the calculation of heats of ion adsorption.

Q1CUH

	T	$\frac{1}{T}$	q	$\log_{10}q$
0.1M	283	3.53×10^{-3}	1205×10^{3}	6.0810
	298	3.36×10^{-3}	795×10^{3}	5.9004
	313	3.2×10^{-3}	545×10^{3}	5.7364
	328	3.05×10^{-3}	355×10^{3}	5.5502
	343	2.9×10^{-3}	235×10^{3}	5.3711
0.01M	283	3.53×10^{-3}	25.5×10^{3}	4.4065
	298	3.36×10^{-3}	16.5×10^{3}	4.2175
	313	3.2×10^{-3}	10.8×10^{3}	4.0334
	328	3.05×10^{-3}	6.1×10^{3}	3.7853
	343	2.9×10^{-3}	3.2×10^{3}	3.5051
0.3M	283	3.53×10^{-3}	7400×10^{3}	6.8692
	298	3.36×10^{-3}	4700×10^{3}	6.6721
	313	3.2×10^{-3}	3100×10^{3}	6.4914
	328	3.05×10^{-3}	2050×10^{3}	6.3118
	343	2.9×10^{-3}	1300×10^{3}	6.1139

S1C CUH

0.1M	283	3.53×10^{-3}	960×10^{3}	5.982
	298	3.36×10^{-3}	690×10^{3}	5.839
	313	3.2×10^{-3}	495×10^{3}	5.695
	328	3.05×10^{-3}	330×10^{3}	5.519
	343	2.9×10^{-3}	230×10^{3}	5.362
0.01M	283	3.53×10^{-3}	21.5×10^{3}	4.332
	298	3.36×10^{-3}	15.0×10^{3}	4.176
	313	3.2×10^{-3}	9.1×10^{3}	3.959
	328	3.05×10^{-3}	5.3×10^{3}	3.724
	343	2.9×10^{-3}	3.2×10^{3}	3.505

S1C CUH
(continued)

	T	$\frac{1}{T}$	q	$\log_{10} q$
0.3M	283	3.53×10^{-3}	5605×10^{3}	6.749
	298	3.36×10^{-3}	4100×10^{3}	6.613
	313	3.2×10^{-3}	2940×10^{3}	6.468
	328	3.05×10^{-3}	1800×10^{3}	6.255
	343	2.9×10^{3}	1230×10^{3}	6.090

APPENDIX V

CALCULATION OF MAXIMUM EXPERIMENTAL ERROR

Conductivity K

Accuracy of the bridge used, at full scale deflection ± 1%

There was no noticeable drift.

Temperature

The temperature of solution entering the cell was controlled to ± 0.5°C; the temperature fell as the solution passed through the cell, the fall being greatest at the highest operating temperature, i.e. 2°C at 70°C. This would give an error

in D of ±1 on 64 ± 1.5%

and in η of ± 0.1 on 4 ± 2.5%

Pressure P

This was measured directly: 1 in 100 for P = 1 ± 1%

1 in 2000 for P = 20

Streaming potential E

The potentiometer used had an error of 0.02% and there was no noticeable drift. The error was considered to be negligible (in fact at the point of zero charge any error in the reading would be infinitely great but only at this exact point).

Permeability

The use of granular material should have given constant permeability to solution flow: certainly no variation in streaming activity was observed.

Total error in calculated ζ ± 6%

N.B. Relative errors are added when the quantities are to be multiplied or divided. A theoretical justification of this is given, for example, by Butler and Kerr.[96]

It is possible that slight errors could arise from the following factors but these were considered to be negligible for the reasons stated.

Polarisation of the platinum electrodes.

This was considered to be negligible as when streaming pressure was reduced to zero the emf very quickly fell to zero; there was no back swing.

Mat effects.

Whatman 541 paper was used as mat material throughout and any mat effect was therefore a constant factor. Measurement of the electrokinetic activity of the mat in the absence of a diaphragm showed it to be consistently 0.5% of that of the diaphragm and it was therefore neglected.

Carbon dioxide uptake by water used for streaming solutions.

This was prevented, during storage, by a soda-lime trap. During streaming the solutions were exposed to air: no conductivity change was detected at the end of the period of a streaming run.

Leaching of salts from the glass.

This was minimised by soaking the glass in acid followed by steaming out. The method was described in section 3.2.1.

Limits of experimental error.

The total maximum error in the calculated value of the zeta potential is, to the nearest whole number $\pm$ 6%. The error is greatest at the lowest values of hydrostatic pressure and at the highest operating temperatures.

APPENDIX VI

SEPARATION OF REQUIRED SIZE RANGES OF POWDERS BY WATER ELUTRIATION

Of the materials studied only silicon carbide could be purchased in suitable narrow size ranges; the only supplies of quartz and chromium diboride obtainable were of -300 mesh, i.e. from 52 μm to dust.

Powder of 37 μm mean diameter was required for streaming studies and of 4.5 μm mean diameter for deposition. Of these two the fine material was by far the most difficult to separate. For both separations water elutriation was used. For the coarse material a very satisfactory separation was achieved using a "Rapid Laboratory Elutriator", (Griffin and George Ltd.) which was a two vessel instrument and was supplied complete with particle size/flow rate tables. This elutriator was unable to separate powders of as small a size as 4.5 μm and it was modified considerably by the addition of two larger vessels, in which lower flow rates could be achieved. The modified elutriator is shown schematically in fig. A6.1. By graphical extrapolation of the particle size/flow rate data given in the supplied tables, see fig. A6.2., it was shown that the flow rate required to separate quartz powder (specific gravity 2.65) in the size range 4-5 μm was 0.07 mm sec^{-1}. This flow rate was achieved in the 4^{th} vessel by a volume flow of 1.8 cm^3 sec^{-1} and the various vessels retained particles with size ranges as follows: second vessel above 0.012 μm, third vessel 0.0055-0.012 μm, fourth vessel 0.0035-0.0055 μm. Particles of size less than 0.0035 μm were carried over from the fourth vessel. The effectiveness of the separation achieved using this apparatus was verified by using a microscope with a suitable graticule eyepiece and a stage micrometer.

Materials which had densities greater than 2.65 were separated in exactly the same way as was the quartz. The water flow rate

was increased to compensate for the increased density according to the relationship

$$\frac{V_1}{V_2} = \frac{(S_1 - S_{H_2O})}{(S_2 - S_{H_2O})}$$

where V_2 was the velocity for separation of the required size of quartz powder; V_1 was the velocity for obtaining the same size of the powder under test; S_2, S_{H_2O} and S_1 were the specific gravities of quartz, water and the material to be separated respectively.

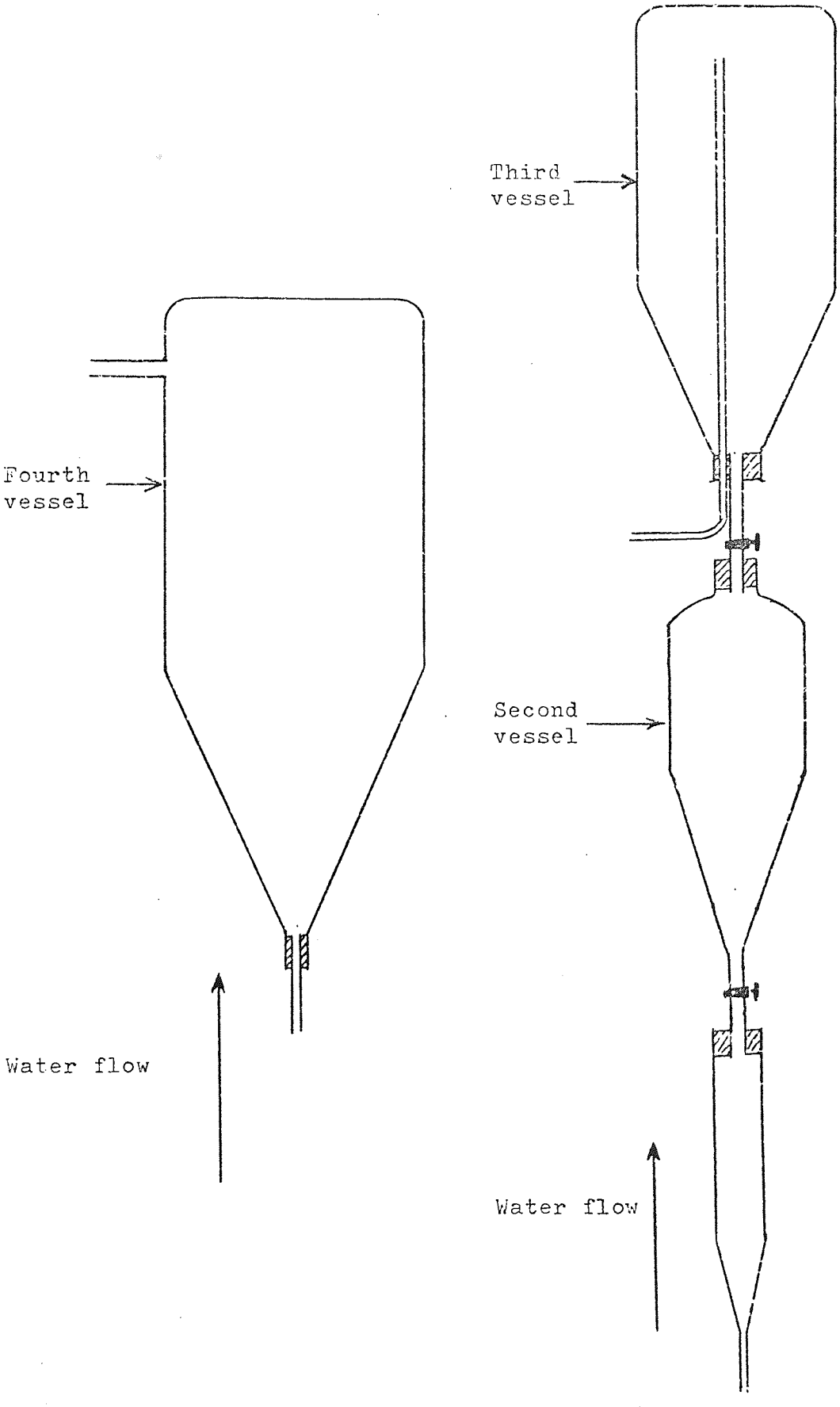

Fig. A6.1. Schematic diagram of elutriator.

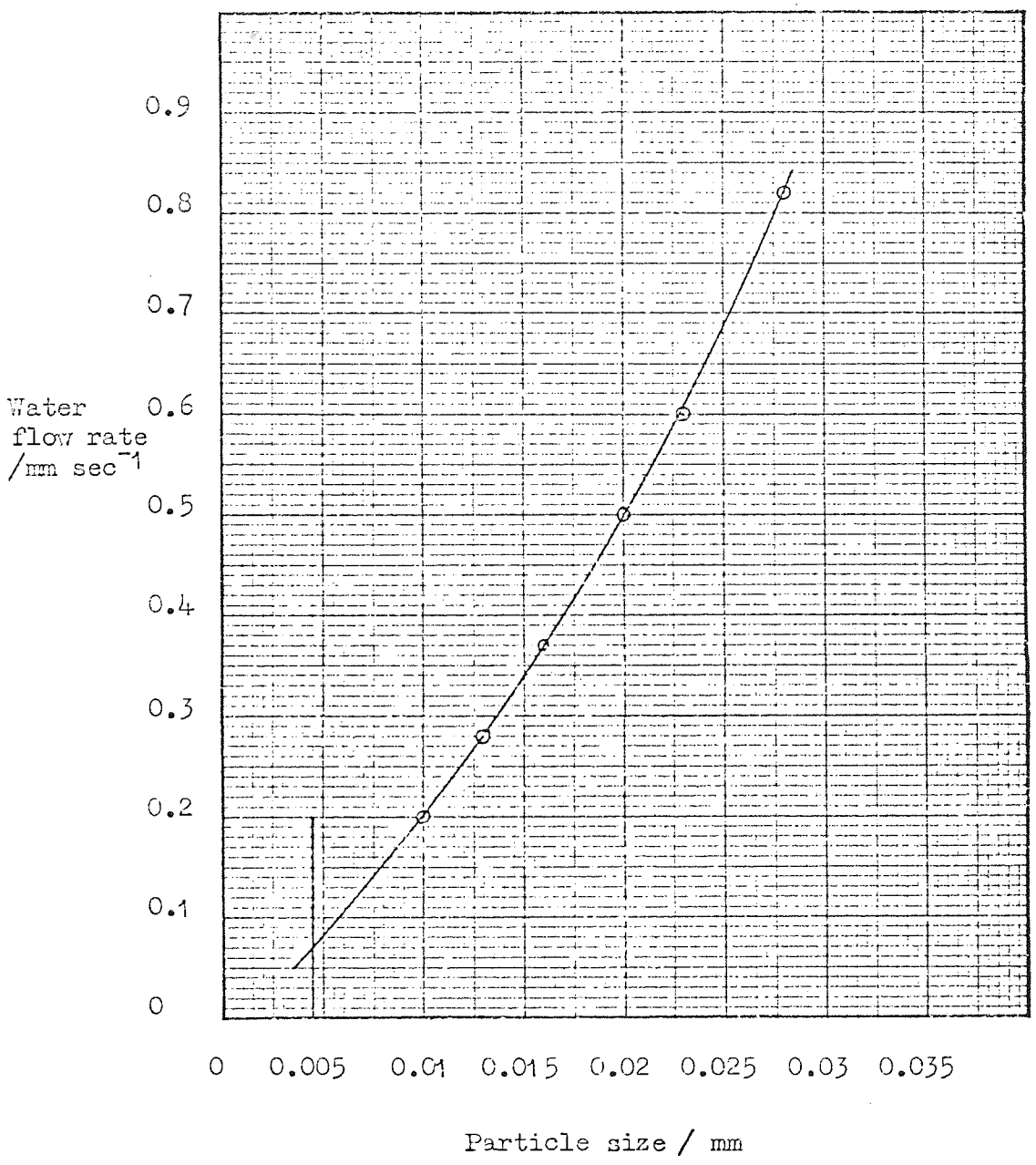

Fig. A6.2. Water flow rate in mm sec^{-1} required for separation of various particle sizes of quartz powder.

APPENDIX VII

BIBLIOGRAPHY

1 D. W. Smaith, M.Sc., University of Aston, 1970

2 I. C. Taig, Composites, (1972), 3(1), 16.

3 T. N. Brennan and K. C. Krieder, Materials Engineering Quarterly, (1969), 9, 5.

4 ASTM STP 427 (1967)

5 ASTM STP 452 (1969)

6 A. G. Thomas, J. B. Huffadine and N. C. Moore, Metallurgical Reviews, (1963), 8(32), 461.

7 A. A. Baker, A. Martin and R. J. Bache, Composites, (1971), 2(3), 154.

8 R. W. Jones, Composites, (1972), 3(1), 34.

9 A. A. Baker, S. V. Harris and E. Holmes, Metals and Materials, (1967), 1, 211.

10 D. J. O'Brien, D. W. Martin and R. V. Williams, Applied Materials Research, (1966), Oct, 241.

11 G. A. Cooper, J. Mat. Sci., (1967), 2(5), 409.

12 J. C. Withers and S. Abram, Plating, (1968), 55, 605.

13 A. A. Baker, M. B. P. Allery and S. J. Harris, J. Mat. Sci., (1969), 4, 242.

14 W. A. Wallace and V. P. Greco, Plating, (1970), 57(4), 342.

15 P. W. Jackson and J. R. Marjoram, J. Mat. Sci., (1970), 5, 9.

16 D. M. Braddick, P. W. Jackson and P. J. Walker, J. Mat. Sci., (1971), 6, 5.

17 M. Chapman, Symposium on Electrodeposited Composite Coatings, (S.E.P.A./I.M.F.), London, Oct. 1972.

18 J. Foster, Private communication.

19 H. von Helmholtz, Wied. Ann., (1879), 7, 337. Translated as Eng. Res. Bull. no. 33, (1951), University of Michigan.

20 M. von Smoluchowski, Bull. Intern. Acad. Sci. Cracovie, (1903), A, 182. Also in Handb. d. Electr. und Magnet., Vol II, Graetz (Ed), Leipzig, (1921), 374.

21 G. Kortum, Treatise on Electrochemistry, 2nd Ed., Elsevier, (1965), 424.

22 J. O'M. Bockris and A. K. N. Reddy, Modern Electrochemistry, Macdonald, London, (1970), 830.

23 J. T. Davies and E. K. Rideal, Interfacial Phenomena, 2nd Ed., Academic Press, (1963), 108-111.

24 A. J. Rutgers, T. Far. Soc., (1940), 36, 69.

25 A. J. Rutgers and H. De Smet, T. Far. Soc., (1947), 43, 102.

26 H. Fricke and H. J. Curtis, J. Phys. Chem., (1936), 40, 715.

27 D. C. Henry, T. Far. Soc., (1948), 44, 1021.

28 N. Street, Aust. J. Chem., (1956), 9, 333.

29 J. T. Davies and E. K. Rideal, Interfacial Phenomena, 2nd Ed., Academic Press, (1963), 131.

30 E. N. Andrade and C. Dodd, Proc. Roy. Soc., (1951), A204, 449.

31 D. C. Grahame, J. Chem. Phys., (1950), 18, 903.

32 B. E. Conway, J. O'M. Bockris and Ammar. T. Far. Soc., (1951), 47, 756.

33 F. Booth, J. Chem. Phys., (1951), 19, 391, 1327, 1615.

34 J. Th. G. Overbeek, J. Colloid Sci., (1953), 8, 420.

35 J. T. Davies and E. K. Rideal, Interfacial Phenomena, 2nd Ed., Academic Press, (1963), 141-147.

36 J. Lyklema, Discussions Far. Soc., (1966), 42, 81.

37 J. T. Davies and E. K. Rideal, Interfacial Phenomena, 2nd Ed., Academic Press, (1963), 84.

38 J. O'M. Bockris and A. K. N. Reddy, Modern Electrochemistry, Macdonald, London, (1970), 924.

39 G. M. Neale, T. Far. Soc., (1946), 42, 473

40 P. Delahaye, Double Layer and Electrode Kinetics, John Wiley, (1965), 44.

41 A. Findlay, Practical Physical Chemistry, 8th Ed., Longmans, (1954).

42 D. W. Smaith and P. D. Groves, Trans. Inst. Met. Fin., (1972), 50(3), 95.

43 D. W. Fuerstenau and H. J. Modi, J. Electrochem. Soc., (1959), 106, 336.

44 J. Foster and A. M. J. Kariapper, Trans. Inst. Met. Fin., (1973), 51(1), 27.

45 I. Langmuir, J.A.C.S., (1916), 38, 2221; (1917), 39, 1848.

46 L. De Brouckere, J. Chem. Phys., (1928), 25, 605; (1929), 26, 250; (1930), 27, 543.

47 M. M. Mooney, J. Phys. Chem., (1931), 35, 331.

48 H. A. Abramson and H. Muller, Proc. Am. Phys. Soc., (1932), 7, 11.

49 L. W. Janssen, Sow. Phys., (1933), 4, 322.

50 D. O. Hayward and B. M. W. Trapnell, Chemisorption, 2nd Ed., Butterworths (London)., (1964), 3.

51 R. A. Beebe and H. S. Taylor, J.A.C.S., (1924), 46, 43.

52 R. A. Beebe and D. A. Dowden, J.A.C.S., (1938), 60, 2912.

53 B. M. W. Trapnell, Proc. Roy. Soc., (1951), A206, 39.

54 H. S. Taylor and A. T. Williamson, J.A.C.S., (1931), 53, 2168.

55 R. A. Beebe, T. Far. Soc., (1932), 28, 761.

56 R. A. Beebe and M. P. Stevens, J.A.C.S., (1940), 62, 2134.

57 D. O. Haward and B. M. W. Trapnell, Chemisorption, 2nd Ed., Butterworths (London), (1964), 194.

58 J. O'M. Bockris and A. K. N. Reddy, Modern Electrochemistry, Macdonald, London, (1970), 1177.

59 W. Mehl and J. O. M. Bockris, J. Chem. Phys., (1957), 27, 817.

60 A. R. Despic and J. O'M. Bockris, J. Chem. Phys., (1960), 32, 389.

61 J. O'M Bockris and M. Enyo, J. Electrochem. Soc., (1962) 109, 48.

62 J. O'M Bockris and M. Kita, J. Electrochem. Soc., (1962), 109, 928.

63 T. Vitanov, A. Popov, E. Budersky, J. Electrochem. Soc., (1974), 121(2), 207.

64 J. Frenkel, J. Phys., (USSR), (1945), 9, 392.

65 W. K. Burton and N. Cabrera, Discussions Far. Soc., (1949), 5, 33.

66 A. Damjanovic in Modern Aspects of Electrochemistry, J. O'M Bockris and B. E. Conway, Eds., vol.3, Butterworths, (1964), 224.

67 N. A. Pangarov, Electrochem. Acta, (1962), 7, 139.

68 M. Volmer, Z. Physik, Chem., (1922), 102, 267; Kinetic der Phasenbildung, Steinkopff, Dresden and Leipzig, (1939).

69 F. C. Frank, Discussions Far. Soc., (1947), 5, 48.

70 W. K. Burton, N. Cabrera and F. C. Frank, Nature, (1949), 163, 398; Proc. Roy. Soc., (1951), A243, 229.

71 M. J. Lighthill and G. B. Whittam, Proc. Roy. Soc., (1955), A229, 281, 317.

72 N. Cabrera and D. A. Vermilyea in Growth and Perfection of crystals, R. H. Doremus, B. W. Roberts and D. Turnbull, eds., John Wiley, N.Y., (1958), 393.

73 F. C. Frank, ibid, 411.

74 H. J. Pick, G. G. Storey and T. B. Vaughan, Electrochem. Acta., (1960), 2, 169.

75 E. Raub and K. Müller, Fundamentals of Electrodeposition, Elsevier, London, (1967), 198.

76 P. Spiro, J. Electrodep. Tech. Soc., (1947-8), 23, 27: Electroforming, Draper, London, (1968), 59.

77 V. A. Lamb and W. H. Metzger, Tool Engineer, (U.S.A.), 33, 55.

78 R. Brugger, Nickel Plating, Draper, London, (1970).

79 J. N. Notley, Trans. Inst. Met. Fin., (1972), 50(1), 6.

80 G. A. Cooper, Composites, (1970), 1, 153.

81 R. V. Williams and P. W. Martin, 6th International Metal Finishing Conference, (1964).

82 T. C. Kedward, Symposium on Electrodeposited Composite Coatings (C.A.P.A./I.M.F.), London, Oct. 1972.

83 R. Bazzard and P. J. Boden, Trans. Inst. Met. Fin., (1972), 50(2), 63.

84 V. P. Greco and W. Baldauf, Plating, (1968), 55(3), 250.

85 N. Guglielmi, J. Electrochem. Soc., (1972), 119(8), 1009.

86 R. S. Saifullin, L. N. Akulova and A. T. Kudryashov, Porosh. Met., (1970), 6(90), 75.

87 P. T. Varadi and K. Ettre, J. Electrochem. Soc., (1962), 109, 292.

88 G. Isserlis, Private communication.

89 T. Gilliam, K. M. McVie and M. Phillips, J. Inst. Metals, (1966), 94, 228.

90 E. Broszeit, F. J. Hess and E. Wagner, Z. Werkstofftech., (1973), 4(7), 374.

91 J. M. Sykes and D. J. Alner, Trans. Inst. Met. Fin., (1974), 52(1), 28.

92 T. M. Tomaszewski, L. C. Tomaszewski and M. Brown, Plating, (1969), 56(11), 1234.

93 R. A. Brandes and D. Goldthorpe, Metallurgia, (1967), 76(11), 195.

94 W. G. Pfann, Zone Melting, 2nd Ed., John Wiley, N.Y. (1966).

95 J. M. Sykes and D. J. Alner, Trans. Inst. Met. Fin., (1973), 51(5), 171.

96 R. Butler and T. Kerr, An introduction to Numerical Methods, Pitman (1962), 6.